EFFECT OF RATE OF WATER TABLE RISE ON LNAPL ENTRAPMENT IN UNIFORM AND WELL-GRADED SANDS

BY

MU'AZU NUHU DALHAT

A Thesis Presented to the
DEANSHIP OF GRADUATE STUDIES

KING FAHD UNIVERSITY OF PETROLEUM & MINERALS

DHAHRAN, SAUDI ARABIA

In Partial Fulfillment of the
Requirements for the Degree of

MASTER OF SCIENCE

In

Civil Engineering

May 2005

KING FAHD UNIVERSITY OF PETROLEUM & MINERALS
DHAHRAN 31261, SAUDI ARABIA

DEANSHIP OF GRADUATE STUDIES

This thesis, written by **MU'AZU NUHU DALHAT** *under the direction of his thesis advisor and approved by his thesis committee, has been presented to and accepted by Dean of Graduate Studies, in partial fulfillment of the requirements for the degree of* **MASTER OF SCIENCE IN CIVIL ENGINEERING.**

Thesis Committee

Dr. Mohammad Al-Suwaiyan (Advisor)

Dr. Rashid Allayla (Member)

Dr. Muhammad Al-Zahrani (Member)

Prof. H.I. Al-AbdulWahhab
(Department Chairman)

Dr. Mohammad Abdulaziz Al-Ohali
(Dean of Graduate Studies)

Date 14-6-2005

عمادة الدراسات العليا
DEANSHIP OF GRADUATE STUDIES

Dedicated to My Beloved Parents

“Each and every inch of my life achievements is credited to you”

ACKNOWLEDGEMENT

All best thanks and praises are always due to Al-mighty Allah (SWT) alone who made everything possible towards achieving this milestone. May peace and blessings be upon His beloved servant, His last messenger and the seal of the prophet-hood, Prophet Muhammad (S.A.W), his house-hold, companions and those that follow their unique and most guided foot-steps till day of resurrection.

Many thanks are to KFUPM for giving me the rare opportunity to study in her conducive academic environment. To my thesis supervisor Dr. Muhammad Al-Suwaiyan whose noble characters reflect ideal characters worth emulating, my special gratitude and appreciations are due for his much caring, encouragement, guidance and assistance throughout the course of this work. I also wish to express similar gratitude and appreciations to my committee members, Dr. Rashid Allayla and Dr, Muhammad Al-Zahrani for their invaluable contributions to the success of this work.

I am highly indebted to express my profound appreciations and thanks -that I am short of apt words to use- that I preserve for my beloved parents for their caring, guidance, prayers and the moral upbringing they put me through right from childhood. Also my deserving thanks are to my brothers, sisters and caring friends for their relentless prayers, supports and concern for my success in my life endeavors.

The proper attention and assistance rendered by Engr. Essa, Dr. Salim, Mr. Hassan and Mr. Hussaini in KFUPM Civil Engineering Laboratories and Mr. Abdul-Samad of KFUPM Petroleum Engineering Laboratory is highly commended and appreciated. My sincere gratitude is due to brothers and colleagues in building 92 and 93 and the Nigerian community in east compound for making my stay in KFUPM an enjoyable and memorable one. Special appreciations are to Sa'idu Waziri and Ahmad Doko for all sorts of invaluable supports and assistance they rendered to me during necessary procedures towards getting to KFUPM and Dr. Mohammad Shazali for the final technical editing of this write-up.

TABLE OF CONTENTS

LIST OF TABLES

LIST OF FIGURES

THESIS ABSTRACT

Name: Mu'azu Nuhu Dalhat

Title: Effect of Rate of Water Table Rise on LNAPL Entrapment in Uniform and Well-graded Sands

Major Field: Civil Engineering

Date of Degree: May 2005

Vertical water table movement is liable to trap part of any light non-aqueous phase liquid (LNAPL) present within the vicinity of capillary fringe and water table in contaminated aquifers. Due to toxicity and low dissolution of LNAPLs in water, the trapped component could be a long-term groundwater contamination source. This present work experimentally investigated and modeled the influence of rate of water table rise on the entrapment of Saudi Arabian light crude oil in natural uniform and blended well-graded sands. Series of laboratory column tests were conducted to simulate a rising water table at several rise rates and the subsequent entrapment of the LNAPL for range of initial water saturations between 0-71%; from which macroscopic quantitative measurements of trapped LNAPL saturation were performed after attainment of quasi-static equilibrium.

The experimental results apparently show that, at high rate of water table rise, in addition to initial water saturation, the entrapment of LNAPL is also significantly influenced by the rate of the water table rise. Increase in the rise rate was found to increase the LNAPL trapped saturation for water-wet initial condition, while it decreases the LNAPL trapped saturation for the LNAPL-wet condition, suggesting that the initial soil matrix wetting status controls the flow condition during water displacing LNAPL processes. The trapped saturation ranges for the water-wet conditions are 1.5-37.3% and 28.1-37.5%, while for the LNAPL-wet conditions the ranges are 33.6-13.4% and 37-15.2% for the two porous media respectively. Marked deviation from the established linearity of trapped saturation as a function of initial water content was observed to amplify with increase in the rise rate. Predictions from a semi-empirical model formulated in the study to account for the rate of wetting fluid imbibition rate imposed by a rising water table provided much better results compared to predictions from linear trapping models of Land [1968] and Steffy *et al* [1996] as they profoundly underestimated the trapped specific volume. It is concluded that LNAPL tapping models are bound to be erroneous when rate of imbibition of wetting fluid is disregarded at high rate of water table rise.

MASTER OF SCIENCE
KING FAHD UNIVERSITY OF PETROLEUM AND MINERALS
Dhahran, Saudi Arabia
May 2005

ملخص الرسالة

الاسم : معاذ نوح طلحة

عنوان الرسالة : تأثير معدل ارتفاع مستوى المياه الجوفية على السوائل الخفيفة في التربة الرملية المنتظمة جيدة التدرج

القسم : الهندسة المدنية

تاريخ منح الشهادة : مايو 2005

تؤدي الحركة الراسية للمياه الجوفية الى حصر أجزاء من السوائل العضوية الخفيفة غير الذائبة التي تتواجد في مجال الجاذبية الشعرية وبالقرب من مستوى سطح المياه الجوفية في المكامن الملوثة نظراً لقلة ذوبان هذه السوائل في الماء بالاضافة لتاثيرها السام، فإن الجزء المحصور يكون مصدراً طويل المدى لتلويث المياه الجوفية. تم في هذا البحث دراسة ونمذجة تاثير معدل ارتفاع مستوى المياه الجوفية على كمية حصر الزيت العربي الخفيف في بيئة رملية منتظمة مخبريا. كما تم اجراء عدد من الإختبارات العمودية لتمثيل تاثير الارتفاع الراسي للمياه الجوفية بمعدلات مختلفة على كمية حصر الزيت الخفيف حيث كان مستوى التشبع بالمياه الاولي ينحصر بين 0-71%. وقد تم قياس نسبة التشبع بالسوائل الخفيفة بعد الوصول لحالة التوازن الاستاتيكي.

اظهرت النتائج ان الكمية المحصورة من السوائل العضوية الخفيفة تتاثر بصورة واضحة بسرعة ارتفاع مستوى سطح المياه الجوفية بالاضافة لنسبة المياه الاولية في التربة. كما وجد ان زيادة سرعة ارتفاع سطح المياه الجوفية تؤدي لزيادة كمية السوائل الخفيفة المحصورة داخل المياه الجوفية بينما تقل هذه الكمية بزيادة درجة التشبع الاولية. وقد تراوحت نسبة الكمية المحصورة في حالة التشبع المائي الإبتدائي بين 1.5-37.3% و28.1-37.5% بينما بلغت في حالة التشبع الإبتدائي بالسوائل الخفيفة 33.6-13.4% و37-15.2% للوسطين المساميين على التوالي. تمت ملاحظة ان نسبة السوائل العضوية المحصورة تجنح بعيدا عن العلاقة الخطية مع نسبة تشبع المياه الاولية وذلك عند زيادة معدل ارتفاع سطح المياه الجوفية.

اظهرت نتائج النموذج شبه التجريبي الذي تم إعداده في هذه الدراسة توافق اكثر مع النتائج المخبرية وذلك عند مقارنتها بالنماذج المعدة من قبل، مثل لاند (1968) و استيفي (1996) حيث وجد ان هذه النماذج تعطي تقديرات لكمية السوائل العضوية المحصورة اقل من الكمية الفعلية. وقد وجد ان النموذج المعد في هذه الدراسة يكون غير صحيح في حالة تجاهل معدل ارتفاع مستوى المياه لاسيما عندما تكون عند معدلات الارتفاع في سطح المياه الجوفية عالية.

ماجستير العلوم
جامعة الملك فهد للبترول والمعادن
الظهران، المملكة العربية السعودية

مايو 2005

CHAPTER 1

Introduction

Groundwater storage in aquifers accounts for more than 96% of global harvestable liquid fresh water [65]. Being one of the world most precious resources ever known throughout ages for sustenance of the world living inhabitants, for centuries this essential asset had been considered pristine and free from human interferences. However, owing to increased industrialization and rapid population growth, recent decades have demonstrated that groundwater is increasingly subjected to dangers of pollution and dwindling supplies. Currently, with variety of toxic chemicals detected in the subsurface environment, aggrieved by steady increase in production with tens of thousands of the chemicals being manufactured; the susceptibility of groundwater to contamination has become a real problem of growing concern day-by-day.

Universal reliance on particularly petroleum products and relentless consumption of such products are advancing the vulnerability of groundwater to pollution that metamorphosed into persistent plague that is widely spread geographically. Majority of the frequently detected soil and groundwater pollutants at affected hazardous contaminated sites, such as oil refineries, offshore services facilities, industrial pipe networks, heavy manufacturing industries, petroleum tank farms and more often, gasoline service station, are highly toxic organic liquid contaminants that slightly dissolve in water, commonly referred to as non-aqueous phase liquids (NAPLs) [9,70]. High percentages of these contaminants are petroleum hydrocarbons; locomotive fuels, chlorinated solvents, transmission oils, coal tar

and so forth. Discharge of NAPLs into the subsurface following accidental spill, leaks from aging underground tanks, pipe leakages, surface spills and negligence and/or improper disposal practices has been identified as momentous soil and groundwater contamination source.

1.1 Classification of Non-Aqueous Phase Liquids (NAPLs)

The fate and transport of NAPLs in the subsurface are very complex. Volatilization, partitioning, dissolution, smearing, sorption, chemical degradation, biodegradation, soil adsorption and convection, diffusion and hydrodynamic dispersion are among the complex mechanisms describing the transport of NAPLs once released into the subsurface [8]. Based on physical properties and behaviors upon reaching water table, NAPLs are generally subdivided into two main classes:

1. Light NAPLs (LNAPLs), hydrocarbons that are less dense than water; they overlay and float atop the water table. This class includes hydrocarbon such as kerosene, light crude oil, benzene and toluene.
2. Heavy NAPLs (DNAPLs) which are denser than water; they migrate down to underlay the water at the impermeable bed at bottom of an aquifer. Examples are creosote, chlorinated solvents (e.g. TCE), coal tar, and polychlorinated biphenyl.

1.2 LNAPL Aquifer Contamination and Water Table Dynamic Effects

Water table which is a surface of water at atmospheric pressure that separates saturated zone below and vadose zone above where the pore-water pressure is positive and negative respectively. For unconfined aquifer, principally with shallow water table, the well-known conceptual model for LNAPL contamination is given in figure (1.1). The figure shows that small LNAPL discharge into subsurface migrates downward and spread laterally under the influence of gravity and capillary forces until it finally becomes discontinuous and immobile before reaching the water table. But plume from a LNAPL spill of sufficient size percolating into the subsurface can eventually reach the water table. Due to its low density, the LNAPL initially spreads laterally in form of pancake-like lens within the water table and the capillary fringe. The water table is locally depressed near the center of the plume and recovers to a degree as the plume continues to spread over the capillary fringe. By returning to its original position, some of the LNAPL will become trapped as it is vertically displaced, forming an "immiscible" lens of water and the contaminant [15]. Similarly, regions holding significant volume of trapped LNAPL in the form of discontinuous blobs or ganglia can be created anywhere the plume comes in contact with the capillary fringe or the water table due to artificial causes such as artificial recharging, pumping and flooding during free product recovery or naturally induced seasonal water table fluctuations [41, 43, 67, 68, 77]. Water table rising, falling or fluctuation renders LNAPL at or near the water table susceptible to "smearing", a typical case of rising is shown in figure (1.2). The residual LNAPL smeared zone also becomes source of trapped LNAPL [9].

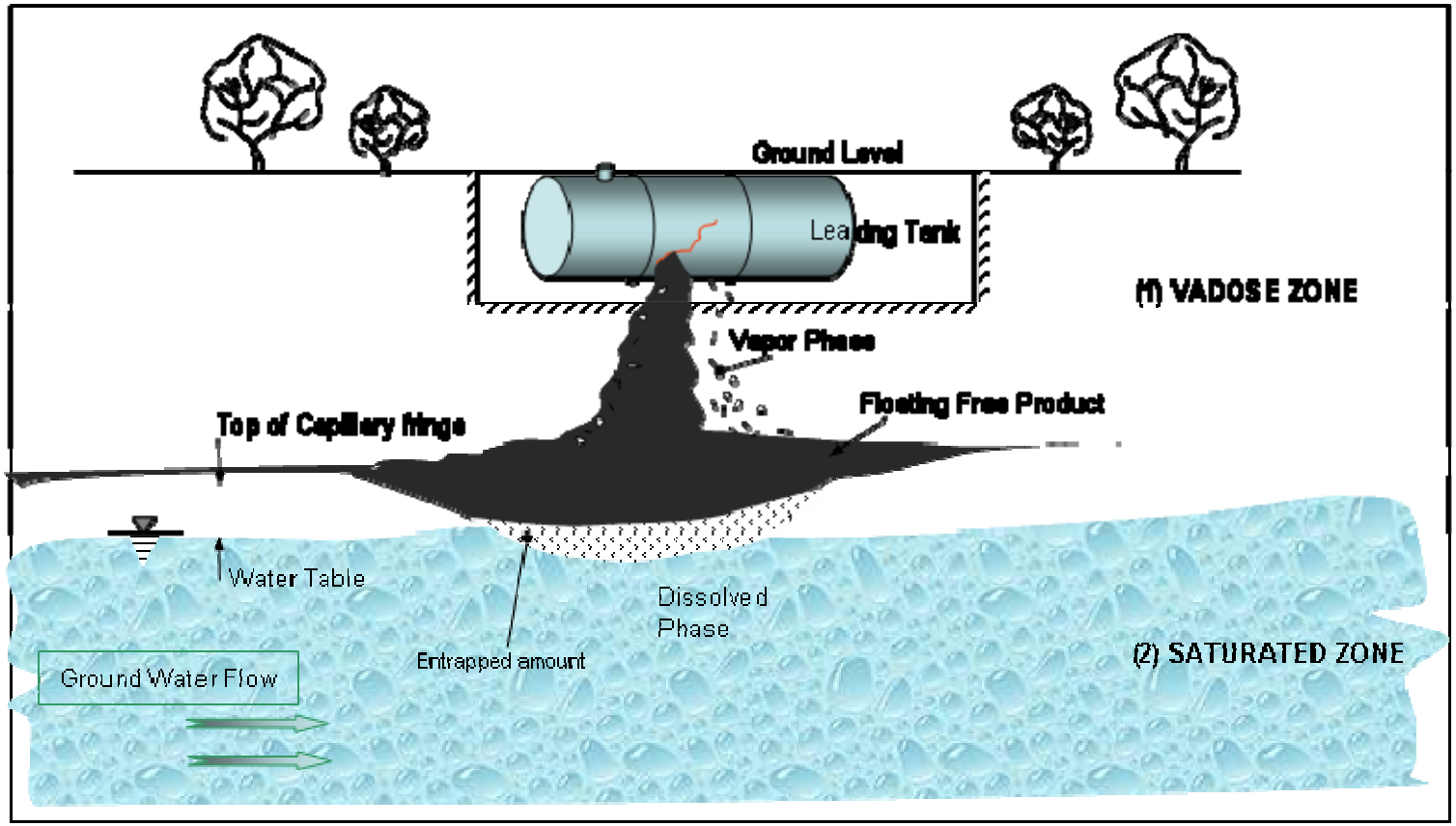

Figure 1.1: Section View in a Contaminated Water Table Aquifer

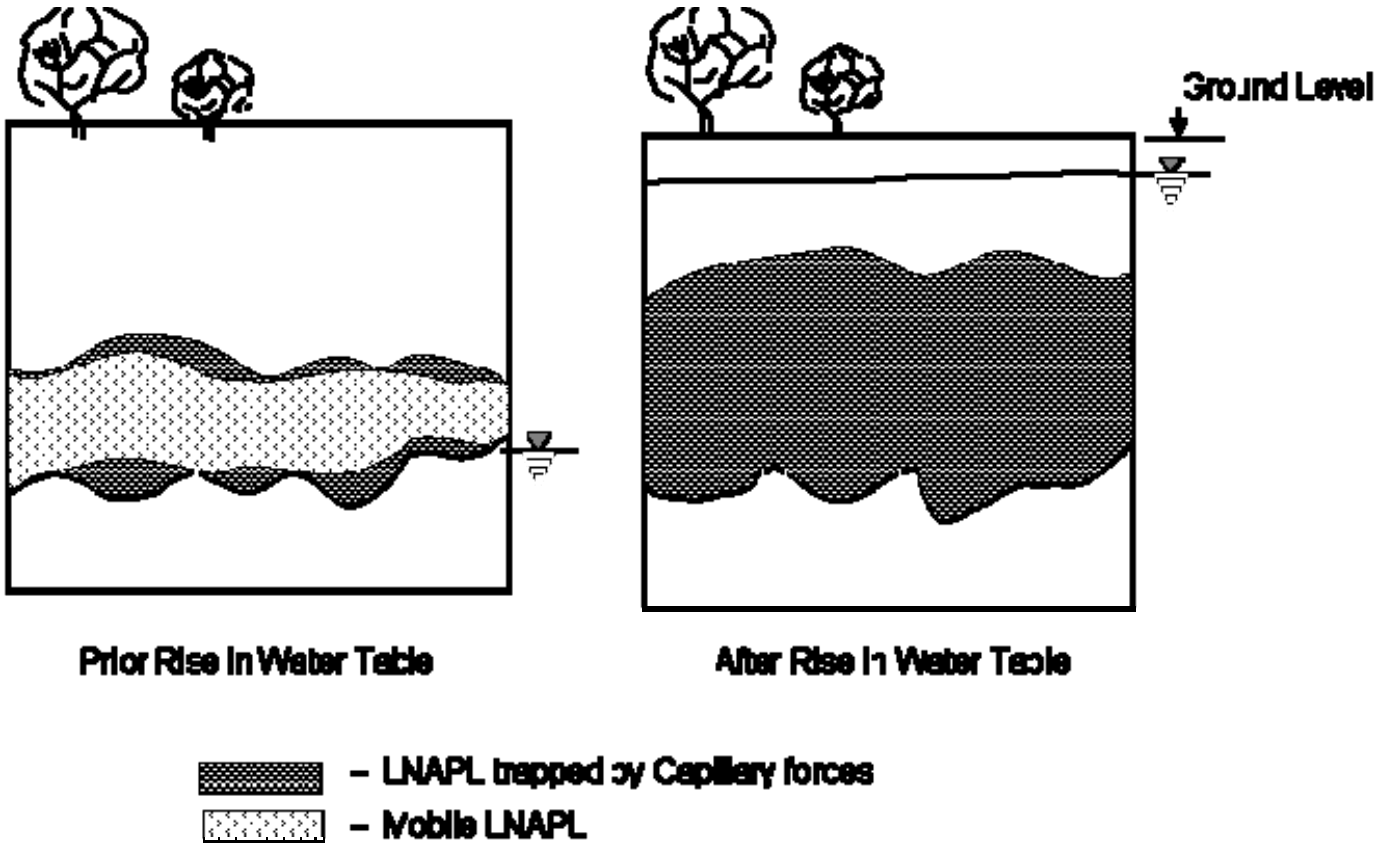

Figure 1.2: Trapped Smeared Zone Due to Water Table Rise Effect [9]

By virtue of its location in the saturated zone, characterized by large interfacial area in contact with the water phase, very slow dissolution rate, toxicity of most LNAPLs even at low concentration and clean-up difficultly, the trapped LNAPL is expected to be a potential persisting danger to soil and groundwater quality capable of spanning for numerous years [43, 58, 68, 72].

1.3 Objectives of the Study

It is evident that the relevance of trapped LNAPL saturation in subsurface contamination investigation as highlighted in the literature survey in section 2.1 cannot be overemphasized. Based on such facts, the LNAPL entrapment is expected to be a multifaceted problem needing more attention in order to have a better understanding of the effects of its various influencing factors. Devising a viable and effective remediation scheme for contaminated soil or aquifer is crucial process that requires in-depth knowledge of both natural and artificial processes that control the fate of the contaminant. Consequently, establishing interaction between water table and LNAPL existing within its vicinity is vital in advancing the understanding of subsurface processes that could follow LNAPL contamination. Moreover, it would be of significance in better estimation of the amount of LNAPL that could be left in both the saturated and unsaturated zones for appropriate strategic clean-up plan and its cost estimates.

The main aim of the present study is to assess the effect of water table rise rate on LNAPL entrapment in sandy soils of different gradations. More specific objectives of this study are:

1. To undertake series of laboratory column tests at various initial water content simulating the rate of water table rise in LNAPL contaminated sandy soils- uniform and well-graded- in order to examine the LNAPL entrapment process in the distinct soils.
2. To assess the influence of initial water saturation on the LNAPL entrapment taken into consideration the effect of water table rate. Moreover, to examine the effect of initial porous media surface wetting condition on the entrapment saturation.
3. To develop an empirical relationship relating LNAPL trapped saturation to the initial water saturation that incorporates the effects of the rate of water table rise.
4. To develop a LNAPL entrapment model that could predict trapped LNAPL's specific volume as a function of initial water saturation taking into account rate of imbibition imposed by the rising water table based on Brooks-Corey (BC) [5] and Van Genutchen (VG) [71] constitutive relationships.
5. To validate the developed LNAPL trapping model and to compare its performance with Land's [31] and Steffy e*t al* [68] trapping models.

CHAPTER 2

Literature Review

Entrapment of fluids in porous media is a multi-disciplinary problem that cut across fields of studies which include petroleum engineering, soil physics, hydrology and geo-environmental/environmental engineering, with bulk of the related research conducted in petroleum engineering. With particular emphases, LNAPL contamination of aquifers has drawn vast attention of policy makers and diverse technical fields concerned with averting environmental deterioration, solely, with common interest of protecting subsurface water resources. Relatively, subject to its complexity, researchers in groundwater contamination habitually resort to attempting to capture the subsurface behaviors of LNAPLs in order to formulate vigorous solutions to various groundwater LNAPL contamination scenarios. A number of groundwater hydrologists have reported LNAPL contamination and related effects of water table dynamics at many contaminated fields and many others have reproduced similar trends in laboratory scale studies [1, 25, 32, 43, 60, 61, 68, 73]. Experience has shown that erroneous assessment and estimate of LNAPL residuals and/or entrapment saturation may lead to failure of frequently cumbersome and costly remediation efforts or atleast yielding results less than the originally intended [72]. Moreover, these estimates are found to be crucial and requisites in contamination modeling studies aimed at more accurate determination of volume of recoverable LNAPL free-product in contaminated aquifer. Such assessment is often based on LNAPL product thicknesses in monitoring wells during remediation programs [9, 23, 41, 51, 52, 60, 75].

Parker and Lenhard [54] further indicated that accurate prediction of contamination source distribution and resulting aqueous and gaseous phase plumes will not be quite possible without consideration of non-wetting fluid entrapment. Consequently, within the past few decades, the foregoing highlights led to considerable efforts towards field and/or laboratory studies and numerical simulations of multiphase fluid flow in porous media. Such efforts focus on release, migration of LNAPLs through the un-saturated zone to water table aquifer, and subsequent entrapment and eventual distribution due to the water table fluctuations effects [12, 21, 25, 27, 32, 36, 43, 53, 60, 61, 66, 67, 64, 68, 76, 79, 80].

In broader perspective, establishment of vertical hydrostatic saturation distribution profile of LNAPL in the subsurface is among the foremost requirement for effective clean-up of LNAPL contamination. Farr *et al* [14] and Lenhard and Parker [33] established that vertically integrating the static LNAPL saturation distribution profile gives the estimated spill specific volume which is helpful for proper remedying scheme. Leveretts [40] pioneered the vertical hydrostatic distribution studies of fluids in porous media. He developed two-phase water-air capillary pressure and saturation empirical correlation for a sand media from which hysteretic behavior was quite obvious. Existing numerical models normally rely on Leveretts [40] assumptions on adopting constitutive saturation-capillary pressure-relative permeability (S-P-*K*) relationships. Most of the models are characterized by either portraying strict conservative monotonic system or more comprehensive system that incorporates effects of fluid entrapment and saturation hysteresis on the *S-P-K* relationship. Although, models that account for two-phase hysteretic and non-hysteretic *S-P* relation have been widely developed [28, 31, 39, 46],

yet, accurate prediction of the subsurface fluid behavior inevitably encompasses consideration of three-phase fluid *S-P* relationships. Difficulty and lack of substantial experimental techniques for direct measurement of *S-P* relationship in three phase systems promoted a number of quests directed towards projecting easier to secure two-phase data from well-documented experimental procedures to the three-phase system [5, 13, 40]. As corroborated to Leveret's [40], Lenhard and Parker [38] and Busby *et al.* [7], both validated the proposed extension of two-phase to three fluids system by noting that order of wettability follows; water >LNAPL > air. In addition, the total liquid and the water saturation are only functions of two-phase LNAPL-air and LNAPL-water fluids interface respectively, also an idea suggested previously by Aziz and Settari [3]. Parker and Lenhard [54] pointed-out the complexity of hysteresis and indispensable need to incorporate it in both two and three-fluid systems multiphase flow analysis. Investigators such as Aziz and Settari [3] and Hillel [20] formerly established that in both cases, hysteresis cannot be neglected since it could lead to significant error in predicting fluid saturation distribution [21, 28, 54]. They and many other researchers have attributed hysteresis essentially to combined effects of difference in contact angles during imbibition and drainage processes, irregular porous medium pore geometry and "non-wetting fluid entrapment" [13, 77].

Taking into account of water table fluctuations, Marinelli and Dunfort [43] developed semi-analytical non-hysteretic and hysteretic models for predicting vertical distribution of LNAPL in relation to thickness in monitoring well based on Brooks-Corey [5] and Van Genutchen [71] *S-P* models. The non-hysteretic model employs the analytical approach

presented by Farr *et al* [14] and Lenhard and Parker [33] with the assumption of succession of quasi-static equilibrium, amongst many other assumptions. The former model extends the Lenhard's [32] model that incorporates hysteresis and non-wetting fluid entrapment for both two and three-phase fluid systems. Though, the authors [43] outlined persisting uncertainties warranting further investigation, they concluded that rampant occurrences in LNAPL thickness behavior in monitoring wells reported from numerous contamination sites can be explained more accurately by employing hysteresis and non-wetting fluid entrapment in LNAPL contamination models. Van Geel and Co-worker [72] argued that hysteretic models need to include residual saturation stressing that neglecting it in multiphase flow simulator may lead to eventual misestimating volume of NAPL reaching the capillary fringe and/or held in the unsaturated zone. They filled the vacuum that existed in the literature by a model modifying Parker and Lenhard [54] and Lenhard's [32] model to account for the residual saturation.

Steffy *et al* [68] investigated the effect of antecedent water moisture content on the maximum possible trappable volumes of diesel and decane hydrocarbon using bead packs as the porous medium. They empirically showed that LNAPL trapped below rising water table can be accurately related to initial water saturation by linear fitting, in agreement with more recent report by Maldal and Co-workers [41]. They lamented that availability of water in the pores prior to water table rise limits the amount of trappable LNAPL, thereby resulting in an inverse linear correlation. They validated the resulting semi-empirical trapping model they presented based on laboratory column experiment and field investigation. Later [67], they [68] further experimentally validated modification they

proposed to multiphase transport model (MOFAT), a finite element program for simulating LNAPL displacement and entrapment developed by Katyal *et al* [26]. For initial water saturations varying from 0.02 to 0.40, George *et al* [18] investigated the effect of initial water on residual organic carbon by allowing gasoline to imbibe into the water wet soil and later forcing air into the system resulting in gasoline residual saturation. Their data indicated that in order to comprehend retention and organics transport in the subsurface, accounting for water saturation is crucial. Positively, they also disclosed that residual organic saturation decreases linearly with initial water saturation up to certain "critical value" of the initial water saturation, above which Leverett's assumption [40] was no longer valid and the residual oil saturation remained constant.

Ryan and Dhir [60, 61] examined the effects of particle diameter and interfacial tension on LNAPL entrapment due to slowly fluctuating water table via series of laboratory column tests and reported that at microscopic scale, trapped LNAPL distribution is fairly uniform, and up to 710μm diameter particle size, average residual saturation is almost constant at about 13%. However, above that limiting diameter, residual saturation decreases with particle size. Moreover, they apparently found that as the bond number approaches unity either due to increased in larger particle sizes or reduced interfacial tension, the residual saturation drops to smaller values due to reduction in the entrapment saturation. The outcome of their investigation was a general empirical model they presented relating residual saturation and bond number for bond numbers between 0.001 and 1.2.

2.1 Significance of Trapped LNAPL Saturation

From the forgoing reviews, accurate estimate of trapped LNAPL saturation in LNAPL contamination investigation and/or mitigation processes provides assistance in:

- Averting negative consequences in the assessment of extent of subsurface contamination.
- Modeling approach in determining volume of recoverable LNAPL free-product in contaminated aquifer during remediation process.
- More reliable measurements of LNAPL product thickness in monitoring wells.
- Accurate prediction of resulting aqueous and gaseous phase plumes from LNAPL contamination.
- Providing comprehensive explanation of hysteresis in *S*-*P* relation.
- Better explanation for rampant occurrences in LNAPL thickness behavior in monitoring wells reported from numerous contamination sites.
- LNAPL mobilization processes during soil and aquifer remediation or hydrocarbon enhanced recovery.

2.2 Saturation-Pressure (S-P) Relationships

Complete subsurface mathematical modeling of LNAPL movement and entrapment requires the knowledge of functional *S-P-K* relationship between air, water and LNAPL, mainly determined through experimentation on porous media [72]. However, the difficulty of establishing such relation owing to direct complicated laboratory measurements has been conquered to a great extent by existence of relationships developed by a number of researchers. Among them are Van Genutchen (VG) [71] and Brooks Corey (BC) [5] *S-P* model, which are empirically generated equations for two-phase immiscible fluid systems that apparently receive broader attention in groundwater and soil physics literature. These models depend on certain porous media parameters that describe the water retention curve for two-phase air-water system. Yet, similar relationships have been markedly presented by Fredlund and Xing [17] and many others as well [72]. A typical plot of the hysteretic retention curve according to the two models for a hypothetical soil is depicted in figure (2.1)

2.2.1 Brooks-Corey S-P Model

As shown in figure (2.1), the BC retention function [5] presupposes that finite capillary pressure called displacement pressure head, h_d , is the minimum pressure required for non-wetting fluid to start displacing wetting fluid on the drainage path. In other words, for any capillary head, $h_c \leq h_d$, the model assumes that the pressure head is insufficient for any effective fluid displacement in the porous medium to occur. Accordingly, the model's

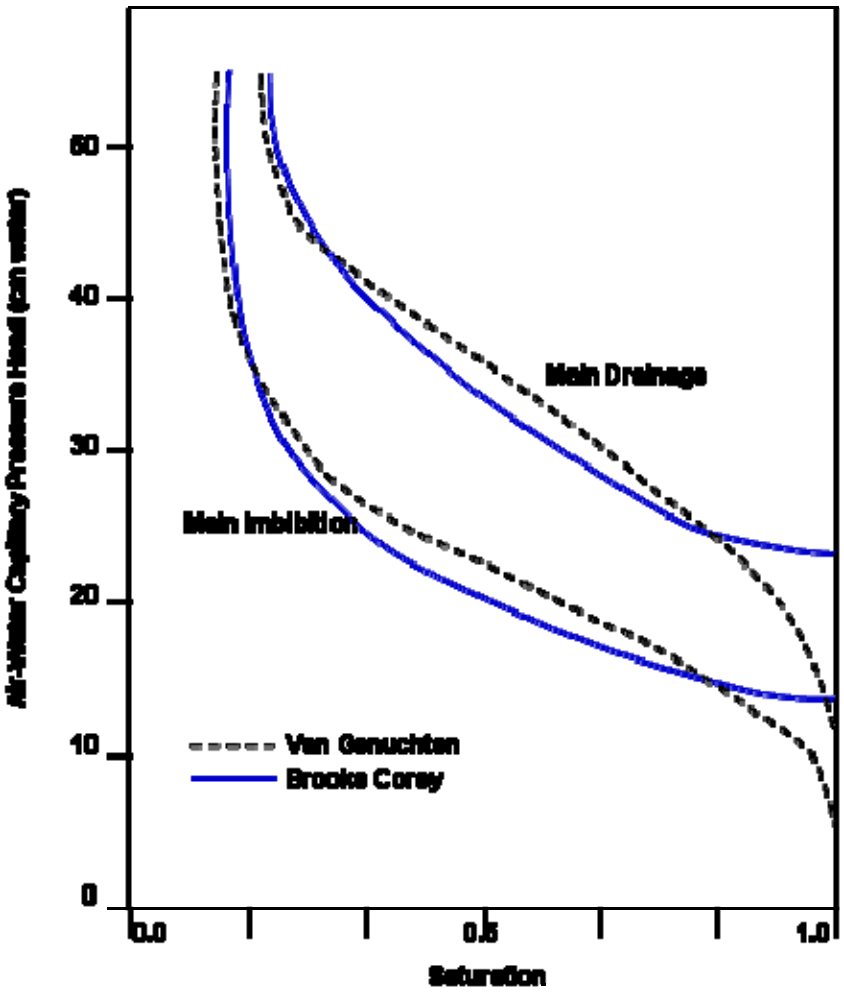

Figure 2.1: Typical Hysteretic Fluid Retention Curves for a Hypothetical Soil

assumption leads to discontinuity which in two-phase system the best fitted *S*-*P* relation for effective wetting fluid saturation, $\overline{S}_w^{nw}$, is stated as

$$\overline{S}_w^{nw} = \left(h_d h_{nw}^{-1} \right)^{\lambda} \qquad \text{for } h_c > h_d \tag{2.1}$$

$$\overline{S}_w^{nw} = 1 \qquad \text{for } h_c \le h_d \tag{2.2}$$

where

$$\overline{S}_w^{nw} = \frac{S_w^{nw} - S_r}{1 - S_r} \tag{2.3}$$

Where, S_w^{nw} = actual wetting fluid saturation, S_r = irreducible wetting fluid saturation, n,w denote non-wetting and wetting fluid, λ = pore size index parameter. S_r , λ and h_d are curve fitting parameters obtainable from experiment or alternatively empirically developed models.

2.2.2 Van-Genutchen S-P Models

In contrast, VG *S*-*P* fitting model [71] suggests that displacement of wetting fluid during drainage could occur at any pressure above zero as displayed in figure (2.1). This assumption produces a continuous characteristic curve throughout the range $h_c > 0$. In other words, the model sets the BC's entry pressure to zero. For this, the VG model is overwhelmingly preferred over BC's model. The model takes the form:

$$\overline{S}_w^{nw} = \left(1 + \left(\alpha_{nw} h_{nw}\right)^n\right)^{-m} \quad \textbf{(2.4)}$$

Similarly, α, n and $m = 1 - 1/n$ are VG model curve fitting parameters obtainable from experiment.

2.3 Parker and Lenhard LNAPL Entrapment Model

Parker and Lenhard [32, 54] gave the most comprehensive closed-form set of algorithms that capture the features of hysteretic and non-hysteretic behaviors in both two-phase and three-phase environment by employing the VG *S*-*P* function given in equation (2.4). The model computes fluid components saturations for any possible path within the main imbibition and drainage paths envelope. The model primarily assumes that Leverett's assumption [40] is valid, in addition it considers hydrostatic equilibrium condition, rigid porous medium with no significant solid-fluid interaction, and that only fluid with greater wettability can trap lesser wettability fluid. Furthermore, the model presupposes entrapped fluids are incompressible and that all pore sizes classes entrap non-wetting fluid in proportion to their volumes.

2.3.1 Description of Primary Drainage and Imbibition and Scanning Curves

Generalized for two-phase fluids system, in lieu of usual actual, S_w^{nw} and effective non-wetting fluid saturation, $\overline{S}_w^{nw}$, apparent wetting fluid saturation, $\overline{\overline{S}}_w^{nw}$, is brought into play so as to account for non-wetting fluid entrapment in similar fashion used by Fayer and

Hiller [16]. To cater for hysteresis, *S*-*P* relationship is parameterized as history dependant function coupled with eliminating fluid pair dependant effects through scaling procedure achieved via:

$$p \overline{\overline{S}}_{w}^{nw}\left(\beta_{nw} h_{nw}\right) = S^{*}\left(h^{*}\right) \tag{2.5}$$

$S^{*}\left(h^{*}\right)$ = is the transformed scaled retention function, p = is the saturation path; main drainage, d, or main imbibition, i, and β = fluid pair scaling coefficient [32].

Customarily, either before reaching irreducible wetting fluid saturation on the drainage path or attainment of maximum trappable non-wetting fluid on the imbibition path within the bound of the two main envelope branches, abrupt reversal may occur. This led to non-parametric scanning pathways predictable via detailed closed-form expressions characterized with enforced closure as elaborately presented by the authors [32, 54]. When drainage path reversed to imbibition path, by generalizing Land's [31] procedure for NAPL-water system algorithm, the model predicts the local maximum amount of trappable non-wetting fluid, $\overline{S}_{nr}^{nw}$, when the wetting fluid saturation increases from arbitrary reversal point, ${}^{d}\overline{S}_{w}^{nw}$, to an apparently water saturated condition at zero capillary pressure yielding fraction of the overall maximum trappable saturation, ${}^{i}\overline{S}_{nr}^{nw}$, if the reversal point were from irreducible saturation, hence :

$$\overline{S}_{nr}^{nw} = \frac{1 - {}^{d}\overline{S}_{w}^{nw}}{1 + R_{nw}\left(1 - {}^{d}\overline{S}_{w}^{nw}\right)} \tag{2.6}$$

Where

$$R_{nw} = \frac{1}{i\overline{S}_{nr}^{nw}} - 1 \qquad \textbf{(2.7)}$$

Linear interpolation is introduced to predict entrapped non-wetting fluid at intermediary points between the two extreme bound set for the arbitrary scanning path from the reversal to the apparent saturated state according to:

$$\overline{S}_{nt}^{nw} = \overline{S}_{nr}^{nw}\left(\frac{\overline{\overline{S}}_{w}^{nw} - {}^{d}\overline{S}_{w}^{nw}}{1 - {}^{d}\overline{S}_{w}^{nw}}\right), \qquad \overline{\overline{S}}_{w}^{nw} > {}^{d}\overline{S}_{w}^{nw} \qquad \textbf{(2.8)}$$

Similarly, with equation (2.5)-(2.8), using the appropriate drainage scanning path expression for reversal from imbibition to drainage, the drainage scanning path could be predicted accordingly. Figure (2.2) illustrates the two-phase Parker and Lenhard [32, 54] model for a hypothetical soil.

Kaluarachchi and Parker [25] modified the Land [31] based procedure stated in (2.6) and (2.7) by assuming that the amount of trapped residual non-wetting fluid at the zero capillary pressure can be estimated as the difference between residual saturation for the actual scanning curve and that for a curve with a reversal point equal to the saturation on

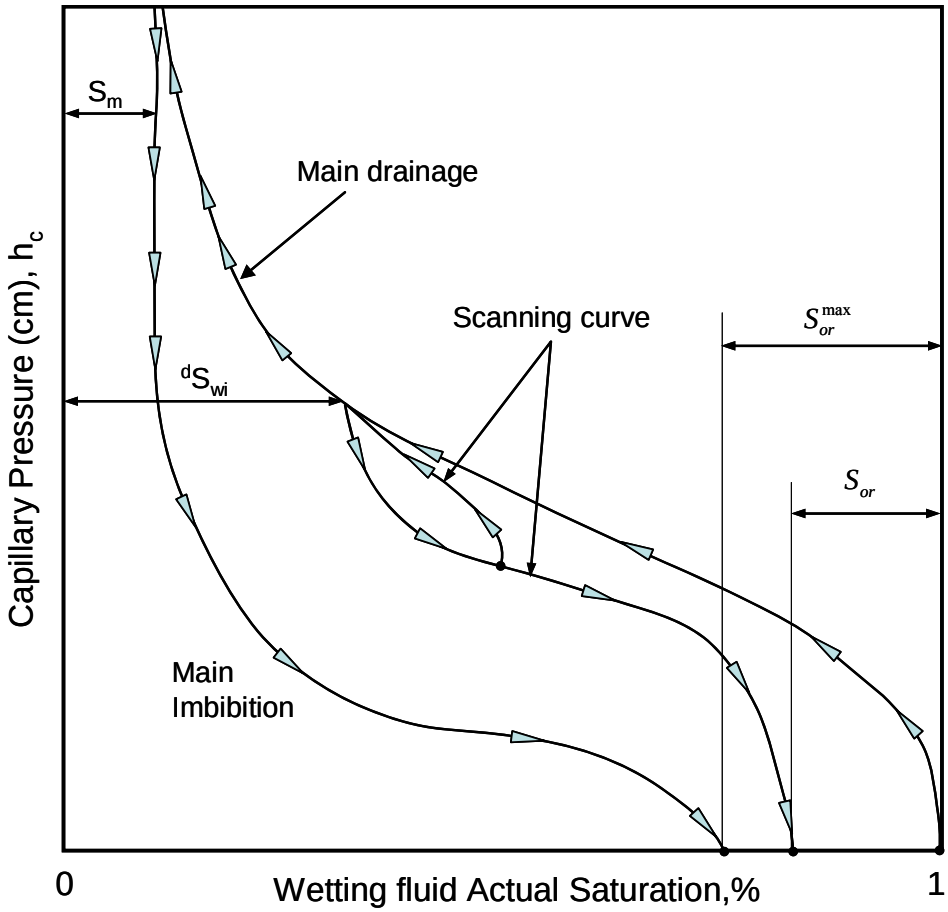

Figure 2.2: Lenhard and Parker Non-wetting Fluid Entrapment Model

the actual path. This approach introduces some sort of non-linearity in the Land's algorithm [31]

2.4 Mechanisms of LNAPL Entrapment in Porous Media

Capillary effects are essentially the key players in LNAPL entrapment processes. Lenhard *et al* [32] highlighted that fluid trapping occurs at zero capillary pressure during displacement by fluid of greater wettability to larger pore spaces where the fluids interface resides on the imbibition pathway. Whillhite [77] microscopically showed that the trapped non-wetting fluid becomes hydraulically isolated discontinuous or immobile pockets of blob or ganglion for a strongly water-wet medium. Non-wetting fluid entrapment process is widely reported in literature on microscopic scale, and it occurs via two key mechanisms namely: Snap-off and pass-by [44, 47, 48, 80].

2.4.1 Snap-off LNAPL Trapping Mechanism

Chatzis *et al* [10] experimentally found that snap-off trapping process is highly dependant on the magnitude of relative wettability of fluids, contact angles and pore geometry. Steffy *et al* [68] showed that this mechanism dominates LNAPL trapping process resulting from vertically rising water table in unconfined aquifers. Due to flow of invading wetting fluid through pores dominantly characterized by high aspect ratios i.e ratio of pore body to pore throat diameter, "snap-off" entrapment mechanism takes place most often [10, 75]. This implies that, as the LNAPL is displaced along the thicker pore body and relatively thinner pore throat, the LNAPL is forcibly "pinched" by the wetting

fluid while exiting the pore thereby leaving a blob of LNAPL disconnected and trapped in the pore body as shown in figure (2.3). This mechanism promotes the formation of singles isolated LNAPL blobs that are one or two bodies in size [10].

2.4.2 Pass-by LNAPL Trapping Mechanism

The pass-by entrapment mechanism occurs due to water preferential flow through a smaller pore rather than an adjacent larger one when LNAPL is displaced by water through two adjacent pathways as depicted also in figure (2.3). Displacement through small pores is faster than through the larger, and this renders the LNAPL contained in the larger pore to break away and become trapped as the water passes. Accordingly, the amount of LNAPL left in the larger pores become trapped creating large and complex blobs as the larger capillary in the small pore favorably draws in the imbibing wetting phase leaving the LNAPL in the larger pores [80]. Chatzis *et al* [10] noted that the total volume of LNAPL trapped in porous medium by this mechanism is usually larger than that of snap-off which ascertains Melrose and Brandner [44] previous report that blob due to bypass can reach up to 10 pore bodies in length.

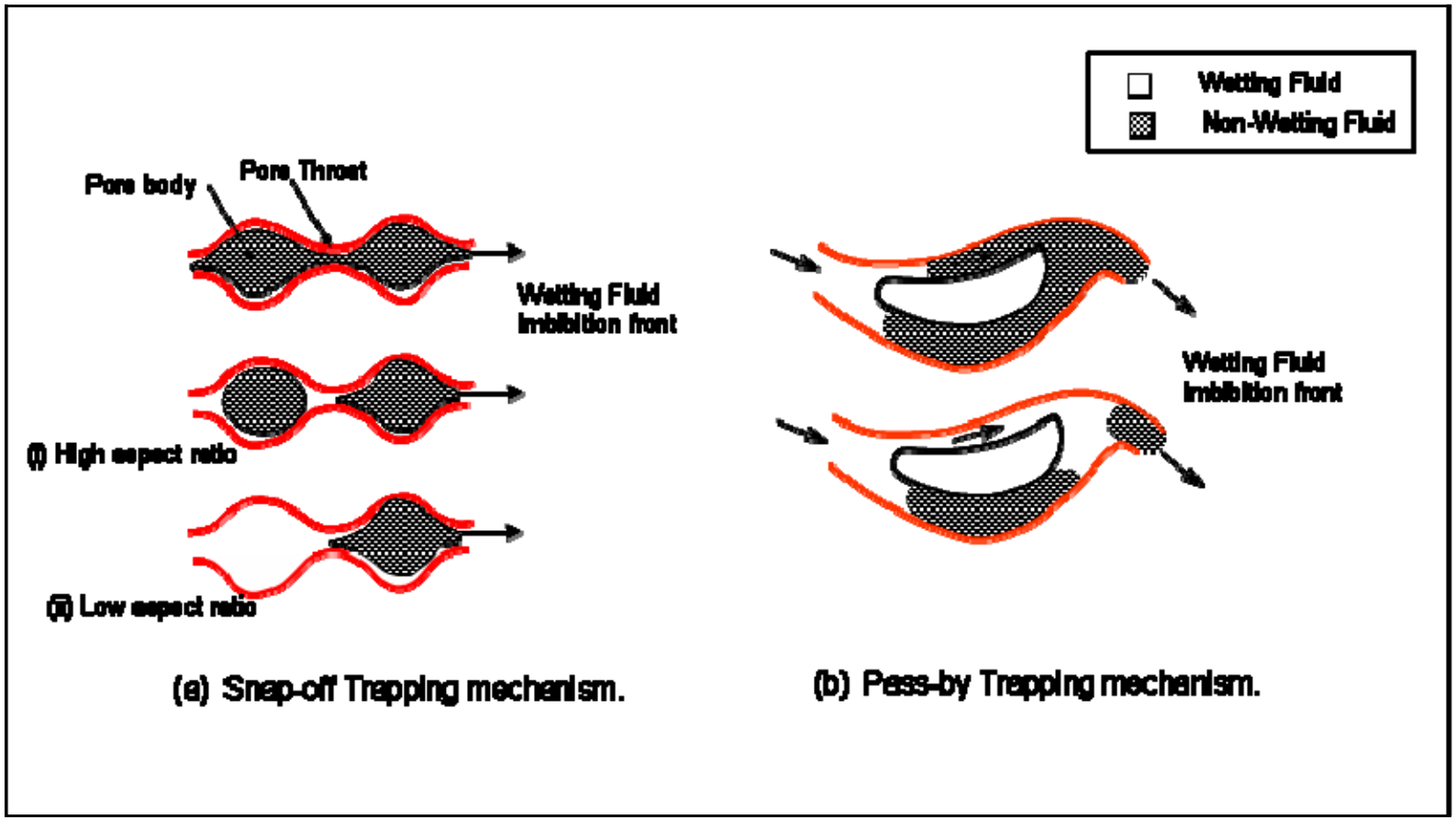

Figure 2.3: Mechanisms of LNAPL Entrapment in Porous Media [10]

2.5 Factors Influencing LNAPL Entrapment in Porous Media

Characterized by complex morphology, the magnitude of trapped non-wetting fluid distribution depends on (i) Degree of saturation, subsurface location and the geometry of the pore space; (ii) fluid-fluid properties such as interfacial tension, density contrast and viscosity ratio (iii) the properties affecting wetting behavior (iv) applied pressure gradient (v) gravity [49] and (vi) soil surface fluid wetting effects. For water-wet porous media, residual LNAPL saturation are relatively higher in two-phase than in three-phase system and may range between 15-50% in the saturated zone, doubling the amount in unsaturated zone as indicated by Mercer and Cohen [45]. They enumerated that these discrepancies could be due to:

1. Potential existence of LNAPL as wetting phase in presence of air resulting in residual held in smaller pores in the unsaturated zone
2. Existence of LNAPL as non-wetting fluid in the saturated zone that results in creating residual present as blob in larger pores
3. Relatively high LNAPL-air density ratio in the unsaturated zone resulting in higher LNAPL drainage flow.

Whillhite [77] offered comprehensive explanation of distinct behaviors of residual oil in initially water-wet cores from oil-wet cores owing to wettability alteration. A number of reports[32, 33] and groundwater contamination models [33, 49] as well categorically assumed water-wet aquifer condition due to some sort of similar reasons strengthened

with the established fact that subsurface region surrounding aquifer are naturally water-wet.

Capillary forces evolving from fluids phases' interfacial tensions and soil matrix wettability inversely varies with soil pore diameter. Wilson *et al* [80] and Powers *et al* [56] reported the effect of soil pore structure on entrapment of residual LNAPL blob. They discovered that residual blobs trapped in well graded soil media tend to occupy several pore bodies rather than single pore bodies. Consequently, soils with wide pore size or particle size distributions would attract a higher number of complex residual blobs spanning several pores whereas in more uniform soils, the majority of residual blobs are often singlet occupying a single pore body [10, 48, 56, 80]. The discrepancy is attributed to differences in capillary effects at pore level which is more pronounced in soil having wider variability and smaller particle sizes.

2.6 Physical Parameters Influencing LNAPL Entrapment

Various studies revealed that LNAPL entrapment processes during immiscible displacements in porous media are controlled by the relative magnitude of buoyancy, viscous and capillary forces [57, 58]. Classical investigations by researchers such as Morrow *et al* [46], Morrow and Songkran [49], Wilson *et al* [80], Melrose and Brandner [44] , Chatzis *et al* [10] and many others unanimously reported that during "stable" immiscible displacement that features dominant capillary trapping mechanism, capillary forces are main precursors of LNAPL trapping. Meanwhile, for vertical upward displacements, hydrodynamic viscous drag imposed by flow gradient and density contrast

forces (i.e. buoyancy forces) tends to overcome trapping. Most often, trapping analysis and mobilizing LNAPL residuals immensely refer to dimensionless parameters relating the influencing forces; namely, capillary number (N_c) and the bond number (N_B), defined as ratios of viscous pressure to capillary forces and gravity to capillary forces as stated in equation (2.9) and (2.10) respectively.

$$N_C = \frac{q\mu}{\sigma} \tag{2.9}$$

$$N_B = \frac{\Delta\rho R^2}{\sigma} \tag{2.10}$$

where q is the displacing (Darcy) fluid velocity, μ is the displacing fluid viscosity, σ is the interfacial tension, $\Delta\rho$ is the fluids density contrast, g is the acceleration due to gravity, and R is the average particle radius of the porous medium. It has been shown that above certain critical Capillary or Bond number capillary trapping of a non-wetting fluid does not occur, whereas below a certain combination of N_c and N_b, trapping is dominated by capillary forces [58]. For upward non-wetting fluid displacement, in lieu of dimensionless trapping number, T_r, Morrow and Songkran [49] amalgamated the effects of the two opposing forces in dimensionless group express as:

$$N_{CB} = N_C + k_{wf} A N_B \tag{2.11}$$

Where k_{wf} is the relative permeability of the wetting phase at the flood front, and A is a constant linking the intrinsic permeability, k, of a porous medium to its average particle radius, viz.,

$$k = AR^2 \quad \textbf{(2.12)}$$

Based on earlier work [51], an average relative permeability k_{wf} = 0.63 was assumed at residual LNAPL saturation for all sands. Boyd and Farley [4] defined a similar relationship called mobility number, N_{mo} expressed as ;

$$N_{mo} = (N_C + K_{rw} N_B)/\varepsilon \quad \textbf{(2.13)}$$

Where ε is the medium porosity. In-addition to aforementioned reasons related to Mercer and Cohen [45], the smaller buoyancy force and the characteristics higher capillary force in an LNAPL-water system as compared to three-phase air-water-LNAPL system are additional explanations to greater LNAPL residual and entrapment saturations in the two-phase system [68, 79]. For water-wet porous media, Steffy *el al* [68] reported that at low N_C where buoyancy forces are no longer negligible, the antecedent moisture content control LNAPL entrapment as displacement of the LNAPL due to viscous drag is non-existing. Explicitly, laboratory studies conducted by Lenormand and Zarcoe [38], Jernauld and Salter [24] and Wilson *et al* [80] indicated that during re-mobilizing trapped residual LNAPL blob, displacement by viscous drag occurs in sands when the N_C is greater than 10^{-3} , 10^{-5} and $2x10^{-5}$ respectively. Data from upward vertical hydraulic flushing at various displacement velocities of uniform silica sand initially fully saturated with soltrol-22

secured by Ratnam *et al* [57, 58] using centrifuge modeling technique clearly showed that at higher values of N_{CB}, tremendous reduction in the proportion of LNAPL trapped in the sand pores is achievable before the residual saturation steadied. The authors indicated that the experimental flows were under stable conditions. On whole, their finding evidently strengthens the idea presented by Morrow and Songkran [49].

2.7 Two-Phase Immiscible Flow Instability Effect and Criterion

Multiphase instability at initial sharp wetting front during immiscible displacement was originally treated vastly in the oil industry [62]. However, the occurrence of unstable flow during water and NAPL infiltration into the subsurface has recently been studied in the hydrology community to handle problems of preferential recharging and contamination of groundwater [19, 29, 59]. Habitually, groundwater flow study is to macro-scale; in contrast, flow instability is observable at pore network scale that exposes flow front's variation in space and time at micro-scale. Saffman and Taylor [62] and Chuoke *et al*. [11] open up studies established that, for viscosity ratio of fluids in two-phase system exceeding unity, displacement velocities higher than gravity drainage of the displaced fluid is liable to create perturbations at fluid-fluid interface leading to flow front instability. It surfaces when displacement of higher viscous fluid by a less viscous one leads to randomness at the micro-scale referred to as "viscous fingering" [11]. The phenomenon of viscous fingering can be explained as the wide variability in easiness with which the wetting front passes the divergent permabilities of irregular-shape and size-pore pathways between the interconnected medium matrix, thereby rendering the wetting front

tips to vary in size and position. However, Kueper and Frind [29] distinctly, regarded fingering as unstable flow caused by density and/or viscosity contrast and channeling as unstable flow caused by macroscopic heterogeneities. In both cases, Whillhite [77] indicated that the result is wetting fluid front bypassing preferential pathways. Confined to upward displacement of oil by water, Chuoke *et al* [11] experimentally proved that unstable flow impends once the magnitude of the wetting fluid front velocity, q, surpasses the difference between the flow critical velocity, V_{crit} (driven by gravity and viscous forces) and the capillary and viscous driving velocity, V_{cap}.

$$V_{crit} = \frac{|\rho_{w} - \rho_{nw}|}{|\mu_{w} - \mu_{nw}|} g k_{eff} |\cos\beta| \qquad \textbf{(2.14)}$$

$$V_{cap} = \frac{|\sigma^{*}|}{|\mu_{w} - \mu_{nw}|} k_{eff} \alpha^{2} \qquad \textbf{(2.15)}$$

Where w, nw denote wetting and non-wetting fluid respectively. $\rho, \mu, k_{eff}, \sigma^{*}, \alpha$ and β are the density, viscosity, effective permeability, wetting front perturbation, effective interfacial tension and angle between gravity and flow direction respectively. Zhi Feyan *et al* [81] comprehensively reviewed this complex instability criterion for all immiscible displacement set-ups, but, the criterion for the peculiar case stated above was simplified by Whillhite [77] for upward displacement in water-wet media as;

$$q > \frac{kg\left(\rho_{nw} - \rho_{w}\right)}{\left(\mu_{nw} - \mu_{w}\right)} \qquad \textbf{(2.16)}$$

CHAPTER 3

Experimental Design and Laboratory column tests

Laboratory column tests are popular in simulating different LNAPL contamination scenarios. The simplicity of the test and the feasibility in reflecting actual situation encountered during subsurface contamination in field sites made it widely attractive. The method is invariably employed in many situations by researchers to help analyze and comprehend nature of simulated contamination problem under investigation in order to reach appropriate solution formulation.

The main objective of this part of the work is to generate experimental data to be used in order to achieve the overall objectives of the study. As usual, laboratory column displacement tests are conducted to simulate interaction between water table and LNAPL present within the vicinity of the capillary fringe and water table of an unconfined aquifer following an LNAPL contamination event. The tests considered only single upward LNAPL displacement imposed by a rising water table and its subsequent entrapment below the raised water table after attainment of quasi-hydrostatic conditions. Furthermore, it is designed to ensure that only two-phase LNAPL-water fluid flow was encountered throughout. All necessary precautions were taken to eliminate air particles as much as possible within the flow regime. Presence of significant air pockets would transform the system into a more complex three-phase system which would undermine the main goal of the investigation.

Experimental materials obtained locally are used for the entire work. The LNAPL used was thick petroleum hydrocarbon, a Saudi Arabian light crude oil. Meanwhile, two unconsolidated porous media possessing great differences in physical and hydraulic characteristics represented the sandy aquifer materials. Detailed description of the materials, experimental set-up and procedure are enumerate and vividly elaborated below.

3.1 Experimental Set-up

The experimental set-up used for the column tests, illustrated in figure (3.1), consisted mainly of a long graduated cylindrical column, two liquid reservoirs and a reversible Masterflux® solid state liquid speed pump and controller.

The designed long column and the two reservoirs were fabricated at the KFUPM central workshop. The column was 100 cm in height and 0.25 inch thick graduated Plexiglas® material having measured internal diameter of 9 cm firmly fixed on a 0.5 cm thick wider rectangular base plate. Designed to accommodate the porous media, the column was provided with circular ring possessing circular central mesh screen located at 15 cm and45 cm measured from the column base to keep exactly 30 cm height of sand firmly in place and to allow free flow of fluid during water table movement. The rational behind this design was to firmly constrain the sand column in order to suppress variability in porosity while flow is taking place through the test column. Two circular ports, each measuring 0.5 cm in diameter, one located at about 20 cm from the base of the column and the other at the column base were connected via hose pipes to 10 cm diameter graduated Plexiglas® cylinder and 25x25x25 cm^3 Plexiglas® cubic box, that functioned as the LNAPL and

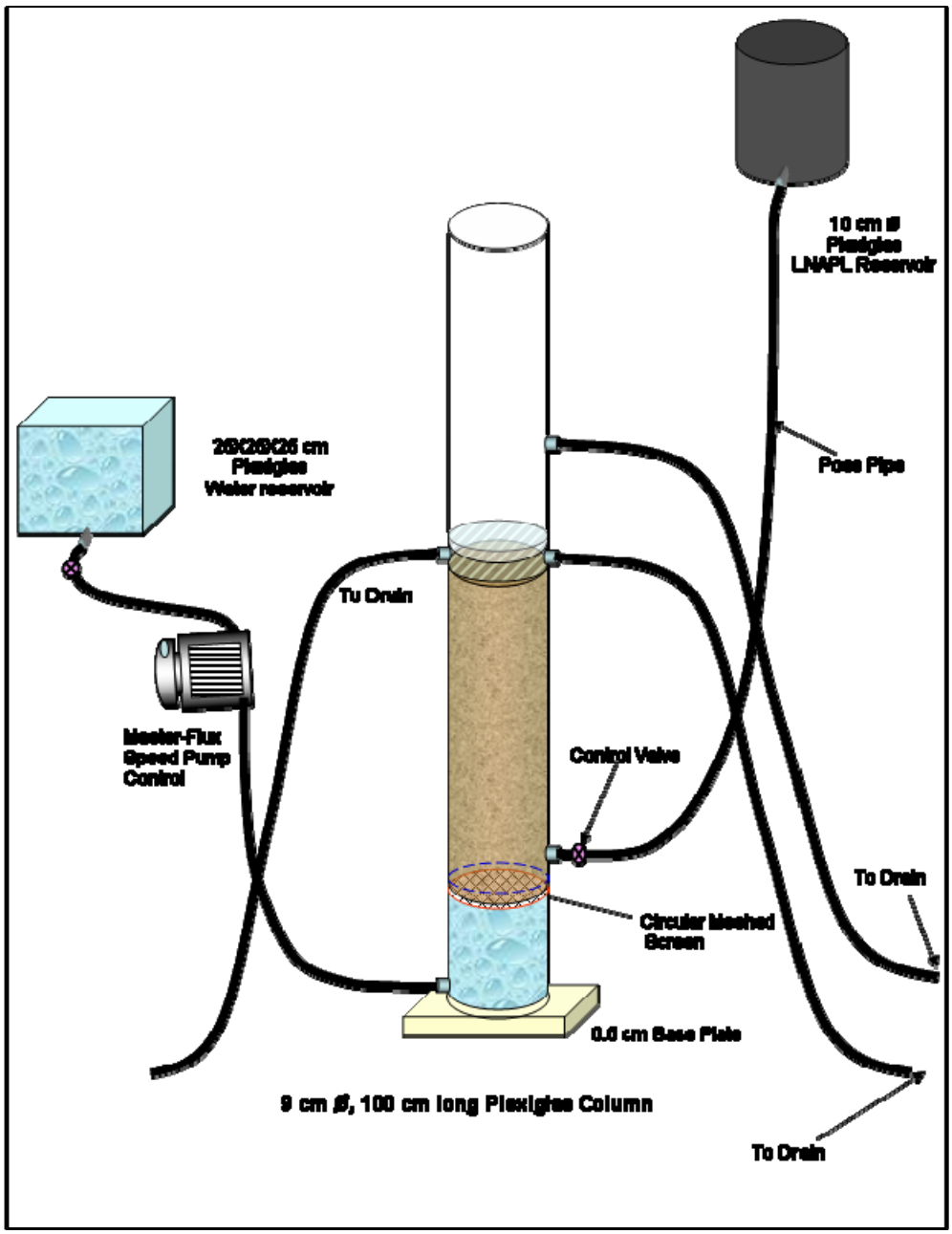

Figure 3.1: Experimental Set-up

water reservoirs respectively.

Elevation and rate of the water table movement within the column was control by the Masterflux® speed pump that draws water from the water reservoir directly into the column through the lower port at the column base. The other port functioned as inlet for injecting the LNAPL into the medium from the LNAPL reservoir. This method was adopted so as to permit exit of air particles as the water or LNAPL enters into the medium so as to avoid their entrapment if the oil were spilled from top instead

3.2 Experimental Materials

The experimental materials consist of two types of sandy porous media and two liquid fluids with details as furnished in the subsections below.

3.2.1 Porous Media

The two types of unconsolidated porous media used for the experiments were carefully selected in order to cover the behavior of LNAPL entrapment in porous medium possessing wide range of grain sizes and as well in porous medium that has narrow pore sizes. The uniform porous medium was local sandy material collected from KFUPM beach at the outskirt of Aziziyah area in the Eastern province of Saudi Arabia possessing the particle sizes distribution shown in figure (3.2). According to the Unified Soil Classification System (USGS), its grain size breakdown shows that it was mainly coarse sand particles which constitute about 94.64% retained on sieve # 30 by weight of a sample volume, while the remaining meager proportion splits into 5.3 % medium sand and 0.08

% fine sand particles. It is characterized by undisturbed and compacted dry density of 1.75 and 1.85 g/cm3 respectively, and porosity of 0.36. The effective grain size (D_{10}), uniformity coefficient (C_u) and Coefficient of curvature (C_c) was 0.65mm, 2, and 0.76 respectively, and hence is classified as a poorly graded soil. In contrast, the well-graded sand was formed by blending three different soils having contrasting particle size distribution. It was comprised of the uniform sand as described above combined with a very fine local uniform sand obtained from KFUPM beach and a soil retained on sieve# 200 from mechanical sieve analysis, all blended together at pre-determined ratio of 1: 1.5 : 1 respectively to give the intended soil characteristics. The resulting blended soil covers a wide range of particle sizes among which about 20 % by weight was between very fine and fine sand particle size range. Also as shown in Figure(3.2) , from the particle size distribution and soil analysis undertaken at KFUPM soil laboratory, the formed sand could be described by; effective grain size (D_{10}), uniformity coefficient (C_u) and coefficient of curvature (C_c) of 0.14mm, 6, and 1.24 respectively according to USGS, thus is classified as well-graded soil. The undisturbed and compacted dry density and the porosity are 1.75 and 2.05 g/cm^3 and 0.288 respectively.

3.2.2 Liquids

The wetting fluid used is KFUPM laboratory tap water at 25 ^{0}C, the prevailing experimental room temperature. While Saudi Arabian crude oil from ARAMCO was the non-wetting fluid. As determined at KFUPM petroleum engineering fluid properties

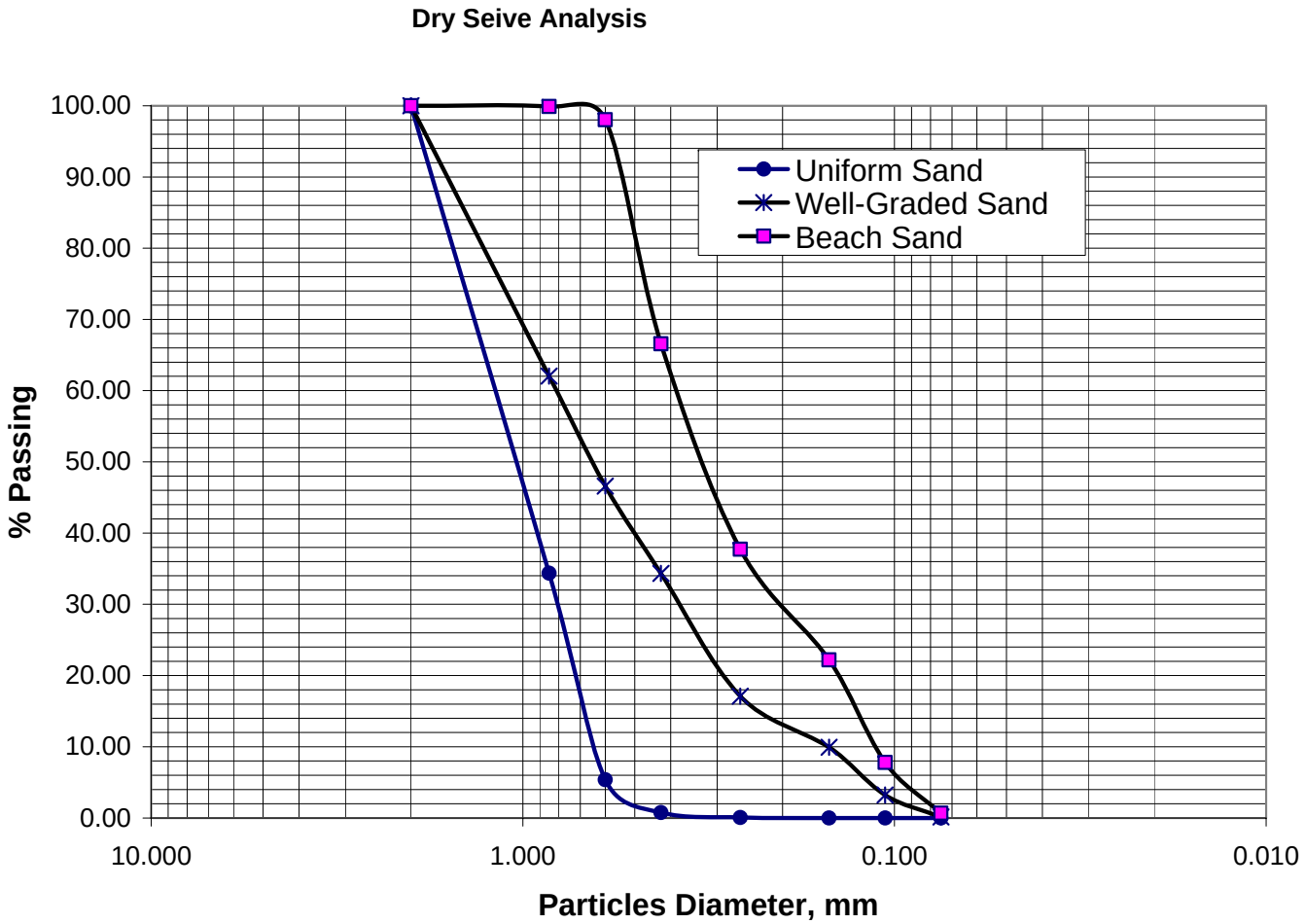

Figure 3.2: Particle Size Distribution of the Porous Media

laboratory using Hydrometer method, it is characterized by a specific gravity, density and API gravity of 0.876, 0.8732 g/cm^3 and 29.36 respectively, thus it is a typical light non-aqueous phase liquid (LNAPL). The viscosity, oil-water interfacial, oil-air and water-air surface tensions were also measured as 18.077 centipoises, 23 dynes/cm, 26 dynes/cm and 70.5 dynes/cm respectively. The viscosity was determined using Oswald viscometer while the interfacial tensions were measured with tensiometer that was calibrated with Benzene. All the measurements of the oil properties were consistently made at 25 ^{0}C.

3.3 Experimental Methodology

In order to achieve greater efficiency in data acquisition, the experimental program was designed to be executed according to three planned separate phases as designated below and elaborated in details in the subsections that follow.

- Phase I Laboratory Column Tests (LCT1); for Preliminary investigation.
- Phase II Laboratory Column Tests (LCT2); for uniform sand experiment.
- Phase III Laboratory Column Tests (LCT3); for well-graded sand experiment.

The experimental design is summarized in Table (3.1) with details given in the following sub-sections.

3.3.1 Phase I Laboratory Column Tests (LCT1)

Preliminary investigation was aimed at designing the framework within which the actual experiment in phase II and phase III were carried-out more efficiently. The wetting fluid

displacement velocities to be used in the other two main phases that satisfy the following experimental conditions were selected:

- Two bounds- upper and lower limits- for the water table rise rates that stroke balance between operational limitations of pump and avoidance of disturbances within the packed soils in the test section while flow takes place.
- The flow is kept at laminar state with Reynolds's numbers within the range of Darcy's law.

Results from this phase showed that for the uniform sand, the controlled water table should maintain a measured rise of 30 cm with average time scale of 42 seconds and 55 minutes yielding operating average minimum and maximum flow rates of 9.1×10^{-5} and 7.14×10^{-3} m/sec respectively. The minimum flow corresponds to the smallest capillary number of 5.69×10^{-5} recorded. However, the well-graded sand matrix renders the flow to be very difficult and much slower both at high and low pump speeds. Therefore, much lower and narrower average flow velocities were set ranging between 4.60×10^{-5} and 3.3×10^{-3} m/sec for time scale of 1.8 hours and 91 seconds respectively. In this case, the smallest capillary number observed was 2.87×10^{-5}. Moreover, the LNAPL height in centimeters (cm) measured in the LNAPL reservoir required to give 0, 20, 30, 42, 60 and 71% initial water saturations were determined for both the two porous media.

Table 3.1: Experimental Design

Test	No of Tests undertaken	Entrapment influencing factors		Packing uniformity
		Water Table rise rate	Initial water saturation	
LCT1	Several Tests	Setting water rise rate range that strike balance between 1. Operational Limitation of the pumping system 2. Avoidance of disturbances in soil 3. Limiting flow between laminar flow bound by setting low Reynolds's number < 10	Setting Volume in cm. of LNAPL in reservoir for various initial Water Saturation	Maximum density packing in test column with mixing as below.
LCT2	More than 80 Tests	•9.1 x 10^{-4} - 7.14 x 10^{-3} m/sec •Maximum Reynolds number=4.6 •Min. capillary number of 5.69 x 10^{-} •Bond number of 1.65	•690, 544, 491, 398, 278 and 199 ml •0, 20, 30, 42, 60 and 71%	Natural
LCT3	More than 80 Tests	•4.60 x 10^{-4} - 3.3 x 10^{-3} m/sec •Maximum Reynolds number=4.61 •Min. capillary number 2.87x10^{-3} •Bond number 0.08	•550, 408, 353, 236, 196 and 117 ml •0, 20, 30, 42, 60 and 71%	Consistently blending 500, 750 and 500 cm^3 of the composite soils for each test run

3.3.2 Experimental Procedure

Initially, the first step in the proposed experimental procedure was to add the porous material gradually into the long column test section already containing de-aired water while concurrently stirring thoroughly in order to homogenize the parking and also to dislodge any air bubble that might be trapped. Implementing this first step proved unfeasible due to flow difficulty encountered as a result of high medium compaction, particularly in the case of the well-graded sand. Alternatively, the same de-aired water saturated medium condition was achieved for the finally implemented procedure, however, by carefully allowing uniformity of packing without any mixing. Thus, the packing that produces maximum medium porosity was adopted. In this regard, the sand medium is at first carefully packed uniformly in the test section through a mesh placed on top of the column and then adequately tightened within the upper and lower protection mesh screens. Sufficient de-aired water is then vertically passed through until the packed sand becomes fully saturated. The slowly rising water level is further allowed to appear far above the top screen until all the air bubbles are eliminated. Afterwards, the water level is then drawn back exactly to the level of the top mesh and the system is allowed to equilibrate. Consequently, the initial condition is water saturated sand. Precise volume of LNAPL as determined in the preliminary investigation is then gradually and carefully injected from the LNAPL reservoir into the water saturated medium by gravity flow. As the LNAPL enters, it displaces the water, draining it to occupy some of the pore spaces. The displaced water is allowed to escape the test column via two exit ports provided on

the column wall directly at the top of the upper mesh screen. The injected LNAPL is allowed to be uniformly distributed throughout the medium. This is opted for in order to permit investigating only effects of the rate of the water table rise on LNAPL entrapment without causing smearing effects which would inevitably occur if the LNAPL distribution were otherwise

One hour later, when the injected LNAPL within the test section became approximately uniformly distributed, the test section is assumed to have attained equilibrium. The porous material is now subjected to two-phase water-LNAPL saturated condition. The water table rise is simulated at a given pre-set constant rate controlled by the Master flux speed pump. Substantial height is allowed to be covered by the rising water level, permitting fluid level to be about 30 cm high above the top mesh. The disturbed sand is left for about 24 hours to reach equilibrium in order to allow total displacement of the mobile component of the LNAPL free-phase and entrapment of the remaining portion. The thickness of the floating LNAPL that clearly appears on top of water above the test section is measured to ascertain the total displaced amount. A volume balance is finally performed for the test run, by noting the difference between pre-flow injected volume and the post-test displaced volume, from which the entrapped saturation in the porous medium could be determined.

At end of each test, the column is emptied and thoroughly cleaned-off from the packed soil, water and oily substances within it to prepare for next test. For each individual test run the same procedure described above was strictly adhered to using fresh sand sample and with varying major parameters of interest.

3.3.3 Phase II Laboratory Column Tests (LCT2)

This second phase of the work proved to be somewhat easier compared to the third phase due to the natural homogeneity of the uniform sand, principally, with regard to difficulty in approximately maintaining packing uniformity. More than eighty (80) successful displacement tests were performed, consisting of some duplicates or even triplicates tests for a single data point to gain increased data credibility. Going by the pre-determined timing scale range covering the test section, seven steady flow rates used are; 0.0911, 0.404, 1.55, 2.47, 3.67, 5.74 and 7.09 x 10^{-3} m/s. Meanwhile, 690, 544, 491, 398, 278 and 199 ml of LNAPL as determined in phase I, corresponding to 0, 20, 30, 42, 60, and 71% initial water saturation prior to when the water table movement is initiated were considered for injection from the LNAPL reservoir. It should be noted here that for the zero initial water saturation, the porous medium was set at initial fully LNAPL saturated condition, hence, at LNAPL-wet condition which differs from the remaining ones that were at water-wet initial condition. Maximum Reynolds number calculated which corresponds to the maximum rise velocity observed was 4.6, which is less than the Darcy's law validity limit of 10.

3.3.4 Phase III laboratory Column Tests (LCT3)

In contrast to the second phase experiments, intricacy of ensuring medium homogeneity in this phase was overcome by consistently blending the three soils that make up the well-graded sand according to the pre-determined stated ratio for each test run. That was achieved by batch blending of 500, 750 and 500 cm^3 volumes of the three composite

sands respectively, to obtain slightly below the quantity of the well-graded sand required to fill the test section.

Similarly, more than eighty (80) successful displacement tests were undertaken, consisting of some duplicates or triplicates tests, also in order to gain increase data points' credibility. In this phase, the maximum Reynolds's number was also 4.61, while the seven steady flow rates used to simulate the water table rise velocity have average values of 0.046, 0.090, 0.61, 0.95, 1.7, 2.5 and 3.3 x 10^{-3} m/s. Similarly, 550, 408, 353, 236, 196 and 117 ml volume of LNAPL that also correspond to 0, 20, 30, 42, 60, and 71% initial water saturation respectively were injected from the reservoir in order to form the two phase water-LNAPL contaminated porous medium as well.

CHAPTER 4

Experimental Results and Discussions

Laboratory column tests performed on the two porous media were aimed to experimentally investigate the effects of initial water saturation and rate of water table rise on LNAPL entrapment. The tests were conducted during each phase of the experimental program while the variability in soils and the LNAPL properties were minimized. Moreover, due to steadiness and relative low room temperature and low solubility of the crude oil in water, the effect of LNAPL dissolution in water was also ignored. The tests were carried-out in accordance with three pre-designed experimental phases designated as LCT1, LCT2 and LCT3. The outcomes from these individual phases are presented and discussed in the following sections.

4.1 Preliminary Investigation (LCT1)

This phase of the study that entails series of column tests on both initially saturated uniform and well-graded sands was very essential in designing and undertaking the actual tests runs performed in LCT2 and LCT3 for the two sands respectively. Result from this phase as detailed earlier underscores the role preliminary study plays, particularly in laboratory column studies.

4.2 Uniform Sand Laboratory Column Tests (LCT2)

More than eighty (80) two-phase water-LNAPL displacement tests were carried-out at varying initial water saturation and rate of water table rise with minimum capillary number of 6.03×10^{-5} and approximated constant bond number of 1.65 in this phase. Mostly, each data point tabulated for analysis is an average of the closest two values recorded during the experiment runs. The summarized results are given in Table (4.1). As the effect of water table rise rate is found to greatly differ for the different state of initial moisture condition investigated i.e. water-wet and LNAPL-wet porous media, the results for two situations are enumerated and independently discussed below.

4.2.1 Effect of Rate of Water Table Rise for Water-wet Uniform Sand

Figure (4.1) displays the effect of changing the rate of water table rise on the LNAPL entrapment amount for initially water-wet saturated uniform sand. Apparently, for all the cases of the initial water saturation values, most of the trends show that an increase in rate of water table rise will result in increase in amount of trapped LNAPL saturation with maximum and minimum overall trapped LNAPL saturation of 37.3% and 1.5%. Moreover, water table rise rates above 3.67E-03 m/sec appear to have insignificantly affected the entrapment amount, unanimously, revealing that maximum trappable LNAPL saturation has been attained in all the cases. However, marked differences are observable at the highest and lowest initial water content. At the lowest initial water

Table 4.1: Summary of Experimental Data for Uniform Sand

Test Run	Rate of WT Rise m/sec	Reynolds's No.	Capillary's No.	LNAPL Trapped Volume, cm^3		
				LNAPL Injected = 690 cm^3 Initial water saturation= 0%	LNAPL Injected = 544 cm^3 Initial water saturation= 20%	LNAPL Injected = 491 cm^3 Initial water saturation = 30%
1	9.11E-05	0.059	5.36E-05	200.384	194.021	33.070
2	4.04E-04	0.258	2.83E-04	232.196	194.021	45.795
3	1.55E-03	0.968	1.06E-03	213.109	213.109	58.520
4	2.47E-03	1.663	1.60E-03	194.021	200.384	58.520
5	3.67E-03	2.527	2.46E-03	155.846	257.647	122.145
6	5.74E-03	3.475	3.74E-03	92.220	251.284	122.145
7	7.09E-03	4.634	4.45E-03	98.583	251.284	122.145
				LNAPL Injected = 398 m^3 Initial water saturation = 42%	LNAPL Injected = 279 cm^3 Initial water saturation = 60%	LNAPL Injected =199 cm^3 Initial water saturation = 71%
1	9.11E-05	0.059	5.36E-05	10.133	56.085	78.236
2	4.04E-04	0.258	2.83E-04	41.946	87.897	90.961
3	1.55E-03	0.968	1.06E-03	92.846	126.073	97.323
4	2.47E-03	1.663	1.60E-03	99.209	126.073	90.961
5	3.67E-03	2.527	2.46E-03	99.209	157.886	116.411
6	5.74E-03	3.475	3.74E-03	92.846	157.886	103.686
7	7.09E-03	4.634	4.45E-03	111.934	151.523	103.686

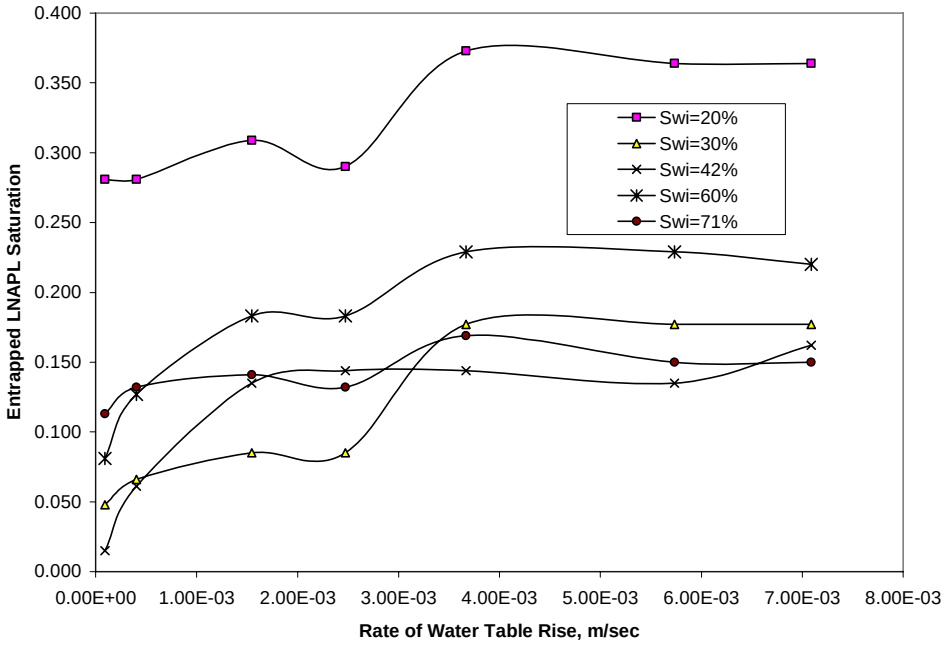

Figure 4.1: Effect of Rate of Water Table Rise for Water-wet LCT2

saturation (i.e.20%), the figure indicates that when the rate of the water table rise is above 4.00E-03 m/sec, the trapped saturation is fairly constant; but can be assumed to vary linearly at lower rates. In case of the highest initial water saturation (i.e. 71%), the trapped saturation ranges between 11.3%-15%, indicating the mild influence of the rate of the water table rise on the trapped LNAPL. This could be attributed to small quantity of the LNAPL present prior to raising the water table.

For some lower varying rate of water rise range at 30%, 42% and 60% initial water saturation, the trapped LNAPL amount was less compared to that at initial LNAPL saturation of 71%. Moreover, it could also be observed that the rise rate ranges decreases with increase in the affected initial water contents. This observation may be attributed to the fact that at 71% initial water saturation, only fewer pore spaces were occupied by the isolated pockets of oil blobs. By that means, the imbibing water preferentially flows through the abundant several pores filled by water as the isolated LNAPLs are difficult of be displaced, and hence leaving behind the LNAPL which was mostly trapped regardless of the displacement rate. Similar trends are portrayed for the overall observations at initial water content of 30% and 42% when compared to LNAPL entrapment saturation at 60%. To some extent, similar explanation could be extended to this observation as well.

4.2.2 Effect of Rate of Water Table Rise for LNAPL-wet Uniform Sand

As displayed in figure (4.2), when the soil was initially LNAPL-wet, the effect of variation of flow velocity on the LNAPL entrapment pattern opposes the previously displayed trend for the water-wet initial condition. Noticeably, it shows that LNAPL

trapped saturation linearly decreases with rate of the water table rise. The maximum trapped saturation of 33.6% was below that observed in the water-wetted condition at 20% initial water saturation that is much closer to the LNAPL-wet condition. It is clear from the figure that the lowest value of 13.4% recorded for this situation considerably narrows the overall trapped saturation range.

4.2.3 Effects of Initial Water Content on LNAPL Entrapment

The trapped LNAPL saturations are plotted against the initial water saturation as shown in figure (4.3). Generally, at fixed water table rise rates the trapped LNAPL saturation shows a fluctuating trend. For clarity, figure (4.3.) is split into figure (4.4) and figure (4.5) considering higher and lower rise rates respectively. Figure (4.4) clearly shows that for lower water table rise rates up to 2.47E-03 m/sec, for transition from 0% to 20% initial water saturation, the entrapment saturation is constant at a given rate of water table rise; whereas, figure (4.5) reveals that for higher rate, there is sharp increase in the entrapment saturation. However, above the 20% initial water saturation, both the two figures show analogous fluctuating patterns at the various rise rates, with least trapped LNAPL saturation between initial water saturation between 40%-50%. While the highest trapped saturation for the lower and higher rise rates occurred at 0% and 20% respectively. The maximum trapped LNAPL at initial water saturation of 20%, 30%, 42%, 60% and 71% are 37.3%, 17.7%, 16.2%, 22.9% and 15% respectively all observable at the highest water rise rate. For the higher rise rates, change in the rate of water table rise seems to have insignificant effects on the entrapment amount, particularly at initial water saturation

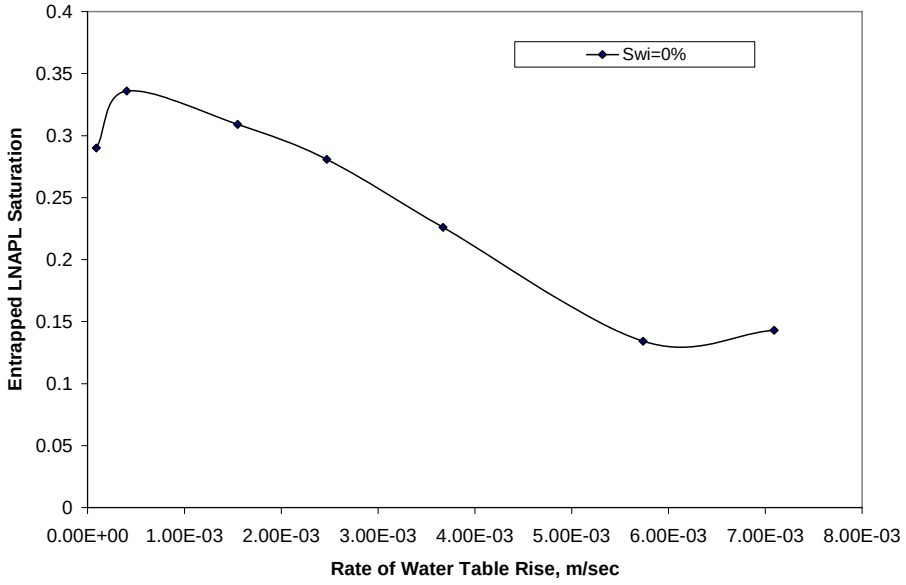

Figure 4.2: Effect of Rate of Water Table Rise for LNAPL-wet LCT2

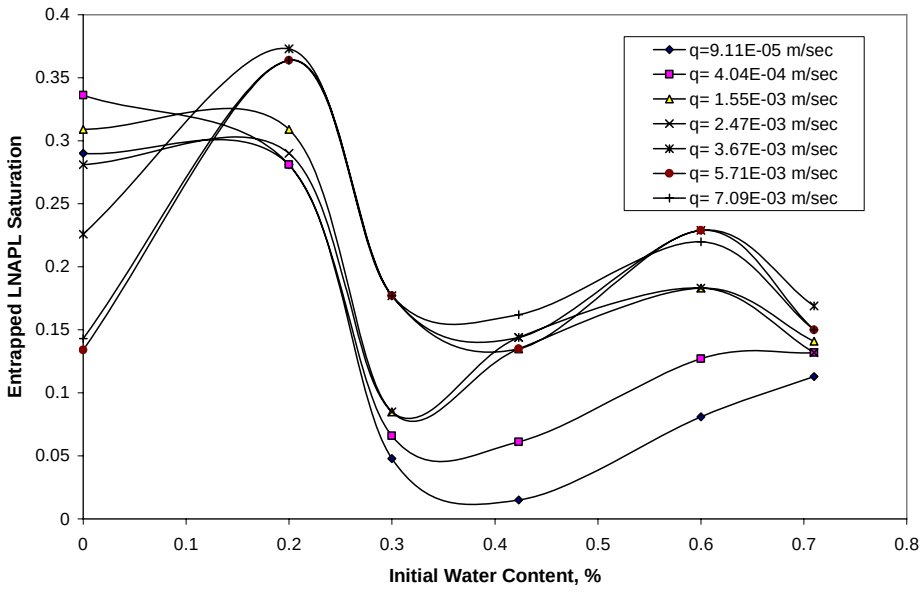

Figure 4.3: Effect of Initial Water Content at Various Rate of Water Table Rise for LCT2

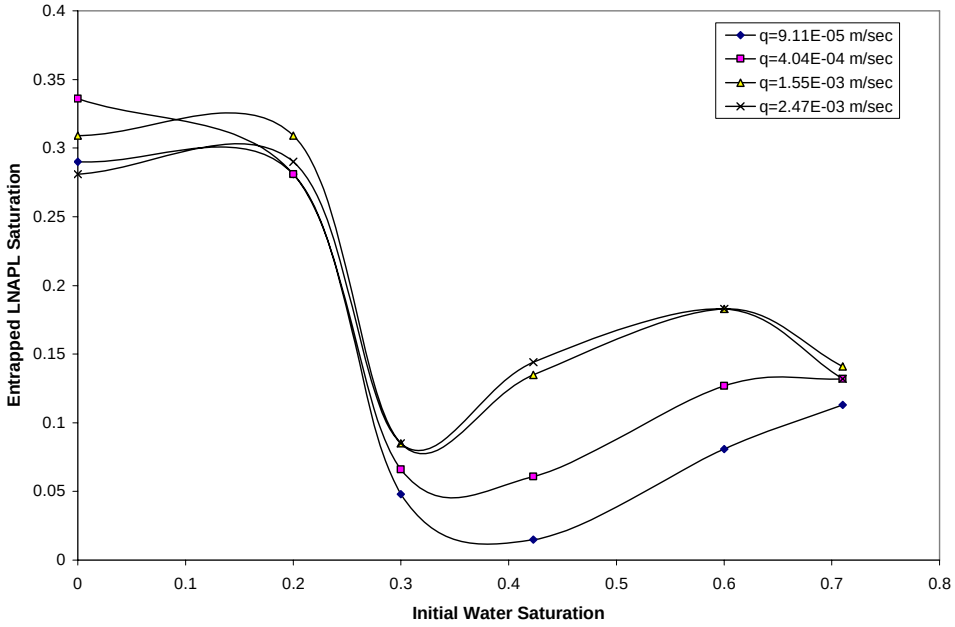

Figure 4.4: Effect of Initial Water Content at Lower Rate of Water Table Rise for LCT2

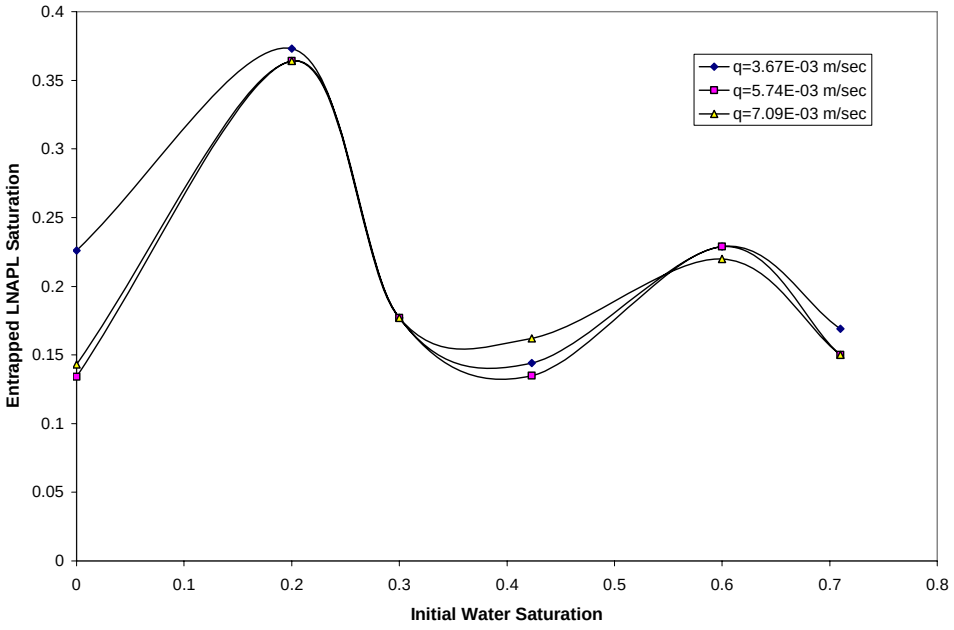

Figure 4.5: Effects of Initial Water Content at Higher Rate of Water Table Rise for LCT2

above 20%.

4.3 Well-graded Sand Laboratory Column Tests (LCT3)

Similarly, more than eighty (80) column displacement tests were carried-out and the data tabulated for analysis using method as described in LCT2. The minimum attainable capillary number here was 2.87 x 10^{-5}, while the bond number was approximated as 0.08. The results are summarized in Table (4.2) and depicted graphically and discussed in sections below.

4.3.1 Effects of Rate of Water Table Rise for Water-wet Well-graded Sand

The effect of rate of water table rise on the LNAPL entrapment saturation shown in figure (4.6) seems to be the same as that of uniform sand for the water-wetted initial condition. While, increase in rate of the water table rise also trapped more LNAPL as in case of the LCT2, there is no attainment of steady entrapment saturation observed in the former case-even as the experimented rise velocities were already stretched for the entire initial water content range. Also the rate at which the trapped LNAPL increases with the rate of the water table rise is much lower than in the case of the uniform sand. The maximum LNAPL trapped saturation of 37% observed at initial water saturation of 20% corresponds to the highest rise velocity of 3.3E-03 m/sec. This observed maximum trapped saturation was the same as that of the uniform sand which was 37.3%, also at very close rise rate of 3.67E-03 m/sec with the exception that this value fairly stabilizes with rise rate till

Table 4.2: Summary of Experimental Data for Well-graded Sand

Test Run	Rate of WT Rise m/sec	Reynolds's No	Capillary's No.	LNAPL Trapped Volume, cm^3		
				LNAPL Injected = 550 cm^3 Initial Water Content = 0%	LNAPL Injected = 433 cm^3 Initial Water Content = 20%	LNAPL Injected = 395 cm^3 Initial Water Content = 30%
1	2.3E-05	0.003	2.87E-05	206.250	143.550	113.131
2	4.6E-05	0.006	5.61E-05	199.650	162.800	120.412
3	6.1E-04	0.085	3.80E-04	193.600	172.150	127.692
4	9.5E-4	0.133	5.92E-04	193.050	188.100	155.415
5	1.7E-03	0.238	1.06E-03	187.000	198.000	169.417
6	2.5E-03	0.349	1.56E-03	176.550	195.800	172.497
7	3.3E-03	0.461	2.06E-03	154.550	203.500	170.638
				LNAPL Injected = 317 cm^3 Initial Water Content = 42%	LNAPL Injected = 221 cm^3 Initial Water Content = 60%	LNAPL Injected =158 cm^3 Initial Water Content= 71%
1	2.3E-05	0.003	2.87E-05	104.013	98.964	83.600
2	4.6E-05	0.006	5.61E-05	111.794	115.512	86.900
3	6.1E-04	0.085	3.80E-04	118.584	127.095	87.175
4	9.5E-04	0.133	5.92E-04	127.844	134.795	88.000
5	1.7E-03	0.238	1.06E-03	131.528	146.314	99.550
6	2.5E-03	0.349	1.56E-03	142.657	151.788	98.450
7	3.3E-03	0.461	2.06E-03	146.925	154.015	107.800

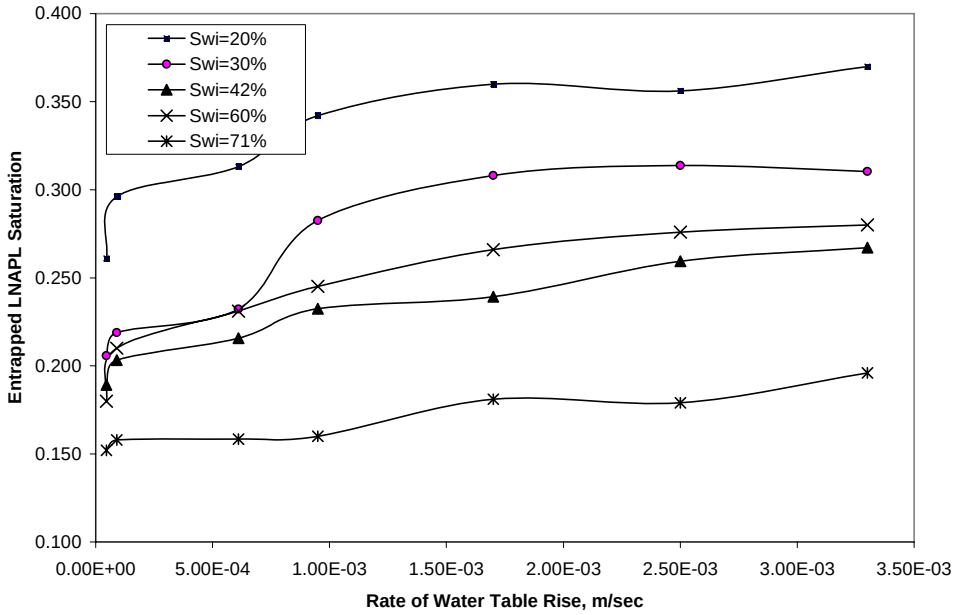

Figure 4.6: Effect of Water Table Rise at Various Initial Water Saturations for LCT3

7.10E-03 m/sec. In contrast, the maximum LNAPL entrapment saturation at 30%, 42% and 60% initial water content corresponding to the highest rate of 3.30E-03 m/sec are 31.4%, 26.7% and 28%. Meanwhile the minimum trapped LNAPL saturation was 15.2% recorded at 71% initial water saturation and the lowest rise rate of 4.6E-05 m/sec. This minimum value is much greater than the minimum entrapped saturation for uniform sand, rendering the entrapment saturation in contrast within somewhat shorter range of relatively higher values. This significant gap between the minimum entrapped saturations in the two sands underscores the role of particle size distribution on LNAPL entrapment saturation.

4.3.2 Effects of Water Table Rise Rate for LNAPL-wet Well-graded Sand

For LNAPL-wetted soil, the trend of LNAPL entrapment is also similar to that of the uniform sand both in terms of the variation with rate and discrepancies when compared with the water-wet state. As illustrated in figure (4.7), increase in the water table rise rate reduces the trapped saturation at a much slower rate when compared to the uniform sand case. The entrapped saturation range is characterized as well by much shorter range of higher values i.e 15.2%-37% , thus resembling the case of the initially water saturated condition.

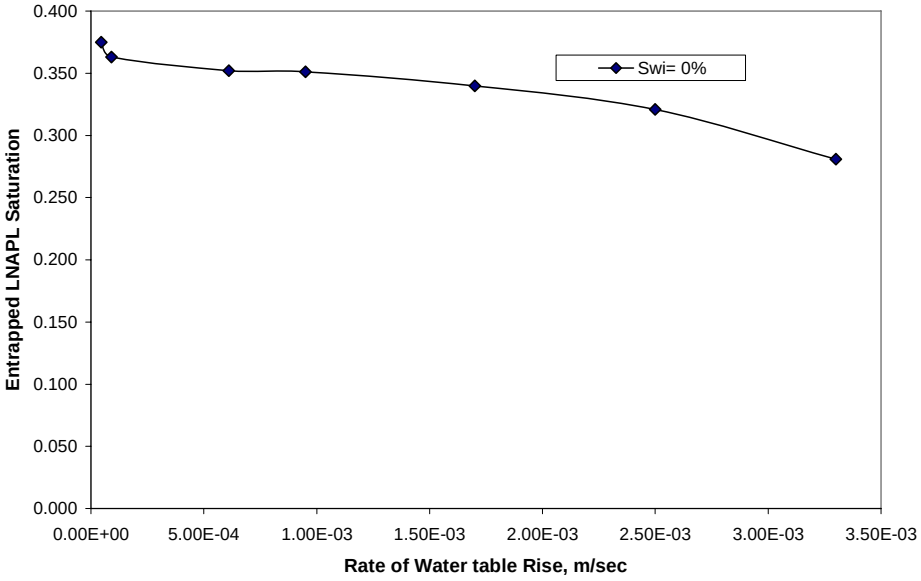

Figure 4.7:Effect of Rate of Water Table Rise for LNAPL-wet LCT3

4.3.3 Effect of Initial Water saturation on LNAPL Entrapment

Figure (4.8) illustrates the influence of the initial water content on the entrapped saturation for the well-graded sand. The trends are analogous to those of the uniform sand for transition from initial water saturation of 0 % to 20% with regard to the distinct behavior between lower and higher rise rate as shown in figures (4.9) and (4.10) respectively. Though in this case, at the lower rise rates, the trapped saturation decreases, while it is fairly constant for the higher rates. However, because of the overall shorter entrapped saturation range as highlighted earlier, figure (4.8) portrays a cluster of curves with mild fluctuations compared to the well-pronounced fluctuations and wider variability trend observed for the uniform sand as shown earlier in figure (4.3) above. Similarly, LNAPL trapped saturation at lower initial water content are observed to be less than that at some higher initial water contents. However, in contrast to the observation in the uniform sand case, at initial water saturation of 42%, the trapped amount is greater than when the initial water saturation is equal to 60%. Moreover, the trapped saturation at 71% initial water content also steadied, this shows the insignificant effect of the water table rise rate. These two points strengthen the idea that the by-passing mechanism which occurred at some higher initial water content has led to the higher entrapment saturation observed at the higher initial water saturations.

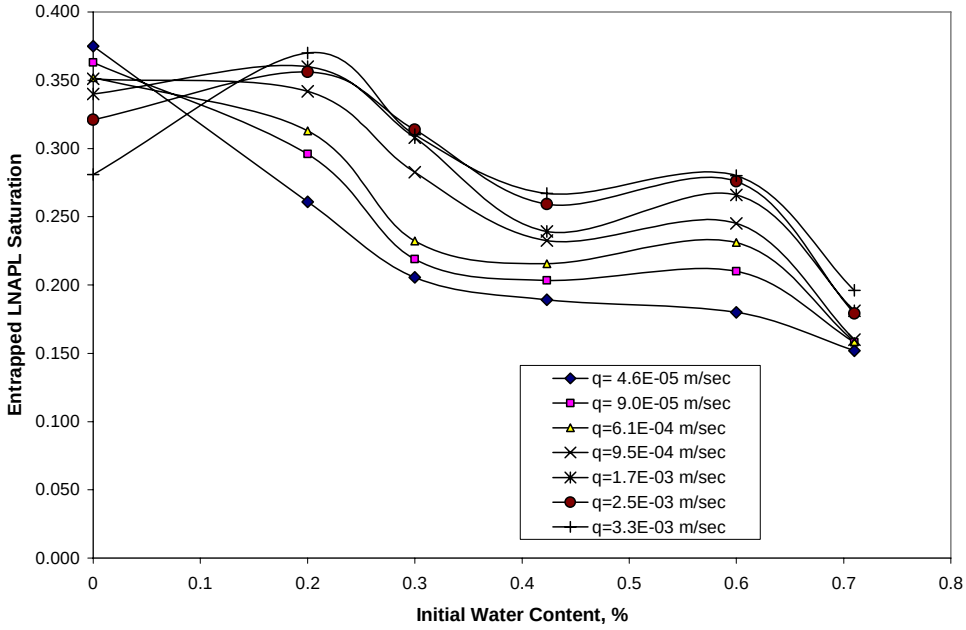

Figure 4.8: Effect of Initial Water Content at Various Rate of Water Table Rise for LCT3

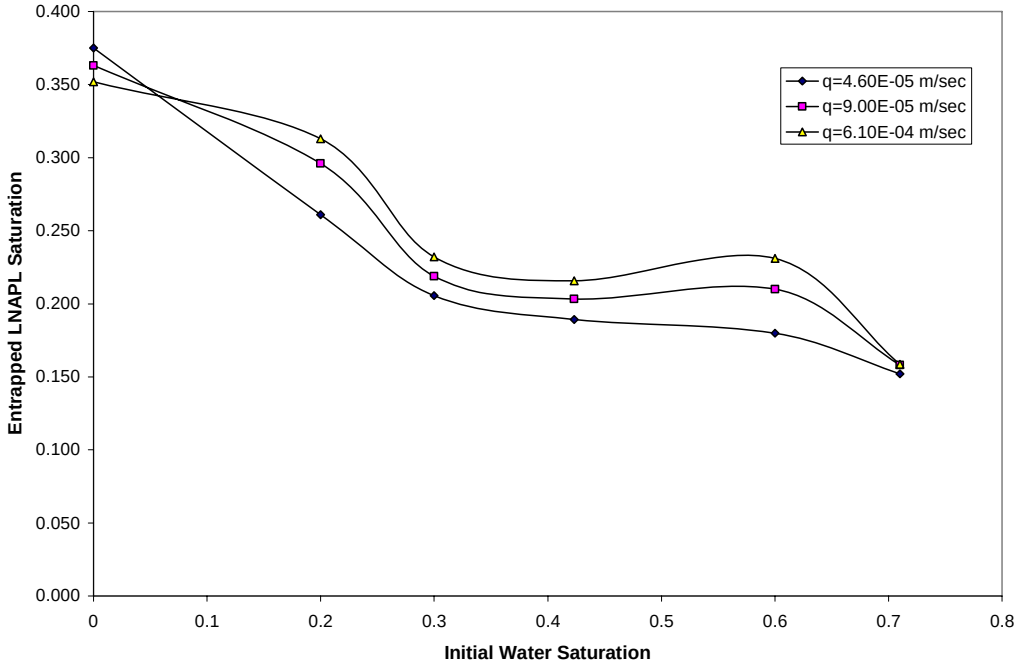

Figure 4.9: Effect of Initial Water Content at Lower Rate of Water Table Rise for LCT3

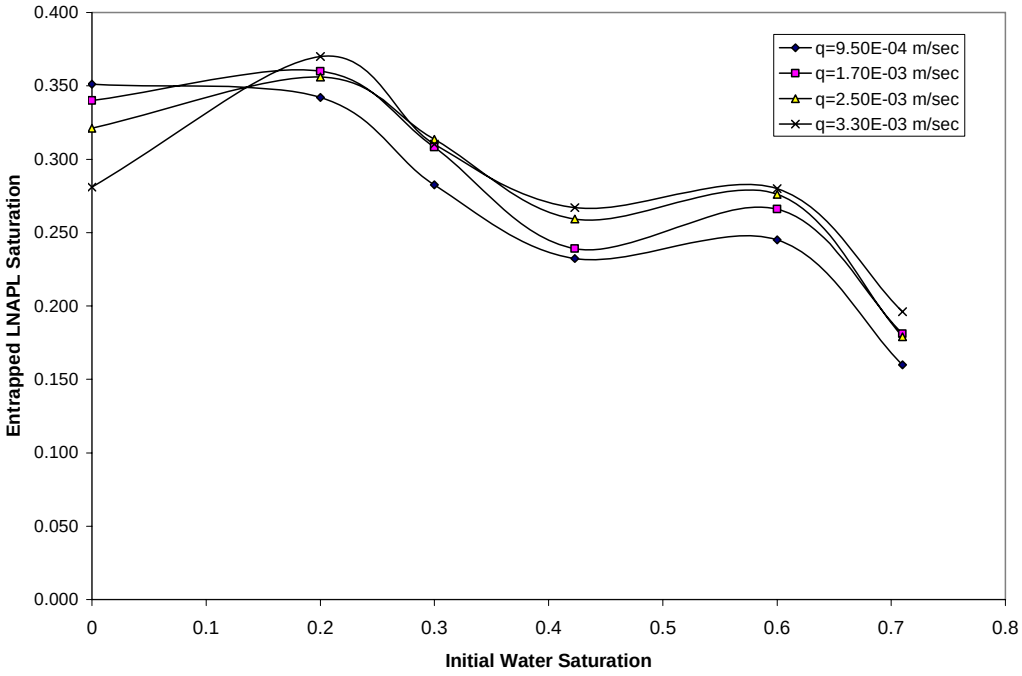

Figure 4.10: Effect of Initial Water Content at Higher Rate of Water Table Rise for LCT3

4.4 Effect of Porous Medium Type

To show the influence of porous medium type on the entrapment amount, figures (4.11)-(4.16) display the entrapped saturation against rise rates for the porous medium at different initial water saturations. Clearly, the figures shows that under similar condition, the well-graded sand that possessing wider range of different particle sizes trapped more LNAPL volume compared to uniform sand. Also, one-to-one comparison as given in Table (4.3) confirms this assertion with some few exceptions at 20% initial water saturation. Thus, despite the fact that the water table rise rate in LCT2 is always higher than that in LCT3, the uniform sand still trapped less LNAPL. For instance, considering the highest water table rise rates, the well-graded sand at 0%, 20%, 30%, 42%, 60% and 71% initial water saturation trapped approximately 196%, 101.65%, 175%, 164% ,127% and 130% of the LNAPL trapped by the uniform sand respectively. This could be attributed to higher heterogeneity and smaller particulate sizes presence in the well-graded sand that render it more prone to higher capillary and lower buoyancy effects.

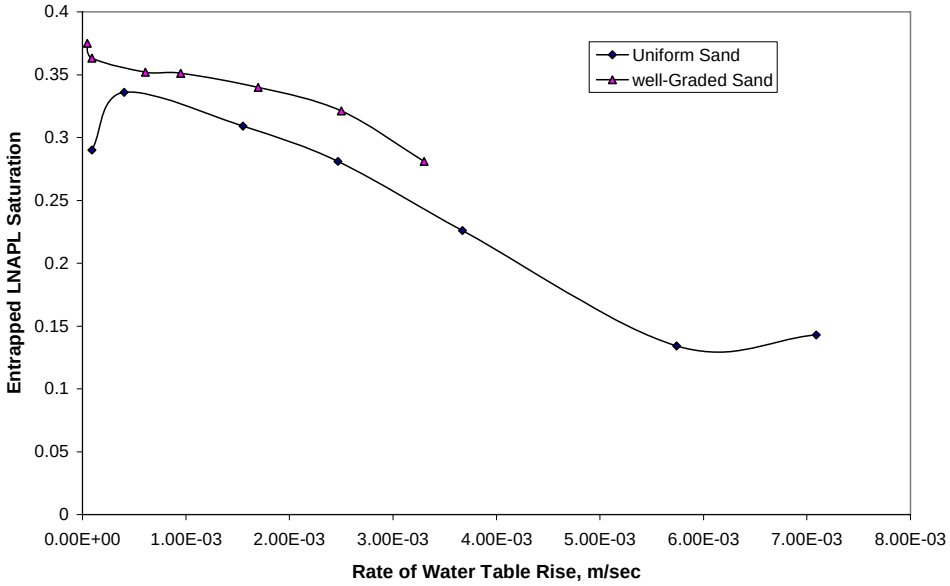

Figure 4.11: Effect of Porous Medium Type at Initial Water Content =0%

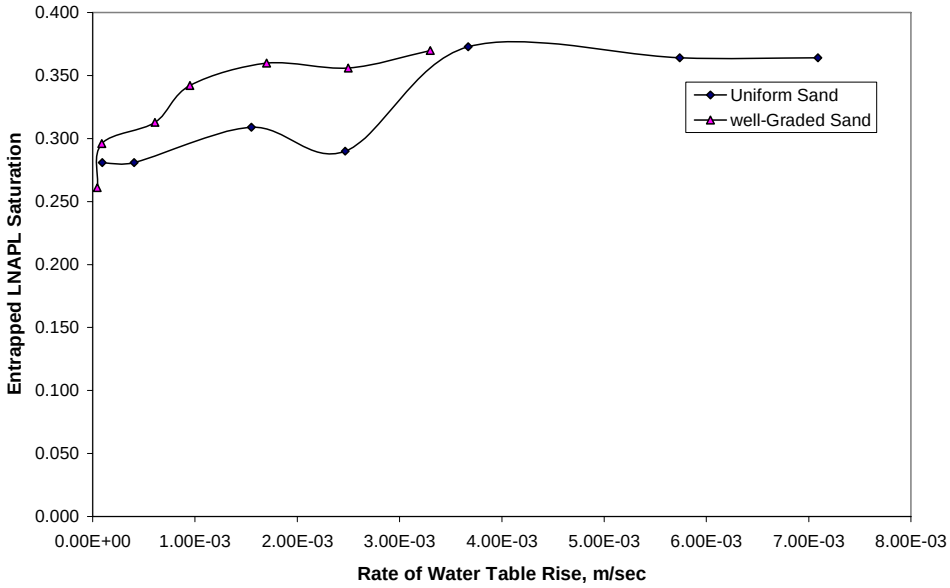

Figure 4.12: Effect of Porous Medium Type at Initial Water Content=20%

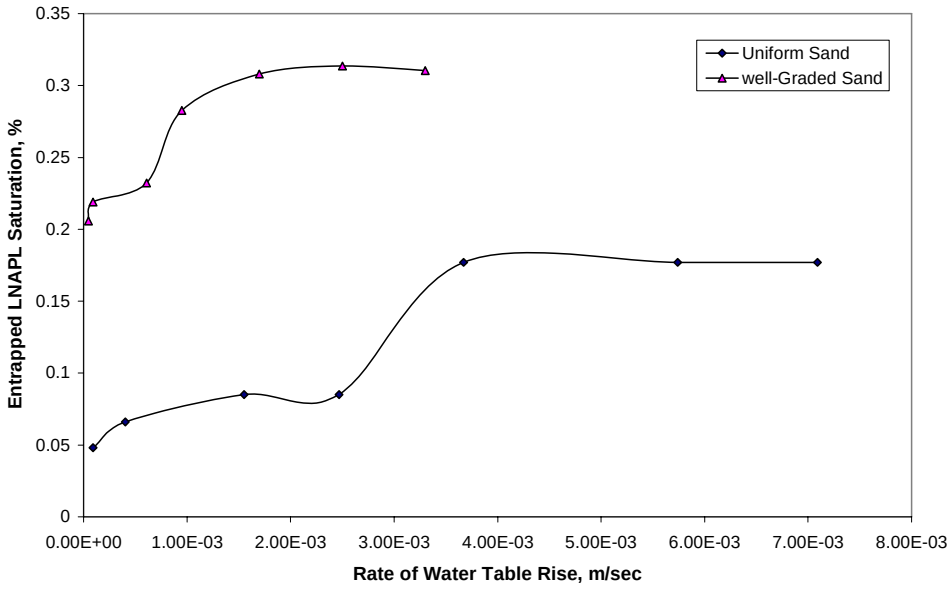

Figure 4.13: Effect of Porous Medium Type at Initial Water Content= 30%

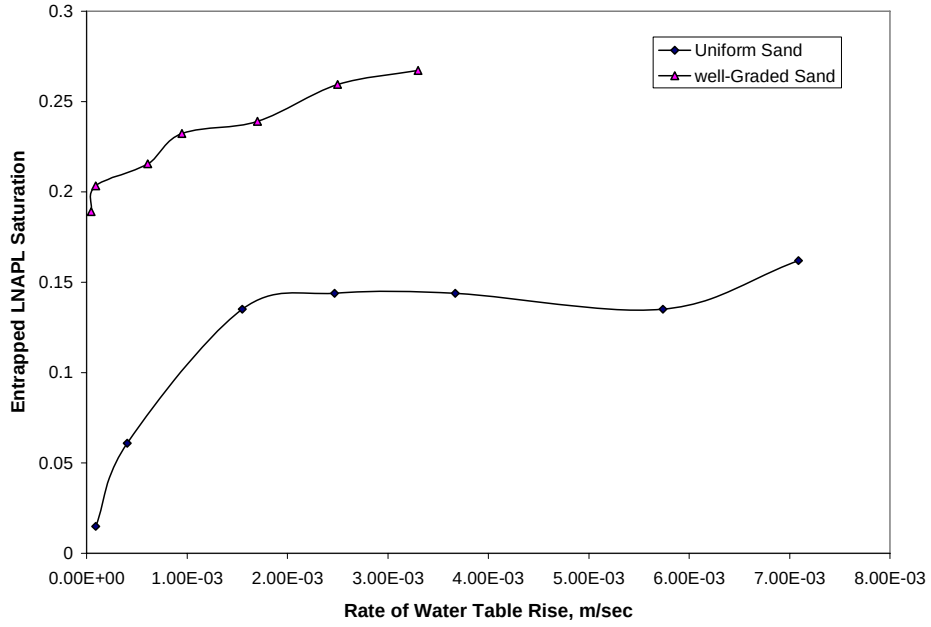

Figure 4.14: Effect of Porous Medium Type at Initial Water Content=42%

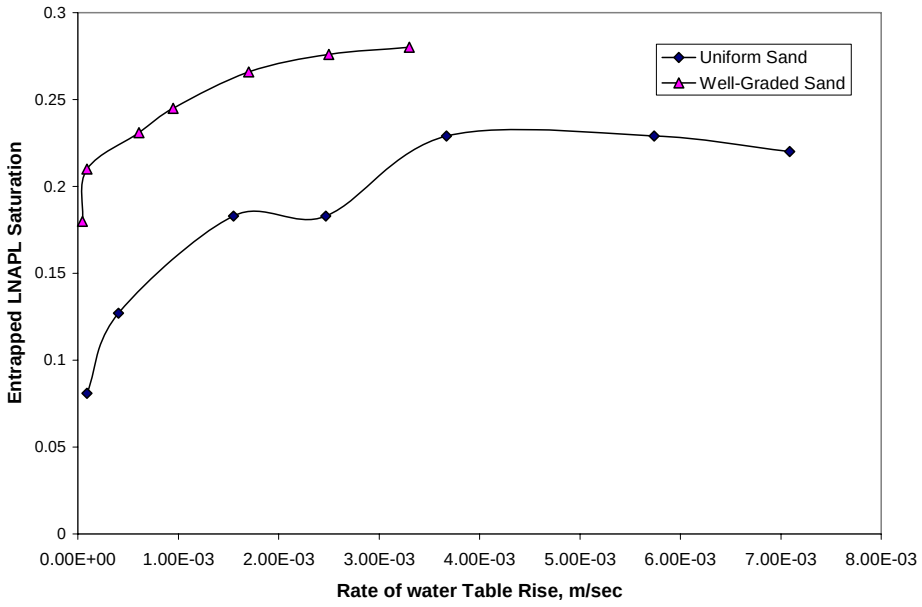

Figure 4.15: Effect of Porous Medium Type at Initial Water Content=60%

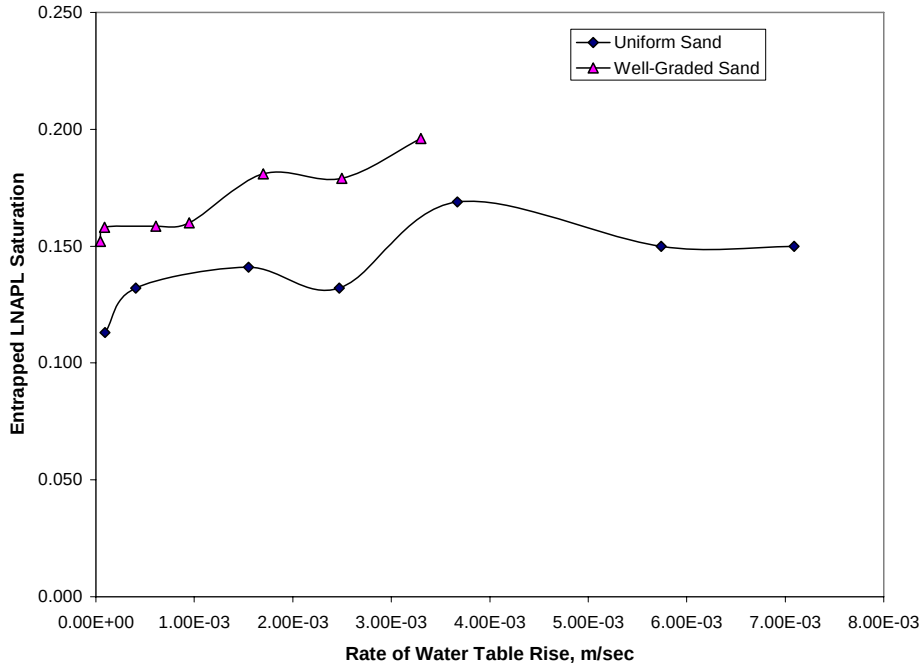

Figure 4.16: Effect of Porous Medium Type at Initial Water Content=70%

Table 4.3: Comparison of LNAPL Trapped Saturation in LCT2 and LCT3

Water table rise rate m/sec		% Increased in Trapped Saturation in LCT3 compared to LCT2					
LCT2	LCT3	Initial Water Content, %					
		0	20	30	42	60	71
9.11E-05	4.60E-05	29.31	-7.12	328.53	1160.77	122.14	34.51
4.04E-04	9.00E-05	8.04	5.34	231.71	233.21	65.37	19.70
1.55E-03	6.10E-04	13.92	1.29	173.14	59.71	26.27	12.41
2.47E-03	9.50E-04	24.91	17.93	232.44	61.42	33.92	21.21
3.67E-03	1.70E-03	50.44	-3.49	74.03	66.07	16.17	7.10
5.74E-03	2.50E-03	139.55	-2.20	77.19	92.13	20.51	19.33
7.09E-03	3.30E-03	96.50	1.65	75.28	64.90	27.29	30.67
	LNAPL Trapped Range for water-wet						
	Minimum				Maximum		
LCT2	1.5%				37.3%		
LCT3	28.1%				37.5%		
LNAPL Trapped Range for LNAPL-wet							
	Minimum				Maximum		
LCT2	13.4%				33.6%		
LCT3	15.2%				37%		

4.5 Analysis and Inferences of Experimental Results

4.5.1 Sensitivity Analysis

The significance of initial water saturation and rate of water table rise on influencing the LNAPL entrapment amount are statistically analyzed using two-way analysis of variance (ANOVA) without replication. For **a** by **b** factor levels, the experimental observations, **y**, could be generally described by a linear statistical model given as:

$$y_{ij=} \mu + \tau_i + \beta_j + \varepsilon_{ij} \quad \textbf{(4.1)}$$

Where **μ** is the overall mean effect, τ_i is the effect of the *ith* level of the initial water saturation effect, β_j is the effect of the *jth* level of rate of water table rise and ε_{ij} is the corresponding random error component. The test of hypotheses about the significance of the two factors could be stated as:

$$H_o: \tau_1 = \tau_2 = \tau_3 = \ldots\ldots\ldots\ldots \tau_a = 0$$

$$H_{1:} \text{ at least one } \tau_i \neq 0 \quad \textbf{(4.2)}$$

Similarly,

$$H_o: \beta_1 = \beta_2 = \beta_3 = \ldots\ldots\ldots\ldots \beta_b = 0$$

$$H_{1:} \text{ at least one } \beta_j \neq 0 \quad \textbf{(4.3)}$$

The two-way ANOVA outputs from SigmaSTAT [83] given in Table (4.4) shows that for both the LCT2 and LCT3, all the ***p***-values are equal to zero which is less than the

operating alpha, i.e *p*-value $0.05 = \alpha$. Also the *F*-values are large compared to the values obtained from statistical table. These support the alternate hypothesis (H_1) against the null hypothesis (H_o). Therefore, it is concluded that there is significant effects of both the initial water saturation and the rate of water table rise on the LNAPL entrapment in both the LCT2 and LCT3.

4.5.2 Wetting Front Instability Analysis

Instability analysis are performed using the simplified criteria presented by Whillhite *et al* [77] as expressed in equation (2.16) in order to check the status of the flow during the column displacement tests. For the set of the initial water saturation, the wetting fluid relative permeabilities were estimated using the parametric relationship presented by Parker *et al* [55]. As given in Table (4.4), the result reveals that the rate of the water table rise of 9.11E-05 m/sec for the LCT2 didn't meet the instability limit for initial water saturation of 60 % and 71%. Meanwhile for LCT3, the rise rate of 4.60E-05 m/sec also violates the instability criteria for both the two aforementioned initial water saturations; in addition to the rise rate of 9.00E-05 m/sec for initial water saturation of 71%. Based on these, it could be inferred that, with some very few exceptions at low rate of water table rise for the initial water saturation of 60% and 71%, the overall flow was dominantly under unstable condition

Table 4.4: Sensitivity Analysis for Factors Affecting LNAPL Entrapment

2-way ANOVA for LCT2					
Source of Variation	DF	SS	MS	F	P
Initial Water Content	4	101271.279	25317.820	92.263	<0.001
WT Rise Rate	6	26389.615	4398.269	16.028	<0.001
Residual	24	6585.826	274.409		
Total	34	134246.720	3948.433		
2-way ANOVA for LCT3					
Source of Variation	DF	SS	MS	F	P
Initial Water Content	4	28403.001	7100.750	116.965	<0.001
WT Rise Rate	6	9866.110	1644.352	27.086	<0.001
Residual	24	1457.001	60.708		
Total	34	39726.112	1168.415		

Table 4.5: Flow Instability Limit at Various Initial Water Saturations

Effective water content	Relative Permeability	Effective Permeability cm^2	Hydraulic Conductivity cm/sec	Instability Limit m/sec
Uniform sand intrinsic permeability = 9.28727E-08 cm^2				
0.2	0.002695171	2.50308E-10	0.000135889	1.77E-06
0.3	0.011964588	1.11118E-09	0.000603249	7.88E-06
0.423	0.042308457	3.9293E-09	0.002133173	2.79E-05
0.6	0.152926939	1.42027E-08	0.007710507	1.01E-04
0.71	0.283939419	2.63702E-08	0.014316096	1.87E-04
1	1	9.28727E-08	0.050419545	6.58E-04
Well-graded sand intrinsic permeability = 6.89174E-08 cm^2				
0.2	0.001706392	1.176E-10	6.38438E-05	8.34E-07
0.3	0.008499633	5.85773E-10	0.000318009	4.15E-06
0.423	0.033136593	2.28369E-09	0.001239788	1.62E-05
0.6	0.13227536	9.11607E-09	0.004949014	6.46E-05
0.71	0.257622067	1.77546E-08	0.009638796	1.26E-04
1	1	6.89174E-08	0.037414482	4.89E-04

4.5.3 General Inferences

The broad observations in the experimental results parallel reports credited to Wilson *et al* [80] and Powers *et al* [56] that found that LNAPL trapped in well-graded sand possessing wider pore size distribution tends to occupy several pore bodies, thereby containing higher number of complex isolated or discontinuous residuals. However, in more uniform sand, majority of the residuals blob are often singlet occupying much smaller pore volumes. Ryan and Dhir [60] experimentally proved that increase in larger particle sizes led to drop in residual saturation due to reduction in the buoyancy effects. Similarly, these differences could be attributed to higher capillary effects which are more pronounced with smaller particulate sizes.

With high experimental flow rates for the simulated water table rise that resulted in capillary numbers of great magnitude in both LCT2 and LCT3, the displacement of LNAPL is influenced by viscous drag effects; therefore, the control of entrapment is no longer limited to initial water saturation [68]. In order to avoid viscous and inertia effects, Ryan and Dhir [60, 61] and Steffy *et al* [64] conducted LNAPL entrapment column tests ensuring low flows. The low flows they used yielded maximum capillary numbers of 2.5E-06 and 1E-09 respectively. Though the inertia effects were also avoided in the course of this study by maintaining low Reynolds's numbers, even the minimum capillary numbers recorded as 5.02E-5 and 2.5E-05 for LCT2 and LCT3 respectively are high. Moreover, as the viscosity ratio (i.e $\mu_{nw} / \mu_w = 20.31 > 1$), at these high capillary numbers, the flows were susceptible to deviations from stability condition. Hence, at

microscopic scale, higher entrapped saturation could be attributed to instability at the interface between the LNAPL and the water that gives rise to more fingering or channeling effects. In addition, this circumstance is prone to be more pronounced at higher velocities that are most likely to be larger than gravity drainage or surpassing the difference between flow critical velocity and the combine capillary and viscous driving velocity as expressed mathematically in equations (2.13)-(2.15). This tendency promotes pre-dominantly bypass entrapment mechanism as favored by Whillhite *et al* [77] observations. The result of the instability analysis given in Table (4.5) corroborates these foregoing inferences.

Kueper and Frind [29] reported that channeling is caused mainly by soil macroscopic heterogeneities and Steffy *el al* [68] noted that increase in trapped and residual saturation occur in finer-grain of more heterogeneous portion of an aquifer. These may explain the reason why the more heterogeneous well-graded sand trapping more LNAPL volume, since for both types of the porous media, factors that influence fingering are kept constant i.e fluids properties were not variables throughout the experiments. Rationally, the different behaviors can be attributed to the contrasting medium heterogeneity between the two soils. It could be suggested that the flow instability has rendered the increase in viscous drag effects to level that advances the LNAPL entrapment rather than to undermine it as expected in the case when immiscible displacements are under stable state conditions.

Considering the remarkable harmony between both the two sands under initial oil saturated condition, corresponding to 0% initial water saturation, the major trend of the

LNAPL entrapment has matched the variation affinity of the data presented by Ratnam *et al* [58, 59]. However, by altering the initial soil wetting condition, the distinct discrepancies between the two wetting scenarios which are in agreement in both the two types of sand emphasizes the significance of the influence of the initial soil matrix wetting on LNAPL residuals and entrapment as reported by a number of authors[12, 18, 49].Based on these findings, it could be inferred that in changing from strongly water-wet to strongly LNAPL-wet initial conditions, the instability that dominated the whole flow in former condition where thoroughly within stable regime when it was completely under the LNAPL-wet state.

Interestingly, considering Table (4.6); it could be noted that by fitting the behaviors of the two porous media using linear model for the various rise velocities, deviation from linearity gets more pronounced as the rise rate increases for both porous media. For the uniform sand, the poor fittings deviation amplified more rapidly from R^2=0.5938 to 0.0021. On the other, for the well-graded variation is slightly within close range of R^2=0.8458 to 0.4016, showing better fittings comparatively. Though both fits are more or less not very good on the whole which could be attributed to large experimental water table rise velocities -leading to very high capillary numbers and flow in-stability -as highlighted above, the later case virtually goes closer in line with prevalent reports [60, 61, 68] observed at smaller displacement rates, which proved not practical under the experimental conditions considered in this study.

Effects of initial water saturation on LNAPL entrapment have received extensive attention from several authors as reviewed earlier in Chapter two. While, linear relationship is

Table 4.6: Goodness of Linear Fitting for Effect of Initial Water Saturation

LCT2		LCT3	
Water table rise rate m/sec	R^2	Water table rise rate m/sec	R^2
9.11E-05	0.5938	4.60E-05	0.8454
4.04E-04	0.5779	9.00E-05	0.8618
1.55E-03	0.3884	6.10E-04	0.874
2.47E-03	0.3096	9.50E-04	0.0485
3.67E-03	0.0914	1.70E-03	0.771
5.74E-03	0.0021	2.50E-03	0.6834
7.09E-03	0.0005	3.30E-03	0.4016

widely reported [18, 41, 31, 68], unique functional relationship binding the two variables apparently remains inconclusive. Lenhard [32] and Parker and Lenhard [54] have advocated for linear fitting for simplicity and in order to facilitate further analysis. In-spite of that, they still admitted that additional experimental investigations are necessary in order to strongly substantiate the linear assumption. Also the fact that for two-phase air-water system, Stonestorm and Rubin [69] data and Kaluarachchi and Parker [25] modified Land [31] based model are evidences that further suggest that nonlinear relation is more appropriate in some instances. Moreover, at larger capillary number that featured in this work, LNAPL entrapment is no longer controlled mainly by antecedent moisture content [68]. This also adds to the suggestion that other capillary number influencing factors- in which flow rate play a leading role- are most likely responsible for the non-linearity already observed in this work. Nonetheless, none of the reviewed studies addressed the issue considering the rate at which the wetting fluid displaces the non-wetting one on the imbibition path. The data presented here implies that exempting this factor in entrapment analysis could certainly lead to misjudgment in estimating the extent of aquifer contamination. This is particularly the case when displacement rates during water table rise are becoming higher and when deviation from ideals of stability is inevitable. According to Steffy *et al* [68], deviation from linearity could be ascribed to fluid surface tension variations when becoming larger and need to be accounted for in LNAPL trapping modeling. However, this work also now infers that pore size distribution that varies from sand to sand type as well as wetting fluid imbibition rate are crucial factors that must be considered in LNAPL entrapment processes and models' estimations. Though, the case of

the pore size distribution has been broadly taken care off, the later inferences arising from this work has not been given due attention by any entrapment model.

The experimental data and the foregoing analysis presented stress the complexity of LNAPL entrapment trend as function of initial water content at varying water table rise rate. These suggest that without considering the effects of rate of non-wetting fluid displacement during imbibition in sandy soils, globalizing a particular relationship could lead to significant error in trapped LNAPL predictions by models; this will eventually undermine the target goals of using the models and their contributions in judging the extent of trapped LNAPL in contaminated sites and remediation attempts extensively.

Remediation schemes employing water displacing LNAPL techniques are more appealing to featuring higher displacement rates than water table rise rates encounter in aquifers. Therefore it is pertinent to mention that great attention and caution should be exercised towards appropriate choice of LNAPL flushing rate and/or hydraulic gradient during water-flooding, pump-and-treat through extraction wells, enhanced hydrocarbon mobilization treatment or any related clean-up program. This is necessary owing to the fact that it could be inferred from the analysis presented here that for cost-effectiveness, several factors should be sufficiently given due consideration during remediation attempts with no exceptions. In this context, flushing rate should be expected to play a great role as its positive impact with intensity has limitation. In other words, a threshold flushing rate does exist above which more amounts of contaminant would be unavoidably trapped. Hence, ignoring this could render supplementary costly aquifer remediation efforts practically ineffective.

CHAPTER 5

Model Development and Validation

Results from the experimental program presented in the previous chapter suggest that trapped LNAPL saturation as function of initial water saturation is complex particularly when rate of imbibition imposed by a rising water table is taken into consideration. The analysis revealed that deviation from widely reported linear relationship amplifies as the rate increases. It is concluded that accounting for the influence of rate of non-wetting fluid displacement on imbibition pathway is necessary for more accuracy of water-wet porous media entrapment models; especially at excessive imbibition rates that pave way to inevitable deviation from wetting front stability during immiscible displacement processes. As an attempt towards catering for such circumstance, a predictive model is developed here to account for rate at which the LNAPL is displaced during imbibition imposed by a rising water table. Empirical relationships were built-up from data generated in the experimental program as detailed in Chapter 3; with the complements of BC and VG derived constitutive relationships the proposed trapping model was formulated and validated. The performance of the developed model is also compared with predictions from linear trapping models of Land [31] and Steffy e*t al* [68].

5.1 Model Development

5.1.1 Proposed Model Assumptions

For convenience, the following fundamental assumptions were made to simplify generating the model and its subsequent application:

1. Flow is vertical, steady, one-dimensional in upward direction and that Darcy's law is valid.
2. Porous medium is homogenous, water-wet and rigid; while fluids are incompressible with invariable properties.
3. Vertical hydrostatic equilibrium flow conditions prevail before entrapment occurs. This implies that pores spaces are assumed to be imbibed by the invading wetting fluid at a rate that allows the fluid pressures to equilibrate before trapping occurs. Therefore, it is assumed that the rate of water table rise in test column is less than rate of LNAPL displacement imposed by imbibition [68].
4. Quasi-static condition is assumed to prevail, i.e rate of displacement during imbibition and LNAPL entrapment are dominated by capillary forces, whereas, viscous effect are ignored. Quasi-static models impose a capillary pressure on the network and consider only the final static position of all fluid-fluid interfaces, neglecting dynamic aspects of pressure propagation within the model and interface dynamics [76]. Also the model neglects buoyancy forces effect.
5. Medium is fully saturated two-phase LNAPL-water system.
6. LNAPL is always available for trapping, and when trapped it is immobile.

For the hydrostatic assumption, the vertical pressure gradient within both water and LNAPL phase in an aquifer satisfied the basic hydrostatic equation under vertical equilibrium conditions. Charbeneau [8] explicitly outlined that the implications of the vertical equilibrium assumption is to provide a basis for:

- Allowing air-water soil water characteristic curve provides sufficient information describing the pore size distribution of the soil.
- To permit characteristic curve for LNAPL-water or air-LNAPL to be estimated from air-water curve by scaling air-water parameters.
- To consider Leverett's [40] assumption of extending two-phase to three-phase valid,

For modeling at pore network level, Wilkinson and Willemson [76] viewed that for limited low capillary number, dynamic network algorithm could be simply reduced to quasi-static algorithm in most porous media systems, including systems mostly relevant to hydrology.

5.1.2 Hydraulic Parameters Estimates and Scaling Procedure

Owing to time consuming, difficult and above all, collective cost of S-P-K experimentation, the feasibility of getting indirect methods requiring lesser experimental commitments for determining VG [71] and BC [5] curve fitting parameters were investigated intensively. In that regard, SOILPROP program, a commercially obtainable package developed employs procedure presented by Mishra *et al* [46] in conjunction with earlier modified Arya and Paris [2] model. The program transforms soil grain-size distribution (GSD) into a pore size distribution from which it establishes a relationship

linking the cumulative pore volume and pore radii. This relationship is further projected to relate S-P for two-phase air-water system, afterwards; the VG parameters estimates are calculated via non-linear regression analysis. Advantageously, the program is capable of estimating an equivalent BC parameters from the calculated VG parameters using BC-VG parameters conversion methodology presented by Lenhard *et al* [35]. Comparably, amongst others, a similar but more comprehensive program that partly require more experimentation is also a procedure incorporated in a more recently computer package; SOILPARA, produced by Marco and Marcello [42].

Busty *et al* [7] showed that for sands porous materials with no clay element, scaling factors for S-P function could be predicted from the interfacial tension as they are assumed to be uniquely fluid dependents parameters in such peculiar case. Therefore, the VG and BC models' parameters of the two soils for air-water drainage process were indirectly estimated using the SOILPROP software. Corresponding estimates for the LNAPL-water system were in turn arrived at by a scaling procedure using the water and the crude oil interfacial tensions in correlations presented by Lenhard and Parker [37] as follows

$$h_d^{ow} \left/ \sigma_{ow} \right. = h_d^{aw} \left/ \sigma_{aw} \right. = h_d^{ao} \left/ \sigma_{ao} \right. \quad \textbf{(5.1)}$$

and

$$\alpha_{ow}\,\sigma_{ow} = \alpha_{aw}\,\sigma_{ow} = \alpha_{ao}\,\sigma_{ao} \quad \textbf{(5.2)}$$

Where *ow, aw* and *ao* denote oil-water, air-water and air-water two phase systems respectively and all other terms as earlier defined in Chapter 2.

Kool and Parker [28] assume constant n for both imbibition and drainage paths and showed that ${}^{i}\alpha/{}^{d}\alpha \approx 2$ for a given system. The resulting estimated LNAPL-water parameters are given in Table (5.1). Alternatively, as demonstrated by Lenhard [32], appropriate scaling of the air-water *S*-*P* function established for drainage and imbibition in whole, yields a single representative hysteretic *S*-*P* function that is characterized by independency on the fluids pair combination effect, which could adequately symbolize the required LNAPL-water hysteretic function as well.

5.1.3 Empirical LNAPL Trapping Models Formulation

Data secured from LCT2 were used to generate the empirical trapping model due to wider and larger range of the water table rise rates. Attempts toward fitting the data to several customs equations using MATLAB [82] and MATHEMATICA [84] proved abortive. An alternative approach was successfully achieved via employing a powerful least square fitting commercial package named "TableCurve3D" [83] that uses Gaussian elimination method. The data were nonlinearly surface-fitted to more than 300 built-in functional relationships; with initial water saturation and rate of the water table rise set as the independent variables. Based on the statistics of the goodness of fit from the optimized function parameters; i.e minimized residuals between the actual the predicted; twenty (20) best fitted functions with adjusted coefficient of regression, R^2, greater than 0.9 were adopted as displayed in Table [5.2], where the variables x, y and z stand for initial water

Table 5.1: BC and VG Hydraulic Parameters Estimates

Porous Medium	Model	Hydraulic Parameter	Estimate for Air-Water from SOILPROP	Estimate for Oil-Water
Uniform Sand	Van-Genutchen	$^{d}\alpha$ (1/cm)	0.0732	0.176
		n	2.7	
		θ_r	0.0	
	Brooks Corey	$^{d}h_d$ (cm)	9.01	3.74
		λ	1.13	
		θ_r	0.0	
Well-Graded Sand	Van-Genutchen	$^{d}\alpha$ (1/cm)	0.0347	0.087
		n	2.37	
		θ_r	0.00407	
	Brooks Corey	$^{d}h_d$ (cm)	18.3	7.6
		λ	0.956	
		θ_r	0.0529	

Table 5.2: Fitted Functions and Summary of their Statistics

	Fit type	Surface-fitted Function	R^2	*p*-value>F
1	Polynomial	Sigmoid Series Bivariate Order 5	0.994	0.0000
2	Polynomial	Cosine Series Bivariate Order 5	0.989	0.0000
3	Polynomial	Chebyshev x, y Bivariate Polynomial Order 5	0.988	0.0000
4	Rational	Chebyshev x, y Rational Order 3/4	0.961	0.0000
6	Rational	Chebyshev Lnx, y Rational Order 3/4	0.950	0.0000
7	polynomial	Cosine Series Bivariate Order 4	0.944	0.0000
8	polynomial	$Z = a+blnx+c(lnx)^2+d(lnx)^2+ey+fy^2+gy^3+hy^4+iy^5$	0.944	0.0000
9	Polynomial	$Z = a+bx+cx^2+dx^3+ex^4+fy+gy^4$	0.936	0.0000
10	Polynomial	$Z = a+bx+cx2+dx3+ex4+flny$	0.934	0.0000
11	Polynomial	$Z = a+b/x+c/x2+d/x3+e/x4+flny$	0.933	0.0000
12	Polynomial	$Z = a+bx+cx2+dx3+elny$	0.903	0.0000
13	Polynomial	$Z = a+bx+cx2+dx3+ex4+f/y+g/y2+h/y3+I/y4$	0.937	0.0000
14	Rational	$Z = (a+bx+clny+d(lny)^2)/(1+ex+fx^2+gx^3+hlny)$	0.938	0.0000
15	Polynomial	$Z = a+b/x+c/x2+d/x3+e/x4+flny+g(lny)2$	0.937	0.0000
16	Polynomial	$Z = a+blnx+c(lnx)2+d(lnx)3+e(lnx)4+f(lnx)5+gy+hy2$	0.947	0.0000
17	Polynomial	$Z = a+blnx+c(lnx)2+d(lnx)3+e(lnx)4+f(lnx)5+gy+hy2$	0.936	0.0000
18	Rational	$Z = (a+blnx+c(lnx)^2+dy)/(1+elnx+f(lnx)^2+gy+hy^2)$	0.914	0.0000
19	Rational	Chebyshev Lnx, y Rational Order 1/2	0.901	0.0000
20	Polynomial	Chebyshev x, Lny Bivariate Polynomial Order 3	0.933	0.0000
21	Polynomial	Chebyshev x, y Bivariate Polynomial Order 3	0.922	0.0000

x=Initial water saturation

y=Rate of water table rise

z=Trapped LNAPL saturation

saturation, rate of water table rise, trapped LNAPL saturation. The robustness of the fits is also portrayed in the sense that the entire tests of hypotheses as stated below performed on the twenty selected empirical functions predictions and their corresponding coefficients are found to be in support of the alternate hypothesis (H_1) against the null hypothesis (H_o) i.e *p*-value $0.05 = \alpha$, which is the selected confidence limit.

Test of Hypothesis

$H_o : \beta_1 = \beta_2 = \beta_3 = ...\beta_n = 0$ For all *n* coefficients

$H_1 : \beta_i \neq 0$ For at least one coefficient **(5.3)**

Where $\beta_1, \beta_2, \beta_3.....\beta_n$ are the fitted function's optimized coefficients.

5.1.4 Analytical LNAPL Trapping Model to Account for Imbibition Rate

The proposed model is an extension to LNAPL linear trapping models to accommodate higher wetting fluid imbibition rate during water table rise. Beside the usual initial water saturation and pore geometric defining parameters, the empirically developed model incorporates rate of imbibition imposed by water table rise. The model take into consideration that reversal from drainage to imbibition from a given reversal point could follow several scanning pathways that rely on the rate at which the wetting fluid imbibes into the porous medium. Hence, the parametrically characterized proposed entrapment model could be reducibly stated as:

$$S_{or} = f\ (S_{wi}, q_w\ ) \quad \textbf{(5.4)}$$

Where q_w is Darcy's velocity for the wetting fluid front expressed as

$$q_w = -\frac{k}{\mu_w}\left(\frac{dP}{dL}\right) \quad \textbf{(5.5)}$$

Where k , μ_w and $\left(\frac{dP}{dL}\right)$ represent the porous medium hydraulic conductivity, wetting fluid viscosity and the pressure gradient respectively. Equation (5.4) could be represented by any of the empirically fitted functions given in Table (5.2). The empirical functions were drastically narrowed down to one optimum function via in-depth analysis involving the whole selected functions. The aftermath of the analysis singled-out the polynomial function number 10 in the Table (5.2) with surface plot shown in figure (5.1)- as the most compatible model; yielding the most superlative output when incorporated in the analytical model stated in equations (5.6)-(5.8). The estimated optimized parameters of the chosen model and their detailed statistics are given in Table (5.3). For a particular reversal point, substituting VG or BC *S-P* function as expressed in equations (2.1)-(2.4) for S_{wi} in equation (5.3) and integrating vertically the area enclosed between the main drainage and the appropriate hypothetical scanning curve from initial water table position, h_{ow} , considered as reversal point on the main drainage pathway to the imbibition scanning pathway for the given initial water saturation and imbibition rate, to the final zero capillary head where local maximum entrapment saturation occurs; yields an estimate of the amount of cumulative trappable specific volume, V_r , in cm^3 of the trapped

Table 5. 3: Statistics of Function and Parameters of the Empirical Trapping Model

R^2	Adjusted R^2	Fit Standard Error	F-value
0.9337402899	0.9195417806	0.0253614661	81.734340165

Parameter	Value	Std Error	t-value	95.00% Confidence Limits		P-value
a	2.76155972	0.35799361	8.854512128	2.43767962	3.902037905	0.00000
b	-20.183787	3.697426938	-6.5815776	-31.8969895	-16.7728151	0.00000
c	57.9350950	13.39734239	5.406153766	45.02745125	99.8287348	0.00001
d	-69.432173	20.32129761	-4.45113482	-132.014556	-48.8911152	0.00012
e	29.6112738	10.98505086	3.683872181	18.00057164	62.93447491	0.00094
f	0.02616234	0.002935045	9.028986652	0.020497638	0.032503319	0.00000

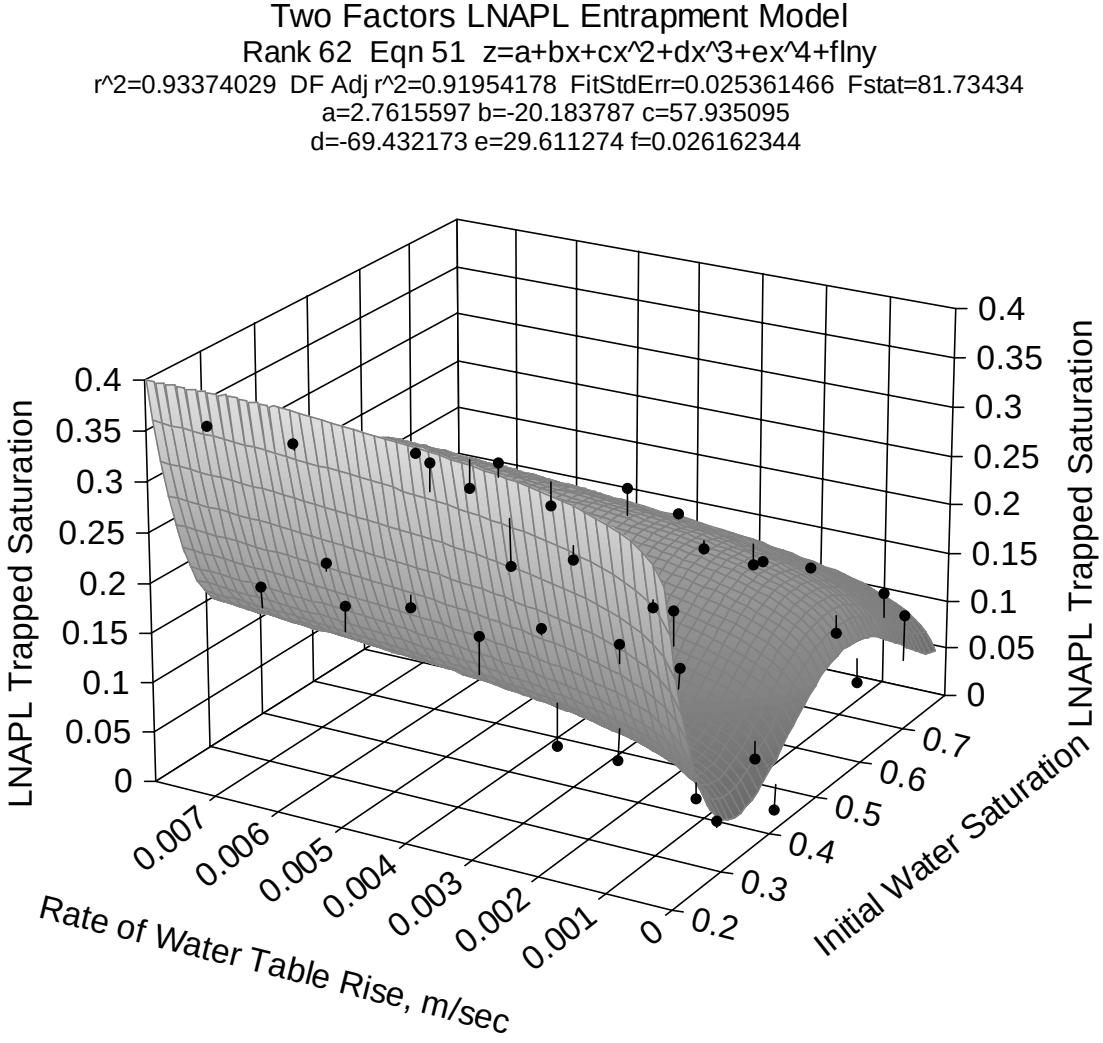

Figure 5.1: Surface-fit Plot of the LNAPL Empirical Trapping Model

LNAPL per cm^2 of an aquifer (i.e cm^3/cm^2). The integration could be achieved by numerically evaluating the definite integral of the volumetric content of the LNAPL, θ_{or}, present in the aquifer after the water table rises, between the two extreme bounds. Hence,

$$V_r = \int_0^{h_{ow}} \theta_{or} dh_{ow} \quad \textbf{(5.6)}$$

Where $\theta_{or} = \phi S_{or}$, ϕ = aquifer porosity and S_{or} = trapped non-wetting fluid saturation presence in the aquifer after attainment of equilibrium.

Hence, this could be written instead for the VG model's assumption as:

$$V_r = \phi \int_0^{h_{ow}} S_{or}(S_{wi}, q) dh_{ow} \quad \textbf{(5.7)}$$

For BC model assumption, the non-zero capillary entry pressure should be accounted for, thus;

$$V_r = \phi \int_0^{h_d} S_{or}(S_{wi}, q) dh_{ow} + \phi \int_{hd}^{h_{ow}} S_{or}(S_{wi}, q) dh_{ow} \quad \textbf{(5.8)}$$

In both cases, the upper bound, h_{ow}, magnitude is obtainable by inverting the appropriate functional relationships S_{wi} as expressed in equation (2.1) and equation (2.3) for the two models accordingly at a given reversal point for any initial water saturation of interest. The constraints of the model are that:

- The cumulative LNAPL present in the porous medium that is available for trapping, (θ_{LNAPL}), exceeds the cumulative amount obtained from equation (5.7)

or equation (5.8), i.e $\theta_{LNAPL} = \theta_{total} - \theta_{water} \geq V_r$. Where θ_{total} and θ_{water} are the total liquid and water volumetric content in the LNAPL-water fully saturated porous medium.

- Initial water saturation between 20%-71% i.e $0.2 \leq S_{wi} \leq 0.71$. Below the lower limit, the model assumes that conditions are moving towards favoring oil-wet media while above the upper limit, most of the LNAPL present is trapped regardless of displacement velocity, therefore the trapped saturation is steady. These conditions were observed from the experimental data.
- The wetting fluid imbibition rate, q_w, satisfies instability limit as stated in equation (2.16). Below this limit, we assume flow rate violates the instability criteria and hence flow could be considered in stable regime for which other entrapment models that advocates linearity could be adequately used.

5.2 Numerical Implementation of LNAPL Entrapment Modeling

The LNAPL entrapment formulated above is coded with programs written in MATLAB language as provided in APPENDIX A and APPENDIX B. The model integration solution was performed using adaptive Lobatto Quadrature numerical technique. The flow chart displayed in figure (5.2) outlines details on how the model works in order to predict the amount of trappable LNAPL specific volume according to the required inputs and stated constraints of the formulated trapping model. Once the constraints stated above are

not met, the model has to be re-run to suit the prevalent initial moisture and water table rise conditions and to ensure that it obeys all the constraints appropriately.

However, models are always bound to deviation from reality due to unavoidable errors and associated uncertainties that could feature in their developments and applications. Therefore, some sources of uncertainties that are likely to impair performance of the developed trapping model could be highlighted as follows:

- Quasi-static model assumption made against complex dynamic model assumption in order to simplify the model formulation.
- Extent of accuracy of indirect estimation of the hydraulic parameters.
- Feasibility of model applicability to field soil conditions.
- Feasibility of extending applicability of model to sandy soils from different classes and hydraulic characteristics.
- Practical significance of the optimized empirical model‘s parameters.

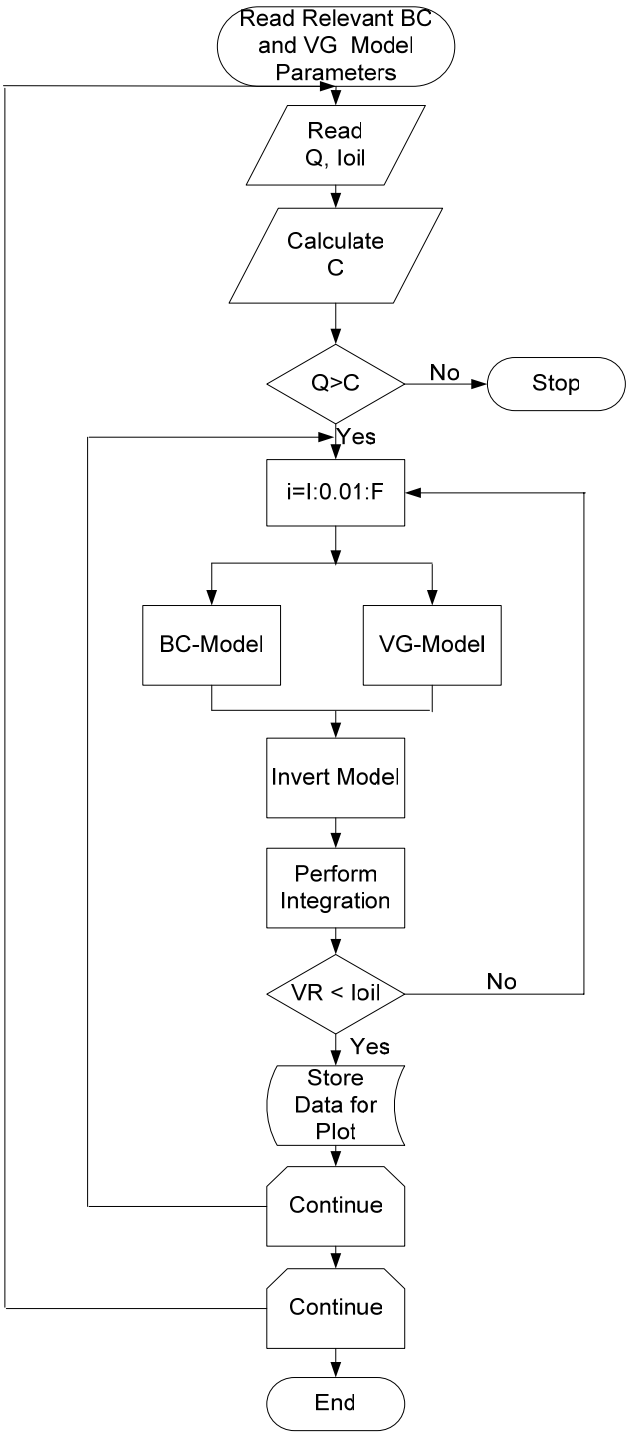

Figure 5.2: Trapping Model Flowchart

5.3 Model Validation

Validation is a process by which performance of a model is tested and evaluated against set of parallel responses that did not partake in its development process. The laboratory data secured in LCT3 was used to evaluate the behavior of the developed trapping model as formulated in section 5.3. The model prediction from the numerical modeling based on VG and BC models for the effect of water table rise rate on the LNAPL entrapment are validated with the experimental data. Also, at fixed water table rise rates, the model's prediction for influence of initial water saturation is validated using the experimental data jointly with the Land [31] empirical algorithm for two-phase oil-water system and Steffy *et al* [68] LNAPL trapping models that advocate for linearity of LNAPL trapped saturation as function of initial water saturation. The predictions results of these two models are compared to that of the developed model in order to show the necessity of incorporating rate of water table rise in LNAPL entrapment models when deviation from the linearity that surface at higher rise rates prevails.

Based on the trapped LNAPL saturation of 0.37, which is the maximum trapped LNAPL saturation obtained from both LCT2 and LCT3 considered as $^{i}\overline{S}_{nr}^{nw}$, the Land's [31] algorithm was evaluated to predict the local maximum trappable LNAPL for reversal point from $^{d}\overline{S}_{w}^{nw}$ drainage to the imbibition scanning curve for $^{d}\overline{S}_{w}^{nw}$ values equal to the initial water saturations considered in the experimental program. On the other hand,

the LNAPL entrapment trend for the lowest water table rise rate corresponding to 4.605E-05 m/s that best fitted linear model was adopted for getting the two additional parameters needed for estimating the trapped LNAPL specific volume using the Steffy *et al* [68] LNAPL trapping model. The values of the model's parameters were therefore estimated as a=-0.356 and b=-0.28 for the well-graded sand. The individual performances of the tested models are analyzed and compared below**.**

5.3.1 Model Validation for Effect of Water Table Rise Rate

Figures (5.3)-(5.7) display the model predictions of the LNAPL trapped specific volume against water table rise at fixed initial water saturations. Despite the fact that both the two approaches captured the major entrapment trends to some extent, the BC-model based predictions apparently are however much higher than the VG-based prediction as shown. The VG-based model prediction was found to perform much better based on the goodness of fit of regression given in Table (5.4). At lower initial water content up to 42%, with increase in water table rise, the VG-based model excellently predicts the experimental values with over or under estimation between 1-14% with corresponding good R^2 in the range between 0.573-0.947. This could be attributed to the fact that the experimental data shows smooth trend of decrease in entrapment saturation with increase in initial water content for initial water content up to 42 %. However, when the initial water saturation was 60 % the trapped saturation increases instead, an observation that could be due to the wetting fluid by-passing that occur which favors higher LNAPL entrapment. On the other side, for the higher initial water saturations, i.e 60% and 71%, the model

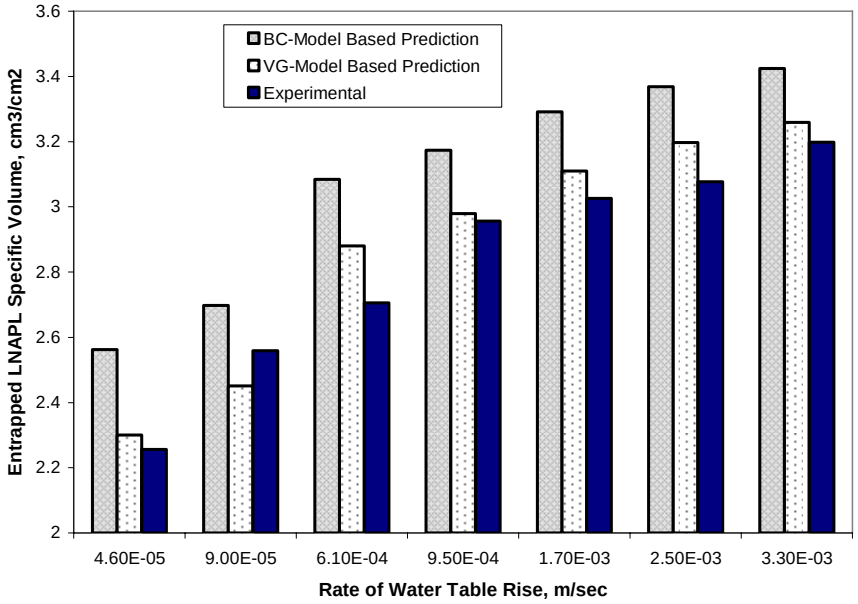

Figure 5.3: Model Validation at Initial Water Saturation=20%

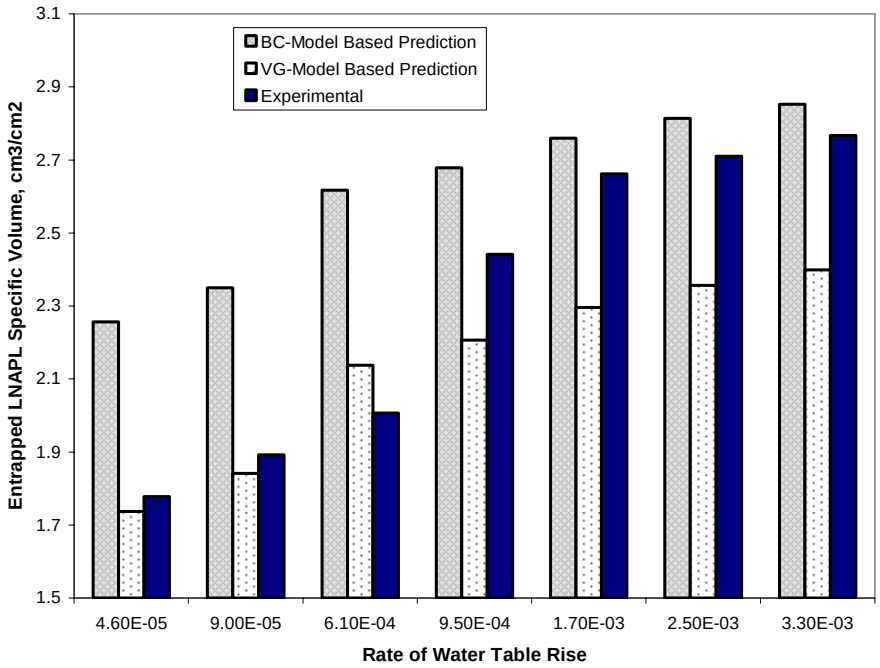

Figure 5.4: Model Validation at Initial Water Saturation=30%

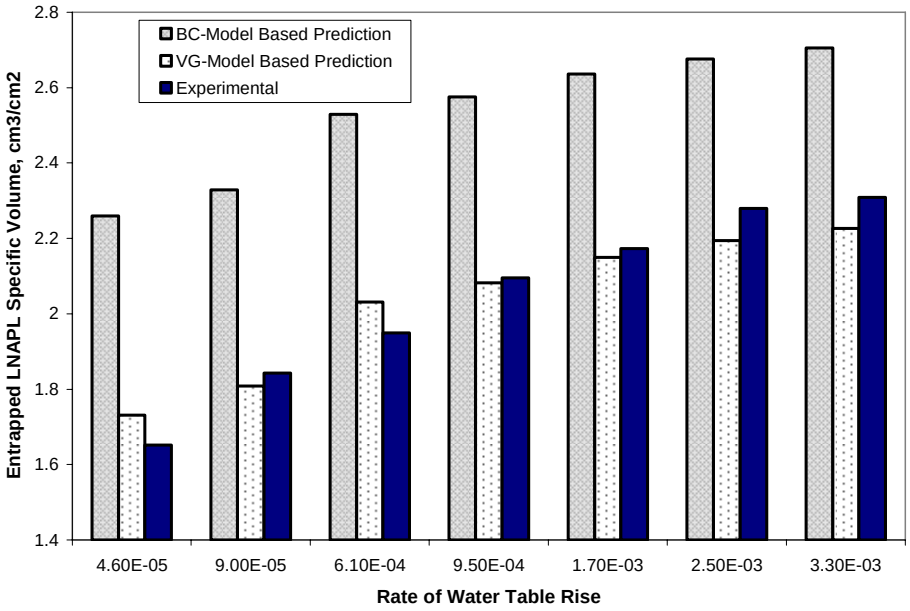

Figure 5.5: Model Validation at Initial Water Saturation=42%

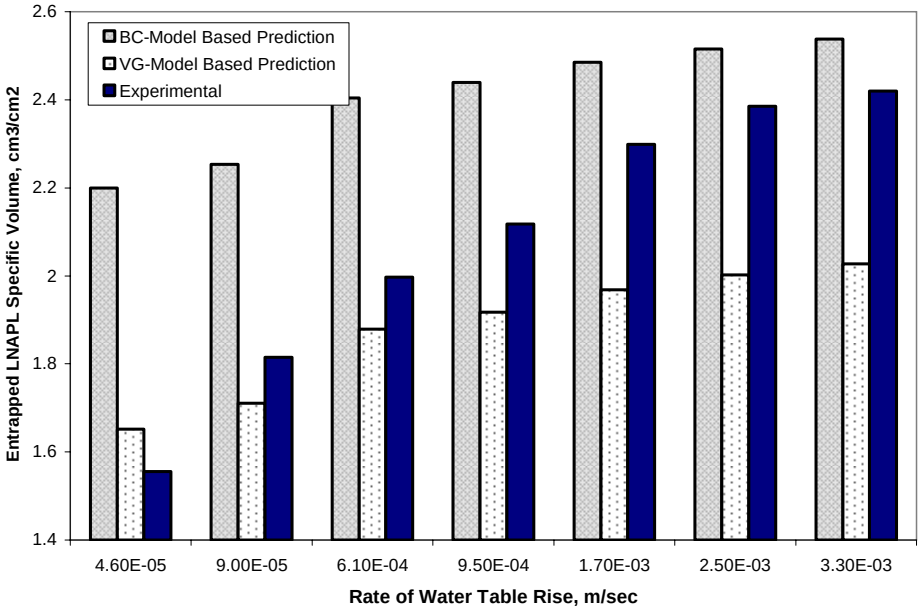

Figure 5.6: Model Validation at Initial Water Saturation=60%

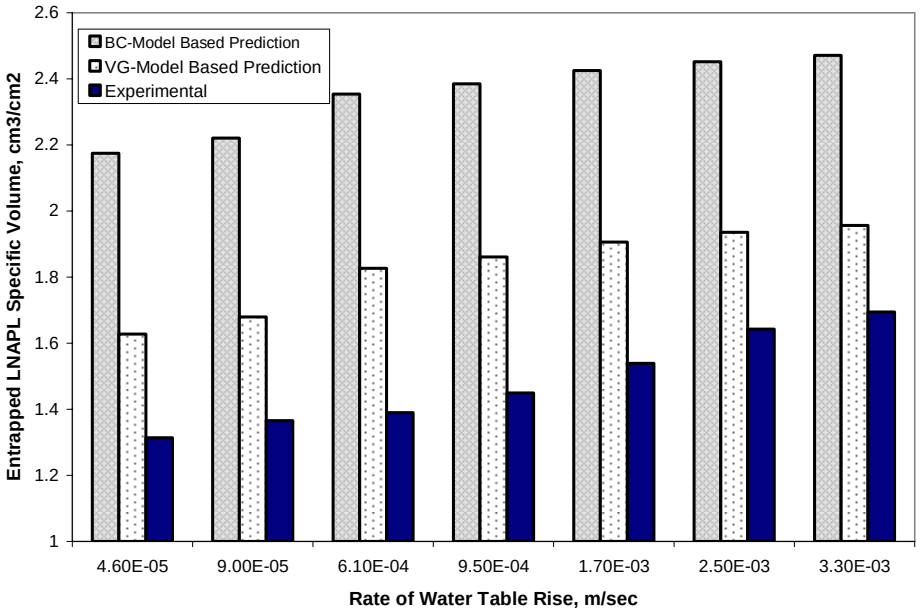

Figure 5.7: Model Validation at Initial Water Saturation=71%

Table 5.4: Coefficients of Regression for the Trapping Model

Factor Affecting LNAPL Entrapment	BC-Model Based Prediction	VG-Model Based Prediction
Water table rise rate, 10^{-3} m/sec		
0.046	< 0	0.7316
0.090	< 0	0.6936
0.61	< 0	0.7476
0.95	< 0	0.6809
1.70	< 0	0.6258
2.50	0.1223	0.6765
3.30	0.2143	0.7294
Initial Water Saturation, %		
20	0.935	0.9457
30	< 0	0.5726
42.3	0.396	0.8788
60	< 0	< 0
71	< 0	0.5577

inaccuracy is by 17-23% with inferior fit of $R^2 \leq 0$ and 0.557 respectively. In contrast, the BC-Based prediction persistently over estimates by 3-67% and portrays exceptionally poor fitness particularly at higher initial water content. For initial water content of 20%-42.3% the prediction was good with R^2 range of 0.396-0.935, while above 42.3% initial water saturation the $R^2 \leq 0$. These differences in the models' estimation that render the BC-Based prediction higher which could be attributed to differences in the way the two models have perceived initial mode of displacement of water by LNAPL on the drainage pathway as discussed earlier.

5.3.2 Model Validation for Effect of Initial Water Content

Behavior of the developed model is checked for effect of initial water on the entrapment trend at fixed rise velocities. Land [31] and Steffy et al [68] linear trapping models are also evaluated in order to display the significance of accounting for the rate of water table rise in LNAPL entrapment models. Clearly, the developed model predictions are good to a considerable extent particularly at lower table rise rates as shown in figures (5.8)-(5.14). Trapped LNAPL decreases with rise in initial water content based on both the VG and BC models' assumptions as observed with the experimental data. Similarly, the coefficients of regression displayed in Table (5.4) shows that the VG-model based prediction is also superior, while, the BC-model based prediction constantly overestimates with relatively greater deviation. Generally, for the whole range of the initial water saturations considered, the VG-based model gives excellent predictions with an average of 6%

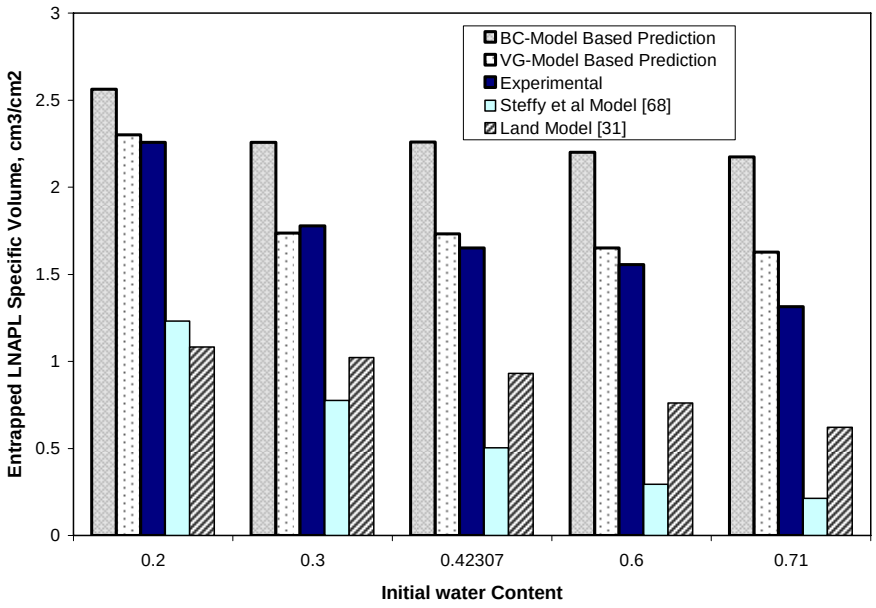

Figure 5.8: Model Validation at Water Table Rise Rate=4.60E-5 m/sec

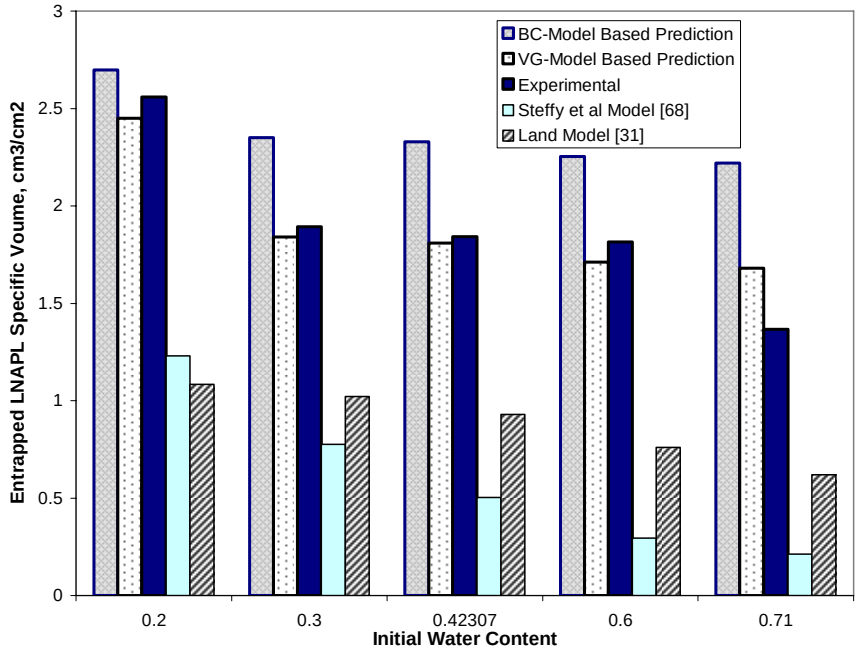

Figure 5.9: Model Validation at Water Table Rise Rate=9.0E-5 m/sec

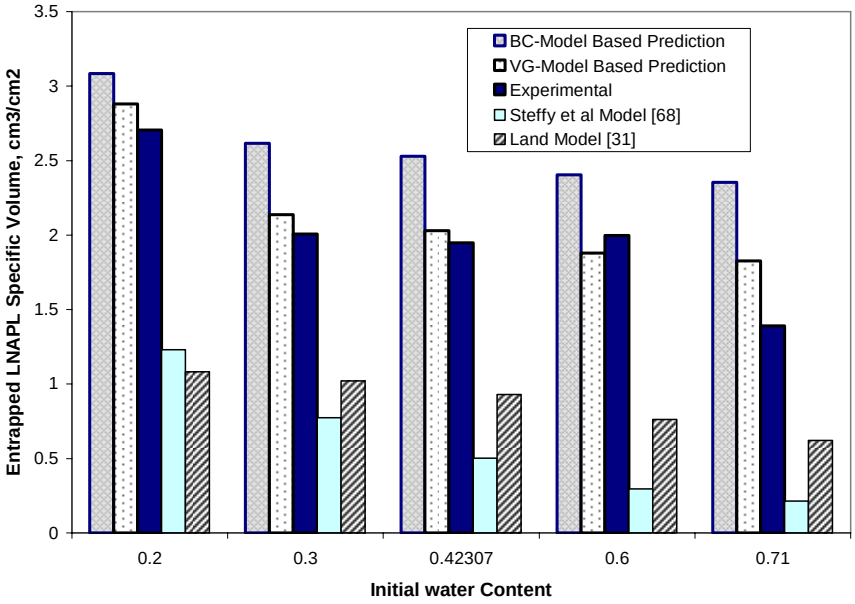

Figure 5.10: Model Validation at Water Table Rise Rate=6.10E-4 m/sec

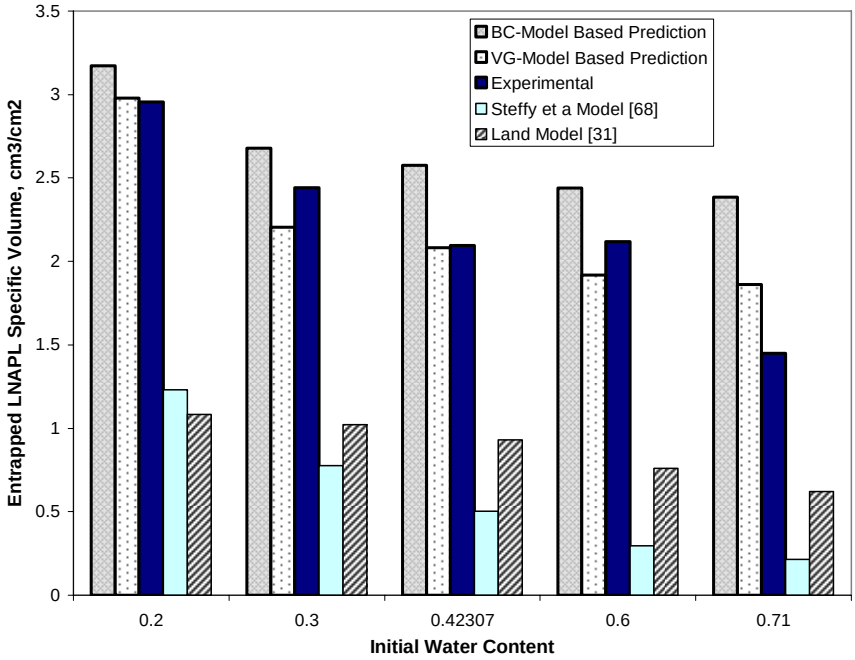

Figure 5.11: Model Validation at Water Table Rise Rate=9.50E-4 m/sec

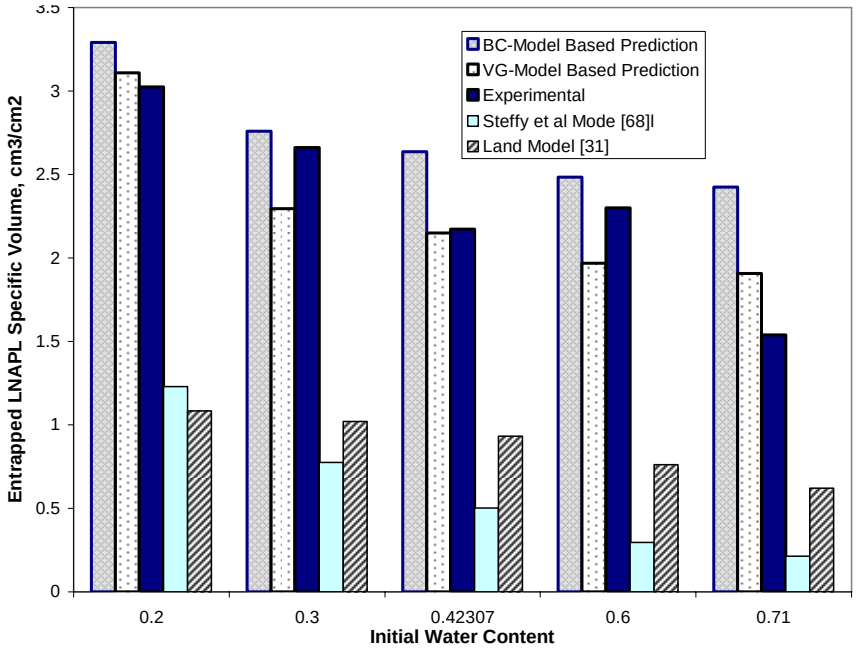

Figure 5.12: Model Validation at Water Table Rise Rate=1.70E-3 m/sec

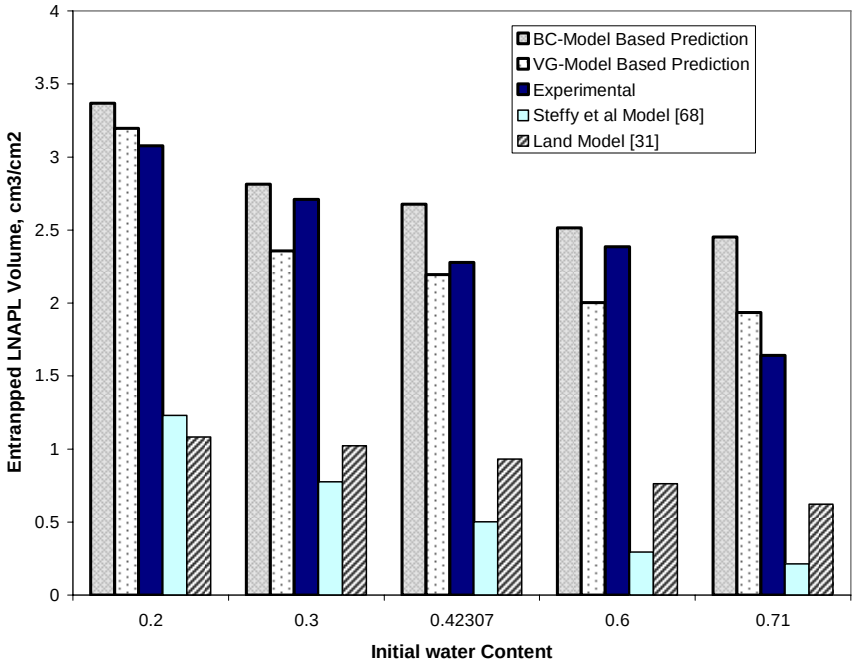

Figure 5.13: Model Validation at Water Table Rise Rate=2.50E-3 m/sec

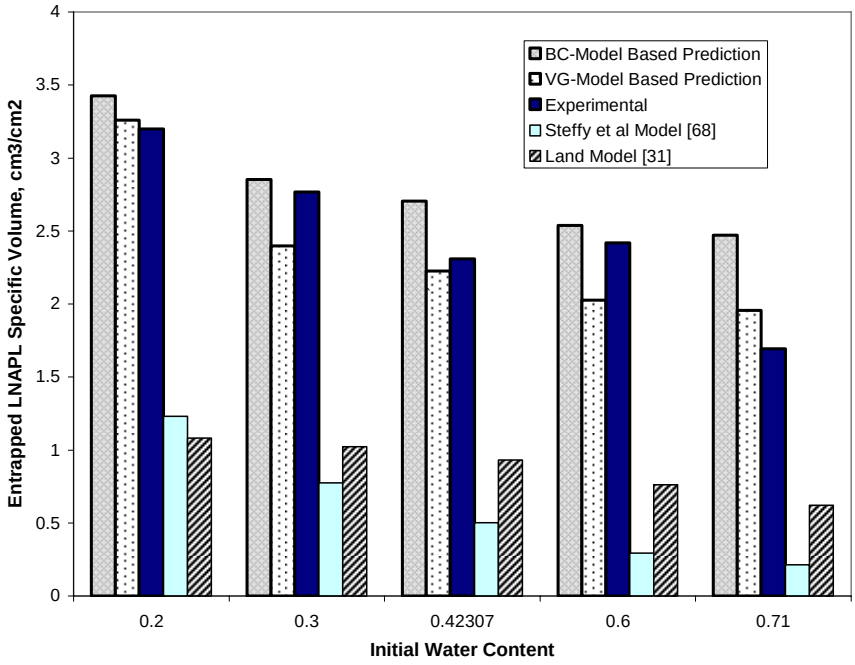

Figure 5.14: Model Validation at Water Table Rise Rate=3.300E-3 m/sec

inaccurate at any fixed rise velocity. The R^2 values are within short range of 0.6258-0.7476, these values of the R^2 are attributed to deviation of the predicted from the experimental at higher initial water content above 60% that impairs the overall accuracy of the prediction. Likewise, based on BC-model, the trapping model consistently over predicts the trapped saturation but portrays the best behavior at higher displacement rates with maximum R^2 = 0.1223 and 0.2143 at rise velocity of 2.50 and 3.30E-03 m/sec respectively.

Eventhough the Land's [31] model performs better than Steffy *et al* [68] model, , as shown also in figures (5.8)-(5.14), it is apparent that in all cases both the two models persistently underestimated the LNAPL entrapment specific volume without restraint. Altogether, their performances are far less than that of the developed model considering both the BC-based and VG-based model's options; owing to the fact that rate of wetting fluid imposed by the water table rise is not taken into consideration.

5.4 Overall S-P Based Models' Performances

To assess the overall performances of the two S-P based models approaches, the predicted LNAPL trapped specific volumes are plotted against the experimental values as displayed in figures (5.15) and (5.16). While the BC-model based trapping model could only explain about 23% of the actual LNAPL entrapment trend, the VG-model showed a better overall performance of about 80 %. The discrepancies between the numerical computations resulted from the two based models' could be attributed to the entry pressure assumption

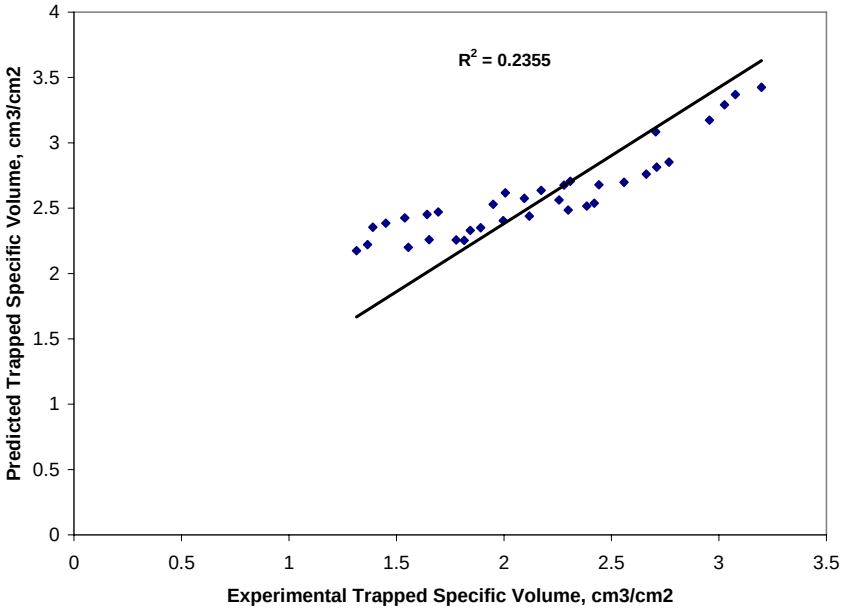

Figure 5.15: Overall Performance of BC-Model Based Prediction

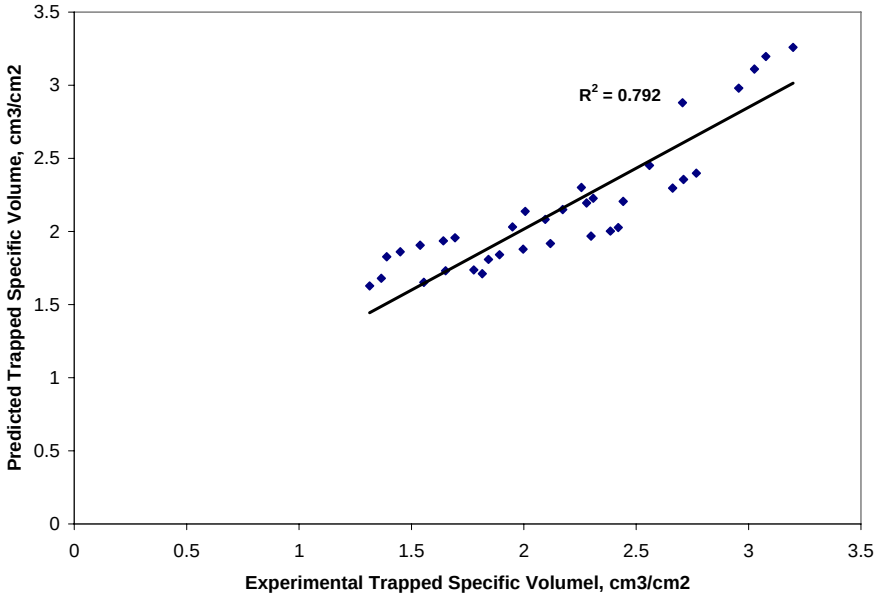

Figure 5.16: Overall Performance of VG-Model Based Prediction

differences which led to the higher trapped specific volumes from the trapping model integration observed when BC's model is used and therefore resulting in more deviation from the experimental values comparatively.

CHAPTER 6

Summary, Conclusions and Recommendations

6.1 Summary

Owing to the fact that greater portion of available fresh water in the globe is stored in underground aquifers and persistence of contaminants spill into subsurface, pollution of groundwater has become a major world-wide problem. Due to widespread petroleum hydrocarbon relevance in modern day-to-day life, most of the contaminants detected in polluted subsurface environment are found to be among the class of highly toxic hydrocarbons referred to as non-aqueous phase liquid (NAPL). Characterized by toxicity and profound low dissolution rate in water; presence of these pollutants in the subsurface could lead to long term deterioration of groundwater quality, thereby depleting the usability potential of large volumes of vital water resources. Following significant NAPL spill or leakage from underground installations into the subsurface and upon reaching an aquifer, it is imminent that it will eventually be carried along by the moving groundwater and/or fluctuating water table. Vast understanding of the fate and behaviors of the LNAPL is paramount because it stands as requisites for efficient design and good decision making towards viable and cost-effective clean-up scheme. Ideally, LNAPL entrapment investigation requires laboratory analysis and modeling to be carried out hand-in-hand with field investigations in order to make them more reliable for contamination problem solving. However, confining to the laboratory and/or modeling option(s) provides an

insight on likely field occurrences; moreover, this approach simplifies the difficulty and huge cost of field investigation.

In the present work, the entrapment of a Saudi Arabian light crude oil, a typical light NAPL (LNAPL), was experimentally investigated and modeled in the light of effects of water table rise rate and initial water content in contaminated uniform and well-graded sandy aquifers. Moreover, these effects were investigated considering the influence of initial porous medium surface wetting on the entrapment saturation of the crude oil. In order to achieve these objectives, the presence of LNAPL within the vicinity of capillary fringe and water table and its subsequent entrapment following a rise in the water table level at some rise rates were simulated at laboratory scale. Three different sets of laboratory column tests designated as LCT1, LCT2 and LCT3 were undertaken for preliminary investigation, experimental analysis on uniform sand and experimental analysis well-graded sand respectively.

Thus, the LCT1 was used to design the experiments in the LCT2 and LCT3. In both the LCT2 and LCT3, the initial water saturation of 0%, 20%, 30%, 42.3%, 60% and 71% were considered for the macroscopic scale quantitative measurements of the trapped LNAPL through several water displacing LNAPL tests undertaken. Due to differences in the two porous media grain size distribution that adversely affects flow characteristics, the average water table rise rates in the LCT2 were set at 0.0911, 0.404, 1.55, 2.47, 3.67, 5.74 and 7.09 x 10^{-3} m/s characterized with capillary number range of 5.36E-05-4.45E-03 . While, the corresponding rise rates for LCT3 were set at 0.046, 0.090, 0.61, 0.95, 1.7, 2.5 and 3.3 x 10^{-3} m/s characterized with capillary number range of 2.87E-05-2.06E-03. By

invoking Brooks Corey (BC) [5] and Van Genutchen (VG) [71] constitutive relationships, the results from the experimental program supplemented the development of a semi-empirical LNAPL trapping model that accounts for the rate of wetting fluid imbibition imposed by a rising water for LNAPL-water two-phase system. The outcome of the investigation could be summarized as follows:

1. At higher water table rise rate, the entrapment saturation as a function of increase in initial water saturation in the well-graded and uniform sands follows fluctuating patterns. The LNAPL trapped saturation decreases smoothly with increase in the initial water saturation except at some higher initial water saturation i.e 60% and 71% when the trapped saturation became higher than at 30% and 42.3% initial water content.
2. For the uniform sand with initial saturations of 20%, 30% 42.3% and 60% at higher water table rise rates, it is apparent that increase in the water table rise rate led to higher entrapment of the LNAPL to occur prior to apparently achieving a steady state when the water table rise rate was about 3.67E-03 m/se. A maximum trapped saturation of 37% was observed at initial water content of 20% and water table rise rate of 3.67E-03m/s.
3. Similarly, with regard to the well-graded sand, increase in water table rise rate resulted in increase in LNAPL entrapment saturation and the maximum trapped saturation of 37.3%. This was also observed at highest water table rise rate 3.3 x 10^{-3} m/s, but in contrast there was no clear attainment of steady state of the trapped saturation.

4. At 71% initial water content, increase in rate of water table rise rate has lesser impact in both the two scenarios for the types of sand grading used. The effect showed minor consequences in trapping more LNAPL, particularly for the uniform sand. The overall saturation range for the water-wet initial conditions for the two soils are 1.5%-37.3% and 28.1%-37.5% respectively

5. For both the uniform and well-graded sand, at initial fully LNAPL saturated condition corresponding to initial water saturation of 0%, increase in water table rise rate significantly decreases the LNAPL entrapment saturation. In this case, the trapped LNAPL saturations for the two soils are within the range of 13.4%-33.6% and 15.2%-37% with the minimum observed at the maximum water table rise rate of 5.40E-3 m/sec and 3.3 x 10^{-3} m/sec respectively.

6. With increase in rate of water table rise, deviation from linear model relationship between initial water content and trapped LNAPL saturation was found to increase. For uniform sand the coefficient of regression, R^2, differs from 0.5938 to 0.0021 while for the well-graded sand it differs from 0.8458 to 0.4016 between the two extreme rise rates.

7. With prime assumption of quasi-static model amongst many others, a semi-empirical model that accounts for rate of imbibition imposed by a rising water table was formulated by coupling the best function that fits the experimental data and soil characteristics curves of BC [5] and VG [71] for the range of initial water saturation of 20-71% and set of water table rise rates that satisfy the instability criteria.

8. The developed model shows a good agreement with the LNAPL entrapment behavior. The BC-model based predictions are higher than the VG-model based predictions and the former model approach seems to always overestimate the LNAPL trapped specific volume. However, both the two model approaches were found to be much better at lower initial water saturation with R^2 within range of 0.396-0.935 and 0.573-0.947 respectively.

9. For effects of rate of water table rise, the VG-model performs fairly well with R^2 between 0.6258-0.7476, whereas the BC-model approach performance was inferior with best fit observed at the two highest rise velocities with $R^2 = 0.1223$ and 0.2143. Comparison of the model predictions with other linear trapping model of Land [31] and Steffy *el al* [68] that disregard rate of wetting fluid imbibition showed that the developed model predictions are more accurate.

6.2 Conclusions

Based on the results of the investigation, the following conclusions are reached:

1. In LNAPL-water contaminated aquifers when rate of water table rise is high, initial soil moisture content does not solely control the entrapment of LNAPL. The effects of wetting fluid imbibition rate imposed by the rising water table also play an important role in the LNAPL entrapment. And in such cases, for a water-wet initial condition, increase in the water table rise increases the amount of LNAPL trapped volume before a limit is reached above which the increase in the rise rate becomes inconsequential.

2. The study verified that soil particle size gradation has significant contribution in LNAPL entrapment. For identical initial soil and flow conditions, the entrapment saturation in well-graded sand is likely to be higher that of uniform sand possessing larger particle sizes.

3. Under similar conditions, removal of LNAPL contamination in well-graded sands possessing finer particles is liable to be more difficult than in uniform sand having higher percentage of larger particles for reason of higher capillary effects in the former type of soil. Moreover, heterogeneous soils are prone to trapping more LNAPL than homogenous ones when rate of water table rise is high due to fingering and channeling effects that are more likely to occur in the former soil type.

4. Due to wetting fluid front instability that could feature at higher rate of water table rise rates, above certain hypothetical critical capillary number, the relationship between trapped LNAPL saturation and initial water saturation is no longer linear, and the deviation from the linearity amplifies as the capillary number increases. In such cases, neglecting the effects of imbibition rate imposed by the rising water table could significantly lead to inaccurate estimation of trappable LNAPL volumes predicted by traditional LNAPL trapping models.

5. Porous medium initial surface wetting condition adversely affects the LNAPL entrapment saturation. Marked distinctions exist between water-wet and LNAPL-wet initial porous medium wetting conditions. The instability criteria are apparently not the same in the two scenarios.

6. The positive impact of increase in displacement or flushing rate on removal of LNAPL in contaminated soils using fluid of greater wettability during remediation has limitation as threshold does exists above which more LNAPL is trappable.

7. Flow instability that could dominate the water-wet initial, quasi-static assumption, indirect hydraulic parameters estimates and field condition could hamper the prediction of the semi-empirical model developed. Moreover, the assumption of quasi-static model could provide good approximation in LNAPL entrapment modeling where the wetting fluid front is unstable.

8. While both the BC and VG based model performed reasonably well, in the course of this study, the later performed much better. The VG-model is therefore considered more appropriate in describing the pore size distribution of the well-graded sand used in this investigation. However, this may not always be the case when other soils of different gradations are considered.

9. Monitoring aquifer's water table fluctuations and its characteristics including the fluctuation history, rising and falling rates etc. would be of significant assistance towards making proper assessment of the potentialities of such effects on proportion of trappable hydrocarbons that could pose greater threat in polluted aquifers.

6.3 Recommendations

The following are recommended for future study:

1. Effect of higher rate of water table rise on LNAPL entrapment should be studied by considering the effects of water table fluctuation and soil layering.
2. As research in instability and preferential flow at wetting fluid front is currently dominated by the oil industry, greater efforts should be directed to this effect in environmental engineering, particularly for LNAPL entrapment analysis. This could provide dependable and concrete explanations that would assist in providing practical solutions to complex flow phenomena and often observations at LNAPL contaminated aquifers.
3. Dynamic pore network models approach should be embraced and enhanced in LNAPL entrapment modeling by concurrently accounting for qualitative microscopic capillary, viscous and buoyancy effects. In-addition, criteria for identifying the critical capillary number above which neglecting the dynamics effects disfavors accuracy in existing models' predictions should be established.
4. In design of LNAPL contamination remediation and/or mobilization using water flushing techniques, choice of appropriate wetting fluid flushing rate should be part of the most crucial decision making process to be made. This will ensure that the flushing rate is optimized for the most cost-effective measure to be taken in the remediation process.

APPENDIX A: INTERACTIVE MATLAB PROGRAM

```
%%%%%%%%%%%%%%%%%%%%%%%%%%%%%%%%%%%%%%%%%%%%%%%%%%%%%%
%%%%%%%%%%%%%%%%%%%%%%%%%%%%%%%%%%%%%%%%%%%%%%%%%%%%
% An Interactive program to predict LNAPL Entrapment specific volume based on  effects of Initial Water
content taking into account the imbibition Rate imposed by a rising water table Model based on Van
Genutchen and Brooks-Corey saturation pressure relationships.
%%%%%%%%%%%%%%%%%%%%%%%%%%%%%%%%%%%%%%%%%%%%%%%%%%%%%%
%%%%%%%%%%%%%%%%%%%%%%%%%%%%%%%%%%%%%%%%%%%%%%%%%%%%
% Enter Porous Medium and LNAPL Properties
K=input('Enter value of hydraulic conductivity >>')
phi=input('Enter value of phi >>')
DW=input('Enter value of density of wetting fluid >>')
DN=input('Enter value of density of non-wetting fluid >>')
VW=input('Enter value of viscosity of wetting fluid >>')
VN=input('Enter value of viscosity of non-wetting fluid >>')
%Enter Water-LNAPL characteristic curve paramaters
Bow=input('Enter value of Bow >>')
Sm=input('Enter value of Sm >>')
%Enter VG-model parameters
n=input('Enter value of n >>');
alphaD=input('Enter value of alpha for drainage >>')
alphaI=input('Enter value of alpha imbibition >>')
m=1-1/n
%Enter BC-model parameters
lamda=input('Enter value of lamda >>')
hdD=input('Enter value of hd for drainage >>')
hdI=input('Enter value of hd for imbibition >>')
% State initial moisture condition and flow
Q=input('Enter value of rate of water table rise >>')
LNAPLI=input('Enter value of initial LNAPL volume >>')
g=9.81
%Optimized empirical trapping model parameters
a=3.169858762 ;
b=-24.3349023  ;
c=72.42809303  ;
d=-90.4528354  ;
e=40.46752327  ;
f=0.026500479  ;
%Calculate instability limiting rate
QL=K*g*(DW-DN)/(VN-VW)
if QL < Q
```

```
%BC-Model Based Trapping model's Predictions
for swi=[0.2:0.015:0.7]
j=1:length(swi)
% Invert BC-Model
h(j)=(hdD./((swi(j)-Sm)/(1-Sm)).^(1./lamdaD))
%Perform Integration
LNAPLBC1(j)=(phi*(a+b+c+d+e+f*log(Q)).*hdD)
F1=@(x)(phi.*(a+b.*(((hdD./x).^(lamda))*(1-Sm)+Sm)+c.*(((hdD./x).^(lamda))*(1-
Sm)+Sm).^2+d.*(((hdD./x).^(lamda))*(1-Sm)+Sm).^3+e.*(((hdD./x).^(lamda))*(1-
Sm)+Sm).^4+f.*log(Q)));
LNAPLBC2(j)=quadl(F1,hdD,h(j))
TLNAPL1(j)=(LNAPLBC2(j)+LNAPLBC1(j));
%Check Model's result compatibility
if TLANPL1< LNAPLI
TLNAPL1(j)=Sor1(j)
else
end
end
else
end
Calculate instability limiting rate
QL=K*g*(DW-DN)/(VN-VW)
if QL < Q
% VG-Model Based Trapping model's Predictions
for swi1=[0.2:0.01:0.7]
g=1:length(swi1)
% Invert VG-Model
h1(g) =((((((swi1(g)-Sm)/(1-Sm)))).^-(1/m))-1).^(1/n)./(alphaD)
% Perform integration
F2=@(y)phi*(a+b*((1+(alphaD.*y).^n).^(-m)*(1-Sm)+Sm)+c*((1+(alphaD.*y).^n).^(-m)*(1-
Sm)+Sm).^2+d*((1+(alphaD.*y).^n).^(-m)*(1-Sm)+Sm).^3+e*((1+(alphaD.*y).^n).^(-m)*(1-
Sm)+Sm).^4+f*log(q));
TLNAPL2(g)=quadl(F2,0,h1(g));
end
end
%Check Model's result compatibility
if TLNAPL2 < LNAPLI
TLNAPL2(g)=Sor2(g)
else
end
end
else
end
```

APPENDIX B: MODEL VALIDATION PROGRAM

```
%%%%%%%%%%%%%%%%%%%%%%%%%%%%%%%%%%%%%%%%%%%%%%%%%%%%%%%%%%%
%%%%%%%%%%%%%%%%%%%%%%%%%%%%%%%%%%%%%%%%%%%%%%%%%%%%%%%%%%%
% Program for VC-Based and BC-Based semi-analytical trapping model validation using experimental data
from laboratory column test
%%%%%%%%%%%%%%%%%%%%%%%%%%%%%%%%%%%%%%%%%%%%%%%%%%%%%%%%%%%
%%%%%%%%%%%%%%%%%%%%%%%%%%%%%%%%%%%%%%%%%%%%%%%%%%%%%%%%%%%
% b=input('Enter porous medium VC and BC parameters >>'}
phi=0.288; Sm=0.0529; hdD=7.77;lamdaD=1.4; n=3.21;alpha=.087;
m=1-1/n;
data =[2.256    1.7776  1.6519  1.555   1.3139
2.559   1.892   1.843   1.815   1.3658
2.706   2.0064  1.9497  1.997   1.39
2.956   2.442   2.0952  2.118   1.45
3.026   2.662   2.1728  2.299   1.5386
3.077   2.7104  2.2795  2.385   1.642
3.198   2.7676  2.3086  2.42    1.694];
z1=data(1,:);
z2=data(2,:);
z3=data(3,:);
z4=data(4,:);
z5=data(5,:);
z6=data(6,:);
z7=data(7,:);
x1=[4.60E-05 9.0E-05 6.10E-04 9.50E-04 1.70E-03 2.50E-03 3.30E-03];
y1=data(:,1);
y2=data(:,2);
y3=data(:,3);
y4=data(:,4);
y5=data(:,5);
%Initial Water content
swi=[0.2 0.3    0.42307 0.6     0.71];
h=(hdD./((swi-Sm)/(1-Sm)).^(1./lamdaD))
% Proposed model empirical parameters from non-linear surface-fit analysis
a=3.169858762 ;
b=-24.3349023  ;
c=72.42809303  ;
d=-90.4528354  ;
e=40.46752327  ;
f=0.026500479  ;
% Wetting fluid Imbibition rates
```

```
q=x1;
for j=1:length(q);
z=length(h);
for i=1:z;
Swi1(i)=((hdD./h(i)).^(lamdaD)) ;
% BC-Based model estimate of trapped volume per unit area
entrappedBC1(j,i)=(phi*(a+b+c+d+e+f*log(q(j))).*hdD)
F1=@(x)(phi*(a+b*(((hdD./x).^(lamdaD))*(1-Sm)+Sm)+c*(((hdD./x).^(lamdaD))*(1-
Sm)+Sm).^2+d*(((hdD./x).^(lamdaD))*(1-Sm)+Sm).^3+e*(((hdD./x).^(lamdaD))*(1-
Sm)+Sm).^4+f*log(q(j))));
entrappedBC2(j,i)=quadl(F1,hdD,h(i))
entrapped1(j,i)=(entrappedBC2(j,i)+entrappedBC1(j,i));
end
end
% Wetting fluid Imbibition rates
q=x1;
for k=1:length(q);
z=length(h);
for l=1:z;
%Initial Water content from VG Model
Swi2(l)=(1+(alpha.*h(l)).^n).^(-m) ;
% VG-Based model estimate of trapped volume per unit area
F2=@(y)phi*(a+b*((1+(alpha.*y).^n).^(-m)*(1-Sm)+Sm)+c*((1+(alpha.*y).^n).^(-m)*(1-
Sm)+Sm).^2+d*((1+(alpha.*y).^n).^(-m)*(1-Sm)+Sm).^3+e*((1+(alpha.*y).^n).^(-m)*(1-
Sm)+Sm).^4+f*log(q(k)));
entrapped2(k,l)=quadl(F2,0,h(l));
end
end
figure(1)
plot(swi,entrapped2(1,:),'k-o',swi,entrapped2(2,:),'k->',swi,entrapped2(3,:),'k-*',swi,entrapped2(4,:),'k-
+',swi,entrapped2(5,:),'k-<',swi,entrapped1(6,:),'k-+',swi,entrapped1(7,:),'k--')
xlabel('Initial Water Content,%'),ylabel('VG-Model Based Trapped LNAPL Saturation,%')
legend('q=4.600E-05 m/s','q=9.0E-05 m/s','q=6.10E-04 m/s','q=9.50E-04  m/s','q=1.70E-03 m/s','q=2.50E-
03m/s','q=3.30E-03 m/s',7)
figure(2)
plot(x1,y1,'k-o',q,entrapped1(:,1),'k-*',q,entrapped2(:,1),'k->');
xlabel('Average Rate of Water Table Rise,m/s'),ylabel('Trapped LNAPL Volume ,cm3/cm2'),title('model
validation at swi=20%')
legend('Experimental','BC-Model Based Prediction','VG-Model Based Prediction',3)
figure(3)
plot(x1,y2,'k-o',q,entrapped1(:,2),'k-*',q,entrapped2(:,2),'k->');
xlabel('Average Rate of Water Table Rise,m/s'),ylabel('Trapped LNAPL Volume ,cm3/cm2'),title('model
validation at swi=30%')
```

```
legend('Experimental','BC-Model Based Prediction','VG-Model Based Prediction',3)
figure(4)
plot(x1,y3,'k-o',q,entrapped1(:,3),'k-*',q,entrapped2(:,3),'k->');
xlabel('Average Rate of Water Table Rise,m/s'),ylabel('Trapped LNAPL Volume ,cm3/cm2'),title('model validation at swi=42.3%')
legend('Experimental','BC-Model Based Prediction','VG-Model Based Prediction',3)
figure(5)
plot(x1,y4,'k-o',q,entrapped1(:,4),'k-*',q,entrapped2(:,4),'k->');
legend('Experimental','Model Prediction',2)
xlabel('Average Rate of Water Table Rise,m/s'),ylabel('Trapped LNAPL Volume ,cm3/cm2'), title('model validation at swi=60%')
legend('Experimental','BC-Model Based Prediction','VG-Model Based Prediction',3)
figure(6)
plot(x1,y5,'k-o',q,entrapped1(:,5),'k-*',q,entrapped2(:,5),'k->');
legend('Experimental','BC-Model Based Prediction','VG-Model Based Prediction',3)
xlabel('Average Rate of Water Table Rise,m/s'),ylabel('Trapped LNAPL Volume ,cm3/cm2'),title('model validation at swi=71%')
% Swi_Sor
figure(7)
plot(swi,z1,'k-o',swi,entrapped1(1,:),'k-*',swi,entrapped2(1,:),'k->')
xlabel('Initial Water Content,%'),ylabel('Trapped LNAPL Saturation,%'),title('model validation at q=4.60E-05m/s')
legend('Experimental','BC-Model Based Prediction','VG-Model Based Prediction',3)
figure(8)
plot(swi,z2,'k-o',swi,entrapped1(2,:),'k-*',swi,entrapped2(2,:),'k->')
xlabel('Initial Water Content,%'),ylabel('Trapped LNAPL Saturation,%'),title('model validation at 9.00E-05m/s')
legend('Experimental','BC-Model Based Prediction','VG-Model Based Prediction',3)
figure(9)
plot(swi,z3,'k-o',swi,entrapped1(3,:),'k-*',swi,entrapped2(3,:),'k->')
xlabel('Initial Water Content,%'),ylabel('Trapped LNAPL Saturation,%'),title('model validation at q=6.10E-04m/s ')
legend('Experimental','BC-Model Based Prediction','VG-Model Based Prediction',3)
figure(10)
plot(swi,z4,'k-o',swi,entrapped1(4,:),'k-*',swi,entrapped2(4,:),'k->')
xlabel('Initial Water Content,%'),ylabel('Trapped LNAPL Saturation,%'),title('model validation at q=9.50E-04m/s')
legend('Experimental','BC-Model Based Prediction','VG-Model Based Prediction',3)
figure(11)
plot(swi,z5,'k-o',swi,entrapped1(5,:),'k-*',swi,entrapped2(5,:),'k->')
xlabel('Initial Water Content,%'),ylabel('Trapped LNAPL Saturation,%'),title('model validation at q=1.70E-03m/s')
legend('Experimental','BC-Model Based Prediction','VG-Model Based Prediction',3)
```

```
figure(12)
plot(swi,z6,'k-o',swi,entrapped1(6,:),'k-*',swi,entrapped2(6,:),'k->')
xlabel('Initial Water Content,%'),ylabel('Trapped LNAPL Saturation,%'),title('model validation at q=2.50E-03m/s')
legend('Experimental','BC-Model Based Prediction','VG-Model Based Prediction',3)
figure(13)
plot(swi,z7,'k-o',swi,entrapped1(7,:),'k-*',swi,entrapped2(7,:),'k->')
xlabel('Initial Water Content,%'),ylabel('Trapped LNAPL Saturation,%'),title('model validation at q=3.30E-03m/s')
legend('Experimental','BC-Model Based Prediction','VG-Model Based Prediction',3)
```

REFERENCES

[1] Abriola, L. M. & G.F Pinder (1985). A multiphase approach to the modeling of porous media contamination by organic compounds 2. Numerical simulation, Water resources research, 21: 19-26.

[2] Arya, L.M. and J.F Paris (1980). A physico-emphirical model to predict soil moisture characteristics from particle size distribution and bulk density data. Soil Sci. Soc. Am. Journal. 45: 1023-1030.

[3] Aziz, K. and Settari, A. (1979). Petroleum Reservoir Simulation. Elsevier Applied science Publications, New York, NY; 385-389.

[4] Boyd, G. R. and Farley, K. J. 1992. NAPL removal from groundwater by alcohol flooding: laboratory studies and applications. In: Hydrocarbon Contaminated Soils and Groundwater, Vol. 2. (Calabrese, E. J. and Kostecki, P. T., Eds.) Lewis Publishers.

[5] Brooks, R.H and A.T Corey (1964). Hydraulic properties of porous media. Hydrology paper No.3, Colorado State University, Fort Collins.

[6] Burden, N. T. (1953). Relative permeability calculations for pore-size distribution data. Trans A.I.M.E, 198; 71-77.

[7] Busby, R. D., Lenhard, R. J and Rolston, D. E (1995). Investigation of saturation-capillary pressure relationship in two- and three-fluid systems for several NAPLs in different porous media. Ground Water, 33 (4); 570-578.

[8] Charbeneau R. J (2000). Groundwater hydraulics and pollutant transport. Prentice Hall Inc. Upper Saddle River, New Jersey 07458.

[9] Charles J. N., Steven D. A, Randall R. R, and Scott, G. H. (1995). Ground Water Issue; Light Nonaqueous Phase Liquids. U.S. Environmental Protection Agency, Washington, DC, EPA/540/S-95/500.

[10] Chatzis, I., Kuntamukkula, M.S., and Morrow, N.R. (1988) Effect of capillary number on the microstructure of residual oil in strongly Water-Wet Sandstones. SPE Res. Eng., Vol. 3, (3); 902-912.

[11] Chuoke, R. L., P. van Meurs, and C. van der Poel (1959).The instability of slow, immiscible, viscous liquid-liquid displacements in permeable media, Trans. Am. Inst. Min. Metall. Pet. Eng., 216; 188–194.

[12] Conrad, S. H., J.L Wilson., W.R Mason., and W. J. Peplinski (1992). Visualization of residual organic liquid trapped in aquifers. Water Resources Research, 28; 467-478.

[13] Corey, A.T (1986). Mechanics of Immiscible fluids in porous media. Water Resources Publications, Fort Collins, CO, 2nd edition ;35-39

[14] Farr, A.M., Houghtalen, R.J and McWhorter, D.B (1990). Volume estimation of light Non-aqueous Phase Liquid in porous media. Groundwater. 28 (1); 48-56.

[15] Faust, C. R (1985). Transport of immiscible fluids within and below the saturated zone: numerical model. Water Resources 21

[16] Fayer, M. J. and Hillel, D. (1986). Air encapsulation 1. Measurement in field soils.

Soil Science Society of American Journal. 50; 568-572

[17] Fredlund, D.G., Xing, A., (1994). Equation for soil-water characteristic curve. Canadian Geotechnical Journal, 31; 521-532.

[18] George C. Z., Roger B. W, and Thomas C. V. (1998). Influence of initial water saturation on the residual saturation of an organic Liquid in the vadose zone. Water Resources Management .12 (2): 81-93

[19] Hill, D. E., and J.Y. Parlange (1972) Wetting front instability in layered soils. Soil Sci. Soc. Am. Proc., 36; 697–702.

[20] Hillel, D., (1980). Fundamentals of Soil Physics. Academic Pre4ss, New York, NY, pp. 152-155.

[21] Hoag, G. E. and M.C Marley (1986). Gasoline Residual Saturation in unsaturated uniform aquifer materials. Journal of Environmental Engineering. ,112; 586-604.

[22] Host-Madsen, J. and Jensen, K. H (1992). Laboratory and numerical investigation of immiscible multiphase-flow in soil. Journal of contaminant hydrology, 135; 13-52.

[23] Hunt, J. R., Sitar, N. and Udell, K. S (1988). Non-aqueous phase liquid transport and clean-up. I. Analysis of mechanisms. Water Resources Research, 24; 1247-1258.

[24] Jerault, G. R and Salter S. J (1990). The effect of pore-structure on hysteresis in relative permeability and capillary pressure: pore-level modeling. Transport in Porous Media, 5; 103-151.

[25] Kalaurachchi, J. J. and Parker, J.C (1992) Multiphase flow with a simple model for oil entrapment. Transport in Porous Media, .7; 1-14.

[26] Katyal, A. K., Kaluarachchi, J. J and Parker, J. C. (1991). MOFAT: A two-dimensional finite element program for multiphase flow and multi-component transport. USEPA/600-2-91-020.

[27] Kia, S.F and A. S Abdul (1990). Retention of diesel fuel in aquifer material. Journal of Hydraulic Engineering, 116; 890-894.

[28] Kool, J.B and Parker, J.C (1987). Development and evaluation of closed-form expressions for hysteretic soil hydraulic properties. Water Resources Research, 23: 105-114.

[29] Kueper, B. H., and E. O. Frind (1988). An overview of immiscible fingering in porous media, Journal of Contaminant Hydrology, 2; 95–110.

[30] Kueper, B.H., W. Abbott, and G. Farquhar. (1989). Experimental observation of multiphase flow in heterogeneous porous media. Journal of Contaminant Hydrology, 5; 8-9.

[31] Land, C. S. (1968).Calculation of imbibition relative permeability for two- and three-phase from rock properties. Trans. AIME (Am. Inst. Of Min. Metall. Eng.) Pet. Eng., 207; 149-156.

[32] Lenhard, R. J (1992). Measurement and modeling of three-phase saturation-pressure hysteresis. Journal of Contaminant Hydrology, 9; 243-269.

[33] Lenhard, R.J and J.C Parker. (1990). Estimation of free product hydrocarbon

volume from fluid level in monitoring wells. Ground Water, 28; 57-67.

[34] Lenhard, R.J and Parker, J. C (1987b). A model for hysteretic constitutive relations governing multiphase flow, 2. Permeability-Saturation relations. Water Resources Research, 23; 2197-2206.

[35] Lenhard, R.J., Parker J.C and Misha S. (1989). Correspondence between Brooks-Corey and Van Genutchen Models. Joutnal of Irrigation and Drainage Engineering, 114 (4); 745-751.

[36] Lenhard, R.J., Parker J.C and Kalaurachchi, J.J., (1989c). A model for hysteretic constitutive relations governing multiphase, 3. Re-definements and numerical simulations. Water Resources Research, 25; 1727-1736.

[37] Lenhard, R.J. and Parker, J.C., (1987). Measurements and prediction of saturation pressure relationships in three phase porous media. Journal of contaminant hydrology, 28 (1); 407-424.

[38] Lenhard, R.J. and Parker, J.C., (1988). Experimental validation of the theory of extending two-phase saturation-pressure relations to three-phase systems for monotonic drainage paths. Water Resources Research, 24; 373-380.

[39] Lenormand, R. and Zarcone, C. (1998). Physics of blob displacement in a two-dimentional porous medium. Soc. Pet. Eng. Form Evaluation, 3; 271-275.

[40] Leverett, M.C., (1941). Capillary behavior in porous Solids. . Trans. AIME (Am. Inst. Of Min. Metall. Eng.) Pet. Eng., 142; 152-169.

[41] Maldal, T., Jacobsen S.R.; Alvestad J., and Årland K.S.(1999) Relationship between

remaining oil saturation after waterflooding and rock/flow properties at laboratory and reservoir scale Petroleum Geoscience, 5; 31-35

[42] Marco, A. and Marcello Donatelli (2003). SOILPAR 2.00: software to estimate soil hydrological parameters and functions. European Journal Agronomy, 18; 373-377.

[43] Marinelli, F. and Dunford, D.S. (1996) LNAPL thickness in monitoring well considering hysteresis and entrapment. Groundwater, 34 (3); 405-414.

[44] Melrose, J. C. and Brandner, C. F. (1974) Role of capillary forces in determining microscopic displacement efficiency for oil recovery by water-flooding. Journal of Canadian .Petrol. Tech., Oct-Dec; 54-62

[45] Mercer, J. W and Cohen, R. M (1990). A review of immiscible fluids in the subsurface; properties, models, characterization and remediation. Journal of Contaminant Hydrology, 6; 107-163.

[46] Mishra, S., Parker , J.C and Singhal, N.(1989). Estimation of soil hydraulic properties and their uncertainty from particle size distribution data. Journal of hydrology, 108; 618-624.

[47] Morrow, N.R. (1976) Capillary Pressure Correlations for Uniformly Wetted Porous Media. Journal of Canadian Petrol. Tech., Oct-Dec; 49-69.

[48] Morrow, N.R., Chatzis, I., and Taber, J.J. (1988) Entrapment and mobilization of residual oil in bead packs. Soc. Petrol. Eng. Res. Eng., August; 927-934

[49] Morrow, N.R. and Songkran, B. (1981) Effect of viscous and buoyancy forces on nonwetting phase trapping in porous media, In D.O. Shah (ed), Surface Phenomena

in Enhanced Oil Recovery: Plenum Press: N.Y.; 387-411.

[50] Mualem, Y. and Miller, E.E.,(1979). A hysteretic model based on an explicit domain-dependence function. Soil Science Society of American Journal, 43; 1067-1073.

[51] Naar, J., Wygal, R.J. and Henderson, J.H. (1962) Imbibition relative permeability in unconsolidated porous media, Soc. Pet. Eng. J., 2(13); 225.

[52] Newell C. J, Steven D. A, Randall R. R and Scott G. Huling (1995). Ground water Issue: Light Non-aqueous Phase Liquids: EPA/540/S-95/500.

[53] Parker J. C, Zhu, J. L., Johnson, V. J., Kremesec, V. J and Hockman, E. L (1994) Modeling free product migration and recovery at hydrocarbon spill sites. Ground Water, 32; 119-128.

[54] Parker, J.C. and Lenhard, R.J. (1987a). A model for hysteretic constitutive relations governing multiphase flow 1. Saturation-Pressure relations. Water Resources Research. 23(12); 2187-2196.

[55] Parker, J.C. and Lenhard, R.J., and Kuppusamy, T. (1987). A parametric model for constitutive propertries governing multiphase flow in porous media. Water Resources Research 23(4); 618-624.

[56] Powers, S.E., Abriola, L.M., and Weber, W.J., Jr. (1994) An Experimental Investigation of Nonaqueous Phase Dissolution in Saturated Subsurface Systems: Transient Mass Transfer Rates. Water Resources Res., 30(2); 321-332.

[57] Ratnam, S., P. J. Culligan-Hensley, and J. T. Germaine (1996). Modeling the

behavior of LNAPLS under hydraulic flushing. Non-Aqueous phase Liquids (NAPLs) in the Subsurface Environment: Assessment and Remediation, ASCE 1996 National Convention, Washington D.C., November 10-14; 595-606.

[58] Ratnam, S., P. J. Culligan-Hensley, and J. T. Germaine (1996). Geotechnical centrifuge modeling of LNAPL entrapment in sands samples under hydraulic flushing. Geotechnical News, 14 (3); 22-26.

[59] Raats, P. A. C (1973) Unstable wetting fronts in uniform and non-uniform soils. Soil Sci. Soc. Am. Proc., 37; 681–685.

[60] Ryan R. G. and Dhir V. K (1993). Effect of soil-partcle size on hydrocarbon entrapment near dynamic water table. Journal of Soil Contamination, 2(1); 59-92.

[61] Ryan R. G. and Dhir V. K (1996). Effect of interfacial tension on hydrocarbon entrapment and mobilization near dynamic water table. Journal of Soil Contamination, 2(1); 59-92

[62] Saffman, P. G., and S. G. Taylor (1958). The penetration of fluid into a porous medium or Hele-Shaw cell containing a more viscous liquid, Proc. Roy. Soc. A, 245; 312–329.

[63] Schiegge, H. O (1988). Considerations water, oil and air in porous media. Water Science and Technology, 17; 467-476.

[64] Scott, P. S., Farquhar, G. J and Kouwen, N. (1983). Hysteresis effects on the net infiltration, American Society of Agric. Engineering Publ. 11-83; 163-171.

[65] Shiklomavov, I. (1993). World fresh water resources in Peter H. Gleick, ed., Water

in crisis: A guide to the world's fresh water resources.

[66] Sleep, B. E and Sykes, J. F (1993). Compositional simulation of ground water contamination by organic compounds: 1. Model development and verification. Water Resources Research, 29 (6); 1697-1708

[67] Steffy D. A, Johnson C. D and Barry D. A (1998). Numerical simulations and long-column tests of LNAPL displacement and trapping by a fluctuating water table. Journal of Soil contamination, 7 (3); 325-356.

[68] Steffy D. A., Johnson C. D and Barry D. A (1997). Influence of antecedent moisture content on residual LNAPL saturation. Journal of Soil contamination, 6 (2); 113-147.

[69] Stonestrom, D. A. and Rubin, J. (1989). Water content dependence of trapped air in two soils. Water Resources Research, 25; 1947-1958.

[70] USEPA. 1992. Evaluation of Ground-Water Extraction Remedies, Phase II, Vol. 1 - Summary Report Publ. 9355.4-05A. Washington, D.C. EPA Office of Emergency and Remedial Response.

[71] Van Genuchten, M.T. (1980). A closed-form equation for predicting the hydraulic conductivity of unsaturated soils. Soil Science Society of American Journal, 44; 892-898.

[72] Van Geel, P. J and Roy, S. D (2002). A proposed model to include a residual NAPL saturation in a hysteretic capillary pressure-saturation relationship. Journal of Contaminant Hydrology, 58: 79-110.

[73] Van Geel, P. J and Skyes, J. F (1994). Laboratory and model simulations of LNAPL spill in a variably-saturated sand II. Comparison of laboratory and model results. Journal of contaminant hydrology, 17; 27-53.

[74] Van Geel, P. J. (1994). Laboratory and simulation of a LNAPL spill in sand porous medium. PhD thesis; University of Waterloo.

[75] Wardlaw, N.C and Miller McKeller, M. (1985). Oil blob population and mobilization of trapped oil in unconsolidated packs. Journal Canadian Petrol. Tech., 63; 525-532.

[76] Wilkinson, D. and J.F. Willemson (1983) Invasion percolation: a new form of percolation theory, J. Phys. A: Math. Gen., 16; 3365-3376.

[77] Willhite, G.P (1986). Waterflooding. SPE publications, Richardson, TX. SPE text book series volume 3.

[78] White, M. D and Oostrom, M., and Lenhard, R. J (1995). Modeling fluid flow and transport in variable saturated porous media with the STOMP simulator: 1. Non-volatile three-phase model description. Advances in Water Resources, 18; 352-364.

[79] Wilson, J.L. and S.H Conrad (1984). Is physical displacement of residual hydrocarbons a realistic possibility in aquifer restoration? Proc. Petroleum Hydrocarbons and Organic Chemicals in Ground Water. NWWA/API, Houston, TX pp. 274-298.

[80] Wilson, J.L., Conrad, S.H., Mason, W.R., Peplinski, W. and Hagan, E. (1990). Laboratory investigation of residual organics from spills, leaks, and disposal

hazardous wastes in groundwater. Rep. prepared by R.S Kerr Environmental research Lab., Ada, OK, for U.S. Environmental Protection Agency, Washington, DC, EPA/600/6-90/004, 267pp

[81] Zhi, W., Feyen, J. and Elrick, D.E (1998). Prediction of fingering in porous media. Water Resources Research, 39 (9); 2183-2190.

[82] http://www.mathworks.com/

[83] http://www.systat.com/

[84] http://www.wolfram.com/

Vitae

- Nuhu Mu'azu Dalhat
- Graduated with Bachelor Degree in Civil Engineering from Ahmadu Bello Univeristy, Zaria Nigeria in 2000.
- Served Osun State Environmental Protection Agency, Osogbo Nigeria as Civil Engineer during NYSC program from April 2001 to May 2002.
- Joined Civil Engineering Department, KFUPM, Dhahran Saudi Arabia as a Research Assistant in September 2002.
- Received Master of Science Degree in Civil Engineering from KFUPM in May 2005.